WARWICK
THE UNIVERSITY OF WARWICK

A Thesis Submitted for the Degree of PhD at the University of Warwick

Permanent WRAP URL:
http://wrap.warwick.ac.uk/81925

Copyright and reuse:
This thesis is made available online and is protected by original copyright.
Please scroll down to view the document itself.
Please refer to the repository record for this item for information to help you to cite it.
Our policy information is available from the repository home page.

For more information, please contact the WRAP Team at: wrap@warwick.ac.uk

warwick.ac.uk/lib-publications

Solubility Studies on Poly(ethylene oxide) and Cellulose

by

Michael Michael

Department of Chemistry

Submitted for the Degree of Doctor of Philosophy

July 1997

CONTENTS

List of Figures

Chapter One

Chapter Two

Chapter Three

Chapter Four

Chapter Five

List of Tables

Chapter One

Chapter Two

Chapter Three

Chapter Four

Chapter Five

Acknowledgements

I would like to thank Dr. O. W. Howarth for his supervision during the course of this project. I would also like to thank Courtaulds research for the CASE award. There are many at Courtaulds I that need to thank; especially my industrial supervisor Dr. R. N. Ibbett, and also Mr. C. Sambrook-Smith and Mr. Peter Laity for all their help and advice.

I would like to thank Dr. J. J. Hastings for his help in training me to operate the solution-state NMR spectrometer at Warwick University.

Finally I thank EPSRC for the studentship.

Declaration

The work described in this thesis is original to the author, except where acknowledgement has been made to results and ideas previously published. The work was carried out at the Department of Chemistry, University of Warwick, between October 1994 and June 1997 and has not been submitted previously for a degree at any institution. Part of this work has been published with the following reference:

C-O and C-O Bond Conformations in 1,2-dimethoxyethane, *Bis*-(2-methoxyethyl)-ether and Poly(ethylene oxide): Dependence on Solvent and Temperature. O. W. Howarth, M. Michael and R. N. Ibbett, *Polymer*, **38**, 355 (1997).

SUMMARY

This study has consisted of two related areas of research. The first area concerned the measurement of the proportions of *gauche* rotamer about C-C and C-O bonds of poly(ethylene oxide) (PEO) from NMR coupling constants. $^3J_{HCCH}$ and $^3J_{HCOC}$ couplings in 1,2-dimethoxyethane and *bis*-(2-methoxyethyl)-ether, both model compounds for PEO, plus $^3J_{HCCH}$ in poly(ethylene oxide), have been obtained in five solvents by iterative fitting. The deduced proportions of *gauche* rotamers are higher than previous estimates, and higher still after allowance is made for the pentane effect. They fit well with gas phase electron diffraction data, with current gas phase theoretical calculations and with standard RIS parameters for the polymer. The influence of solvent arises more from its H-bond donor properties than in its dielectric. This study was undertaken partly in order to elucidate likely conformations of the glycosidic bond in the ensuing work on cellulose dissolution.

The second area of research was concerned with the dissolution of cellulose in amine oxides. Courtaulds PLC have successfully used N-methylmorpholine-N-oxide (NMMO) to produce cellulosic spinning solutions. However, the interaction between cellulose and NMMO is not clearly understood. We have therefore sought to amplify the understanding of this polymer-solvent interaction, first with optical microscopy experiments, and then with solution-state and solid-state NMR techniques.

Optical microscopy experiments showed several different behaviours of ramie fibres (natural, highly crystalline cellulose I) as they dissolved in NMMO with added H_2O. In 81.2 % NMMO solution, the fibres were observed to swell without dissolution, or burst into tiny fragments or else bend at certain regions creating a "zigzagging" pattern before dissolution. The rates of dissolution were also variable. Some amine oxides that are non-solvents for cellulose were also found to swell ramie, though in this case without subsequent dissolution.

The changes in the proton NMR chemical shifts of NMMO and N-ethylmorpholine-N-oxide (NEMO), dissolved in dry DMSO-d_6, on addition of water or methyl-β-D-glucopyranoside (a soluble model compound for cellulose) were used to obtain binding constants. The binding between methyl-β-D-glucopyranoside and NMMO (a solvent for cellulose) is about twice as strong as the binding between the non-solvent NEMO and the same saccharide, under these conditions. In contrast, the binding between NEMO and water is stronger than that measured between NMMO and water. The stronger interaction of NMMO (relative to the interaction of NEMO) with the saccharide helps to explain its potency as a solvent for cellulose, but the reason for its occurrence, and the weakened interaction with water, is not fully understood. The carbon NMR shift differences of methyl-β-D-cellobioside on addition of various amine oxides (both solvents and non-solvents for cellulose) were found to be similar. We propose that the 1:1 interactions of all amine oxides with cellulose may be similar but that the competing interaction between amine oxide molecules decides if they become a solvent or non-solvent for cellulose. The variation of spin-lattice relaxation measurements on the cellobiose carbons upon addition of NMMO was also studied. It indicates an increase of mobility of the C5-C6 bond in the presence of NMMO. This implies the breaking of H-bonds in this region.

Solid-state NMR spectra (both CPMAS and HPDEC/MAS) were run on aliquots of cellulose samples in NMMO, taken out at various stages of the dissolution process. A faster disappearance of the C4 peak from the crystalline phase relative to the C4 peak from the amorphous phase suggests that the crystalline phase must first be penetrated by the solvent before dissolution. In contrast ramie treated with the non-solvent NEMO was found to have been converted from cellulose I to cellulose III_I. The amorphous phase of ramie fibres treated with the non-solvent trimethylamine-N-oxide was found to increase at the expense of the crystalline phase, although in this case no cellulose III_I was detected. Evidently, some amine oxides that are non-solvents for cellulose can nevertheless penetrate between layers of cellulose that are held together by Van der Waals forces, even though they cannot pull apart adjacent chains of cellulose (necessary for dissolution to occur) that are held together by strong H-bonds.

List of Abbreviations

DME	1,2-dimethoxyethane
BMEE	*bis*-(2-methoxyethyl)-ether
PEO	poly(ethylene oxide)
NMMO	N-methylmorpholine-N-oxide
NEMO	N-ethylmorpholine-N-oxide
TMAO	trimethylamine-N-oxide (TMAO)
TEAO	triethylamine-N-oxide (TEAO)
PNO	pyridine-N-oxide (PNO)
DMCHAO	N, N-dimethylcyclohexylamine-N-oxide
DS	degree of substitution
DP	degree of polymerisation
RIS	rotational isomeric states
DMSO	dimethyl sulphoxide
DMF	dimethylformamide
TMS	tetramethylsilane
TPS	3-trimethylsilyl-2,2,3,3-tetrapropionic acid sodium salt
DSS	2,2-dimethyl-2-silapentane-5-sulphonic acid sodium salt
COSY	correlation spectroscopy
TOCSY	total correlation spectroscopy
CPMAS	cross polarisation in combination with magic angle spinning
HPDEC/MAS	high-power decoupling in combination with magic angle spinning
CSA	chemical shift anisotropy
CA	cellulose acetate
Tr-Cell	tritylcelulose
MCC	microcrystalline cellulose
TCH	trans-1,2-cyclohexanediol

CHAPTER ONE

Introduction

1.1 Aims of this study

This project has two main related areas of study. The first part was concerned with the establishment of the conformational preferences of poly(ethylene oxide) (PEO) in a range of environments using NMR data. This important compound has many uses (see section 1.8.1) and is also used as a block copolymer with poly(propylene oxide) (PPO) in the coatings industry as a surfactant. The ether link of these compounds also resembles the glycosidic (1→4) linkage between saccharide molecules and so serves as a model for cellulose. Thus a study of PEO may help to explain the conformational preferences of cellulose and other polysaccharides. This work has started by using 1,2-dimethoxyethane (DME) and *bis*-(2-methoxyethyl)-ether (BMEE) as model compounds for PEO, together with PEO itself. DME and BMEE can be considered as the methoxyl-terminated monomer and dimer of PEO respectively. DME is often used as a model compound for PEO and has also been the subject of numerous computational calculations.[1-8]

The second area was concerned with the dissolution of cellulose. Courtaulds PLC uses NMMO (N-methylmorpholine-N-oxide) as a solvent to dissolve cellulose. Although this process has been successful[9] in producing cellulosic spinning solutions that are subsequently used to produce regenerated cellulose fibres (known commercially as *Tencel*) for the textile industry, the mechanism of dissolution is not fully understood. Water is added for the purpose of suppressing the melting point of NMMO but it is not known whether it has any other purpose. Therefore, the purpose of this project was to increase the understanding of the interaction of cellulose with NMMO and water, and to determine its conformational states and conformational freedoms. Some of these

conformations are fixed by the rigid structure of the sugar ring, but those about the glycosidic link and the C5-C6 bond are flexible and would be expected to change on dissolution. It has been demonstrated that shifts (mainly because of the γ-*gauche* effect) are seen when moving from the regular crystal structure, through the amorphous solid into the true solution. The γ-*gauche* effect is the apparent observed shielding of the carbon nucleus when substituents in the γ-position move to a *gauche* configuration. A γ-*gauche* shielding of about 5 ppm is observed for carbon atoms in a *gauche* conformation to another carbon or about 7 ppm if it is in a *gauche* conformation to oxygen.[10] In order to establish how the cellulose crystal is disrupted by the attack of solvent, these shifts need to be identified and semi-quantitatively explained. Ultimately it is hoped that the "rules" for getting cellulose into solution will be discovered. A more complete understanding of the mechanism of dissolution is important for the long term development of the fibre spinning process, and will also help to increase the range of other commercial opportunities for the technology.

An important aspect of this investigation was to obtain an insight on why some amine oxides, such as NMMO, can dissolve cellulose while others are non-solvents. Figure 1.1 shows a range of amine oxides relevant to this project.

Most experiments involved solution or solid-state NMR spectroscopy. However, some optical microscopy and wide-angle X-ray diffraction experiments were also performed on various cellulose samples.

Column 1 solvents for cellulose

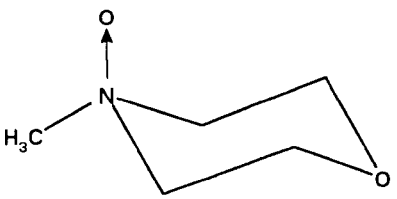

N-methylmorpholine-N-oxide (NMMO)

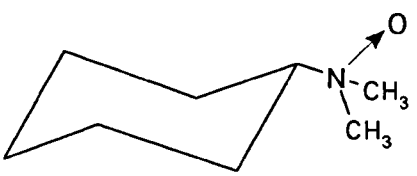

N, N-dimethylcyclohexylamine-N-oxide (DMCHAO)

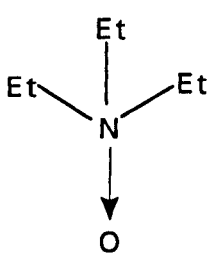

triethylamine-N-oxide (TEAO)

Column 2 non-solvents for cellulose

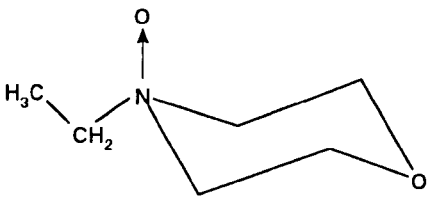

N-ethylmorpholine-N-oxide (NEMO)

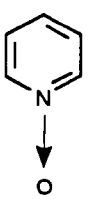

pyridine-N-oxide (PNO)

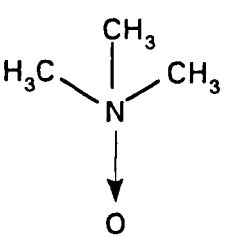

trimethylamine-N-oxide (TMAO)

Figure 1.1 Amine oxides (solvents for cellulose in the first column and non-solvents in the second column) relevant to this work.

1.2 NMR techniques

Since the advent of pulse Fourier transform instruments the importance of NMR spectroscopy in the study of carbohydrates has increased tremendously. With FT instruments measurement of ^{13}C spectra has become routine while the sensitivity of ^{1}H NMR spectra has increased by several orders of magnitude. This increase in sensitivity has facilitated the measurement of relaxation times and nuclear Overhauser enhancements (NOE). New experiments have been made possible and others simplified because of computer controlled instruments.

This section will discuss some of the NMR techniques available for structural and conformational investigations. Although emphasis is placed on the study of saccharides, the principles of the techniques can be applied to other types of molecules.

1.2.1 ^{1}H NMR spectroscopy of carbohydrates

The assignment of NMR peaks is essential for the application of NMR in carbohydrate structural investigation. With modern high field NMR spectrometers most monosaccharides can be analysed on a first order basis and give well-resolved spectra. Assignment difficulties of complex oligosaccharides can often arise with ^{1}H spectra because of protons being located at the surface of the molecule making interunit shielding and deshielding effects important.[11] This is in contrast to ^{13}C spectra that do not suffer from these difficulties.

De Bruyn *et al.*[12,13] have published proton spectra for a series of mono- and oligosaccharides in D_2O. They concluded that individual proton resonances could be identified by shift increments and the position of the glycosidic linkage could also be

determined. The ^1H NMR chemical shifts of protected carbohydrate derivatives (*e.g.* acetates) follow general rules.[14] However, it is essential that comparison of ^1H chemical shifts with literature data should only be done if all data are obtained under identical conditions (*e.g.* temperature and solvent).

Difficulties can often arise when interpreting ^1H spectra of mono- and oligosaccharides because of overlapping peaks in the region between 3.6 and 4.3 ppm. There are several techniques to facilitate the assignment of these overlapping peaks. One such method involves deuterium substitution which causes the substituted proton to disappear in the ^1H spectrum and also removes spin-spin coupling to all neighbouring protons. Another widely used and simple experiment to assist assignment is homonuclear decoupling, but limitations occur when the shift separation of the saturated and observed resonances becomes too small. However, these can often be overcome by the use of more sophisticated experiments such as TOCSY[15] and COSY.[16]

1.2.2 ^{13}C NMR spectroscopy of carbohydrates

Proton-decoupled ^{13}C spectra are well resolved and usually provide an unequivocal identification of monosaccharides, especially when a collection of ^{13}C chemical shifts is available. Peaks usually appear typically within a 40 ppm shift range (60 to 100 ppm). Because ^{13}C chemical shifts are very sensitive to structural changes these spectra can provide information on the anomeric configuration, the monosaccharides sequence and the conformation of polysaccharides. It has been shown that the chemical shifts of monosaccharides are essentially the same as the shifts obtained with a polysaccharide of the same units.[17] It has also been found that substituent groups attached to a carbon atom will cause a large downfield shift of this atom which indicates the location of the glycosidic linkages. Determination of the anomeric configuration of pyranoses can be

achieved from the one bond coupling ($^1J_{C1H1}$) which is in general 10 Hz larger for the α-anomer.[18] The one bond coupling is solvent dependent so comparison must be made with the same solvent.[19] Finally, the conformation of the glycosidic bond can be determined by measurement of $^3J_{COCH}$ couplings, and comparison made then with a Karplus type curve.

Hobley *et al.* used γ-*gauche* and a number of other steric parameters to predict ^1H and ^{13}C NMR chemical shifts for various aldopyranose and aldofuranose monosaccharides in D_2O and DMSO.[20] They concluded that the hydrogen bonding network for each monosaccharide is similar in both solvents since their chemical shifts do not vary widely. Their parameters were successful in predicting ^{13}C shifts in aldofuranose monosaccharides within an average error of 0.74 ppm.

The NOE of ^{13}C produced by proton-decoupling can lead to an almost threefold increase in signal-to-noise ratio reducing the acquisition time required. However, this effect disappears in the absence of proton irradiation. Therefore, proton-coupled carbon spectra are usually obtained using a gated technique. This gives a fully coupled spectrum while retaining the signal-to-noise ratio produced by the NOE. The technique relies on the fact that the appearance of the couplings in a spectrum is determined only by the presence or absence of proton-decoupling during the actual acquisition of the signal and is independent of the decoupling conditions immediately prior or subsequent to this. Therefore, proton-decoupling is applied and then switched off prior to the pulse to produce proton-coupled carbon spectra with full NOE.

Another useful technique to help interpret NMR spectra is that of heteronuclear two-dimensional shift correlation spectroscopy. This is similar to a COSY experiment as discussed above but usually has carbon chemical shifts on one axis and proton chemical

shifts on the other axis. This provides a link between ^{1}H and ^{13}C spectra and can be set up to show ^{1}J or longer range CH couplings.

1.2.3 ^{13}C solid-state NMR spectroscopy

Solid-state NMR spectroscopy has proved to be very useful in characterising crystalline and amorphous regions of cellulose. This technique not only identifies various crystal forms of cellulose but also distinguishes different forms within a grouping such as cellulose I (see section 1.4.2).

1.2.3.1 Magic angle spinning

In the solution-state ^{13}C NMR spectroscopy of a compound, one observes peaks at particular chemical shifts characteristic of the environment of carbons in the molecule. However, the chemical shifts recorded are the isotropic values from the averaging of all possible orientations of the nucleus to the magnetic field by the random motion of the molecule. A single signal will appear for one ^{13}C type in a single crystal but its chemical shift will depend on the orientation of the molecules containing these nuclei, relative to the magnetic field. All orientations are possible for a polycrystalline material resulting in an envelope of signals. This variation of shift with molecular orientation is known as the shift anisotropy.

The envelope of signals may be averaged to its isotropic value by spinning the sample rapidly (2-20 kHz) about an axis at the magic angle of $\theta = 54.74°$ to the magnetic field. This is known as magic angle spinning (MAS). The chemical shift alters according to the term $3\cos^2\theta - 1$ where θ is the angle between the spinning axis and the magnetic field vector. Thus, if $\theta = 54.74°$ then the term $3\cos^2\theta - 1$ is reduced to zero, thus giving the isotropic shift in the solid environment. To succeed in narrowing the line, the rotation

rate must be at least of the order of the chemical shift anisotropy (CSA) in Hz. However, because this isotropic shift value is for the solid-state, it may be different from the solution-state for there will generally be environmental and structural differences between the two phases.

1.2.3.2 High-power decoupling combined with MAS (HPDEC/MAS)

In the isotropic solution-state the random motions of molecules also average the dipolar coupling between ^{1}H and ^{13}C nuclei to zero. However, in the solid-state where there is relatively little motion this interaction is not averaged, but may instead be removed by high power decoupling (HPDEC). HPDEC experiments are usually combined with MAS to remove the CSA and dipolar broadening. Some gums may have enough motion for self decoupling to take place. HPDEC/MAS generally reveals the more mobile components of molecules, because carbons in rigid regions relax inefficiently and thus become saturated.

1.2.3.3 Cross polarisation / magic-angle spinning (CPMAS)

Pines *et al.* introduced one advantageous refinement in solid-state NMR studies, a technique known as cross polarisation.[21] The combined cross polarisation / MAS experiment was first published by Schaefer and Stejskal[22] and has been principally responsible for a rejuvenated interest in solid-state NMR of dilute spin nuclei such as ^{13}C. This technique has the following pulse sequence:

^{1}H $\quad$ $(\pi/2)_x$-$(CP)_y$-CW

^{13}C $\quad$ (CP)-Acquire

where (CP) is the contact pulse and is distinct from the usual pulse used in solution-state NMR in that it is much longer, being milliseconds in length. The $(\pi/2)_x$ pulse applied to

to the proton channel will generate magnetisation along y. Because of the phase of the proton radio frequency field in the rotating frame of reference, the magnetisation becomes spin-locked. Thus the proton magnetisation precesses about the y-axis at an angular frequency of ω_1:

$$(\omega_1)_H = \gamma_H(B_1)_H$$

where B_1 is the magnitude of the applied magnetic field and γ_H is the magnetogyric ratio for protons. A pulse applied to the ^{13}C spins will result in rotating frame precessional frequency of:

$$(\omega_1)_C = \gamma_C(B_1)_C$$

Thus, there is an oscillating component of the proton magnetisation $(\omega_1)_H$ at the carbon nuclei and an oscillating component of the carbon magnetisation $(\omega_1)_C$ at the proton nuclei. Mutual spin flips or relaxation may occur if the two frequencies are the same. This matching of the rotating frame precessional frequencies is given by the Hartmann-Hahn[23] condition such that:

$$(\gamma B_1)_C = (\gamma B_1)_H$$

Since the magnetisation for the proton is larger than for carbon, cross relaxation from ^1H to ^{13}C will cause the carbon magnetisation to increase. A gain in signal amplitude of magnitude γ_H/γ_C is obtained (*i.e.* the magnitude of the ^{13}C signal depends on the magnetogyric ratio of ^1H). The theoretical maximum increase in S/N is fourfold but this is not usually obtained in practice. In addition, the repetition time is now determined by the shorter spin-lattice relaxation time of ^1H, since the carbon signal is generated from the proton magnetisation. To provide dipolar decoupling as with the HPDEC/MAS

technique, the ^{1}H transmitter is left on during acquisition. No NOE is generated, because of the slow tumbling rate.

CPMAS experiments are generally useful in revealing rigid or crystalline components of molecules; in these regions cross polarisation is much more efficient. Saturation becomes less important as with HPDEC/MAS (see above) because of the repetition delay being dependent on ^{1}H relaxation and not on the much longer relaxation times of ^{13}C nuclei.

1.3 The Anomeric and related conformational effects

The anomeric effect[24] is the preference of axial over equatorial C1 electronegative substituents in pyranose rings. This is contrary to the usual order of conformational stability and many attempts have been made to rationalise this effect and many review articles are available.[25,26] A conformational effect is said to have occurred when deviation of a certain phenomenon from usual behaviour is observed.[27] In this case a standard or reference compound whose conformational behaviour is considered as "normal" is needed. Although the anomeric effect was first observed in pyranose rings (and hence its name) it soon became clear that the effect is not confined to carbohydrates. Thus, the "generalised anomeric effect" is defined as the preference of the *gauche* position over *trans* in segments C-X-C-Y (X = O, N or S and Y = O, Br, Cl, F or S).[28] Preference for the *gauche* position has been shown to increase with increasing electronegativity of the Y substituent.[29]

The anomeric effect was first considered to arise from electrostatic interactions between bond dipoles or between bond pairs. However, the most frequently discussed theory is now the delocalisation of oxygen (X) lone pairs into the antibonding σ^* orbital of the

C-Y bond.[30] Measurements of bond lengths are compatible[31] with this interpretation, *i.e.* the C-Y bond is longer and O-C bond shorter in a C-O-C-Y segment for an axial substituent in pyranose rings. It has been shown by David *et al.*[32] that this delocalisation stabilisation is associated with different energies of the two lone pairs on the oxygen atom. Highly polar solvents decrease the preference for the axial conformation, which supports this model.[33]

There also exists a related phenomenon which is comparable in magnitude in X-C-C-Y systems, where X and Y are electronegative groups.[34] This preference of the *gauche* conformation was rationalised by Wolfe[34] in terms of attractive nuclear-electron attraction between X and Y. This dominates over nuclear-nuclear and electron-electron repulsive terms. However, a more satisfactory explanation of the "*gauche* effect" is stabilisation because of overlaps between bonding and antibonding orbitals.[35] The disappearance of this effect for elements of low periods having lone pairs (*e.g.* Br, I and SR) was described by Zefirov[36] using the hockey stick effect, and has been rationalised in terms of orbital repulsion.

In this work the *gauche* effect is very important. Using NMR data PEO will be shown to have a strong preference for the *gauche* conformer about the C-C bond, and also a significant tendency for *gauche* conformations about the C-O bond.

1.4 The structure of cellulose

Cellulose is a polymer composed of β-(1→4)-linked D-glucose residues (figure 1.2). There are important structural relationships between adjacent cellulose chains and the grouping of chains that form microfibrils. Inter- and intramolecular relationships change when cellulose is treated with swelling agents, thus, this supermolecular structure is of considerable research interest.

It is important to understand the detailed structure of β-D-glucopyranose (figure 1.3). A precise knowledge of the ring structure is crucial because none of the measuring techniques gives enough information to delineate the cellulose structure completely.

In defining the structure of cellulose there are principally three structural levels;

1. The molecular level: the chemical constitution, the steric conformation, the molecular weight, the molecular weight distribution, intramolecular interactions, the presence of functional sites, *etc.*
2. The supermolecular level: the aggregation of the chain molecules to elementary crystals and fibres, the degree of order inside and around these fibrils, the perfection of their orientation with respect to the fibre axis, *etc.*
3. The morphological level: the spatial arrangement of the fibrillar crystallites strands in the "cross-morphology" of the fibre, the existence of native cell wall layers or of skin-core structures in man made fibres, the presence of interfibrillar interstices and voids, *etc.*

In order to be able to analyse the relationship between the physical and chemical properties of cellulose with its structure, a profound knowledge of the structural features

of cellulose substrates needs to be known. This account gives a summary of what is known about the structure of cellulose fibres, with a brief history on the subject.

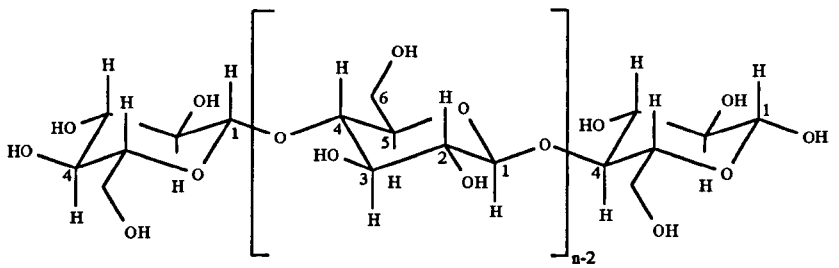

Figure 1.2 Constitutional formula of the cellulose molecule.

a)

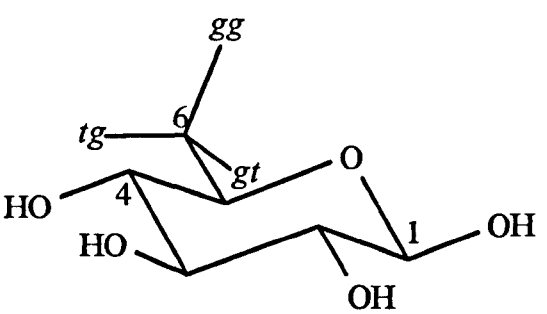

b)

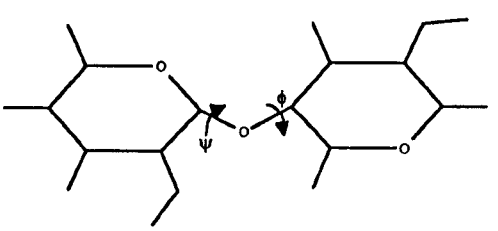

Figure 1.3 (a) Labelling of atoms in β-D-glucopyranose with 3 possible staggered positions for O6 (the first letter refers to the position of O6 relative to the ring oxygen and the second letter is the position relative to C4) and (b) A glycosidic linkage and location of the torsional angles.

1.4.1 Polymorphism of cellulose

At least six different crystalline structures of cellulose are currently known.[37] The best characterised polymorphs are cellulose I (also known as native cellulose) and cellulose II (mercerised or regenerated cellulose). Less detailed information is available for other polymorphs (*i.e.* celluloses III_I, III_{II} and IV_I, IV_{II}). It has been suggested that some of these six polymorphs may have the same conformation and packing but differ in the spatial arrangements of microfibrils.[37] Celluloses III_I or III_{II} are made by the action of ethylamine or a solution of 70 % ethylenediamine on celluloses I and II respectively. These polymorphs can be converted to celluloses IV_I or IV_{II}, depending on the starting material, by heating at 260 °C.

1.4.1.1 Cellulose I (native cellulose)

Native celluloses come from a variety of sources; bacterial cellulose (*e.g. Acetobacter xylinum)*; algal cellulose (*e.g. Velonia ventricosa*); and from the higher plants (*e.g.* tunicin, cotton and ramie). All these sources have a similar structure but vary in the degree of regularity and order of the crystal structure (see below).

Payen published the elemental composition of cellulose in 1838.[38] Subsequent observation on the formation of glucose in hydrolysis treatment lead to todays accepted view that cellulose is constructed from β-(1→4)-linked D-glucose residues. Haworth[39] recognised that there were bonds between atoms in the glucose units, but it was Staudinger[40] who first delivered the final proof of the high polymer nature of the cellulose molecule.

In 1926 and 1937 Mayer, Mark and Misch[41-43] proposed the unit cell structure of cellulose I. Their monoclinic lattice model is in agreement with both the chemical evidence formulated by Haworth and with the X-ray diffraction pattern observed. The

unit cell has dimensions of 0.835 nm for the a-axis, 1.03 nm for the b-axis, 0.79 nm for the c-axis, and 84° for the β-angle. With respect to the β-(1→4)-linkage along the cellulose molecule the two molecules are positioned antiparallel. The chains are staggered by 0.24 nm along the longitudinal axis of the unit cell, and are rotated by 180° around the same axis.

Gardner and Blackwell[44] suggested in 1974, on the basis of X-ray diffraction on *Valonia ventricosa*, a unit cell concept derived principally from the Mayer-Mark-Misch model. Their structure was also based on the monoclinic lattice type with similar parameters. However, it assumed that cellulose chains lie parallel. They claimed that their structure takes into account more completely the observed X-ray diffraction patterns. Their model consisted of a $P2_1$ space group, a twofold helix repeating at 1.038 nm intervals, and torsional angles of $\Phi = 23°$ and $\Psi = -23.7°$. They also concluded that the hydroxymethyl oxygen is near the *tg* conformation.* The authors also suggested the possible existence of a unit cell having twice as long a- and b-axis as previously believed. Although Gardner and Blackwell's model was disputed, the work of Sarko and Muggli supported their structure through conformational energy and X-ray intensity analyses.[45,46]

The crystal structure of ramie was studied by Woodcock and Sarko[47] using X-ray diffraction simultaneously with the stereochemical refinement method developed by Zulgenmaier and Sarko.[48] Their structure (figure 1.4) is almost identical to that obtained from *Velonia*,[44] *i.e.* parallel chains, hydroxymethyl oxygen in the *tg* position, sheets of cellulose staggered by c/4 (0.258 nm) relative to one another, *etc.*

From X-ray diffraction, IR spectroscopy and NMR experiments[49,50] it is known that intramolecular hydrogen bonds are formed between the hydroxyl groups on C3 of one

* The first letter refers to the position of O6 relative to the ring oxygen and the second letter is the position relative to C4.

glucose unit and the ring oxygen of the adjacent glucose unit in the chain. A second intramolecular hydrogen bond occurs between the hydroxyl groups on the C6 and C2' carbon atoms.[51] These intramolecular hydrogen bonds are known to occur in all polymorphs of cellulose and is the main cause of the stiffness and rigidity of cellulose molecules. There is a single intermolecular hydrogen bond[49] in the cellulose I structure between the hydroxyls on C6 and C3". There are no hydrogen bonds between adjacent layers of cellulose chains; only Van der Waals forces hold these sheets together.

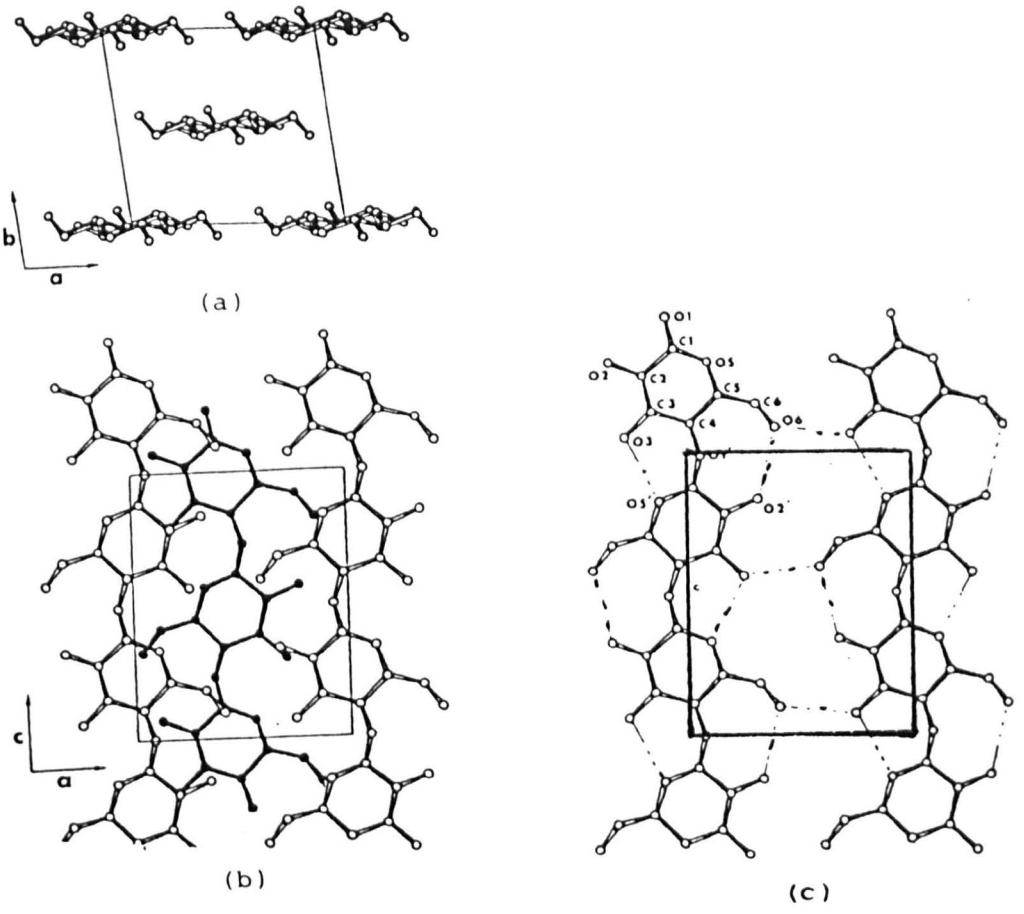

Figure 1.4 The structure of the crystal lattice of cellulose I. Dashed lines indicate the hydrogen bonding network; (a) perpendicular to the ab-plane along the fibre axis, (b) perpendicular to the ac-plane and (c) the 020-plane hydrogen bond network.

1.4.1.2 Cellulose II

If native cellulose is dissolved and precipitated from solution, or treated with an alkaline swelling agent (mercerised) then cellulose II is formed. This conversion is thought to be irreversible since cellulose II is more stable than cellulose I. The crystal structure of cellulose II was investigated by Sarko *et al.*[45,52] using *Fortisan* and Blackwell *et al.*[53-55] using *Rayon* and mercerised cotton.* All these sources of cellulose II maintain a $P2_1$ space group in common with cellulose I.

Stipanovic and Sarko[52] used stereochemical packing refinement and X-ray diffraction analysis to study regenerated cellulose. They found the cellulose II chains lie antiparallel with an extensive hydrogen bond network (figure 1.5). The cellulose II structure consists of hydrogen bonds between adjacent sheets of chains (figure 1.6) that are absent in cellulose I. Hydroxymethyl oxygens on the outside chains have the *tg* conformation while those in the centre chains have the *gg* conformation.

Blackwell *et al.* studied the cellulose II structure of *Rayon* and mercerised cotton using intensity data and rigid-body least squares refinement developed by Arnott and Wonacott.[56] They found these two structures have similar cell dimensions, both possess a $P2_1$ space group and two cellulose chains per cell. The intramolecular bonds are the same as already discussed for the cellulose I lattice structure. For the intermolecular bonding Blackwell *et al.* assumed hydrogen bridges from the hydroxyls on C6 to hydroxyls on C3" alternating in direction for "down" chains neighbouring one another in the centre 002-plane (see figure 1.6a) and hydrogen bonds from the hydroxyls on C6 to hydroxyls on C2" for "up" chains neighbouring one another in the corner 002-planes (figure 1.6b). Furthermore, the same authors assumed hydrogen bonds between neighbouring antiparallel chains in the 101-planes involving hydroxyls on the carbon atoms C2 and C2" from each second glucose unit of centre "down" and corner "up"

* *Fortisan* and *Rayon* are trade names for commercially produced cellulose II.

chains (figure 1.6c). Their antiparallel packing structure has hydroxymethyl oxygens with conformations of *gt* in the corner chains and *tg* in the centre chains. This packing combination gives a very stable structure, lower in energy and helps to explain why conversion to cellulose II cannot be reversed to give cellulose I.

A mechanism for conversion from the parallel cellulose I structure to the antiparallel cellulose II structure during mercerisation, without dissolution, has been proposed by Okano and Sarko.[57,58] They suggested that during the swelling process microfibrils from adjacent chains intermix and then reform to create the cellulose II structure.

1.4.1.3 Cellulose III

Cellulose III is a fairly stable polymorph and has two subclasses, *i.e.* III_I and III_{II}, depending on the starting material used. The only "modern" study on this polymorph was on cellulose III_I derived from ramie.[59] It was proposed that this structure has the same conformation and intramolecular hydrogen bonding as cellulose I, the only difference is the relative stagger between adjacent sheets; c/4 or 0.26 nm for cellulose I and 0.09 nm for cellulose III_I. Sarko *et al.*[59] also concluded that the chain conformation and hydrogen bonding in cellulose III_{II} are also the same as those in the cellulose II structure.

1.4.1.4 Cellulose IV

In common with cellulose III, cellulose IV also has subclasses depending on whether it is created from celluloses I or II.[60] It is thought that the lattice structure of the two subclasses differs only slightly from their corresponding starting material. However, there are no complete structural determinations of cellulose IV.

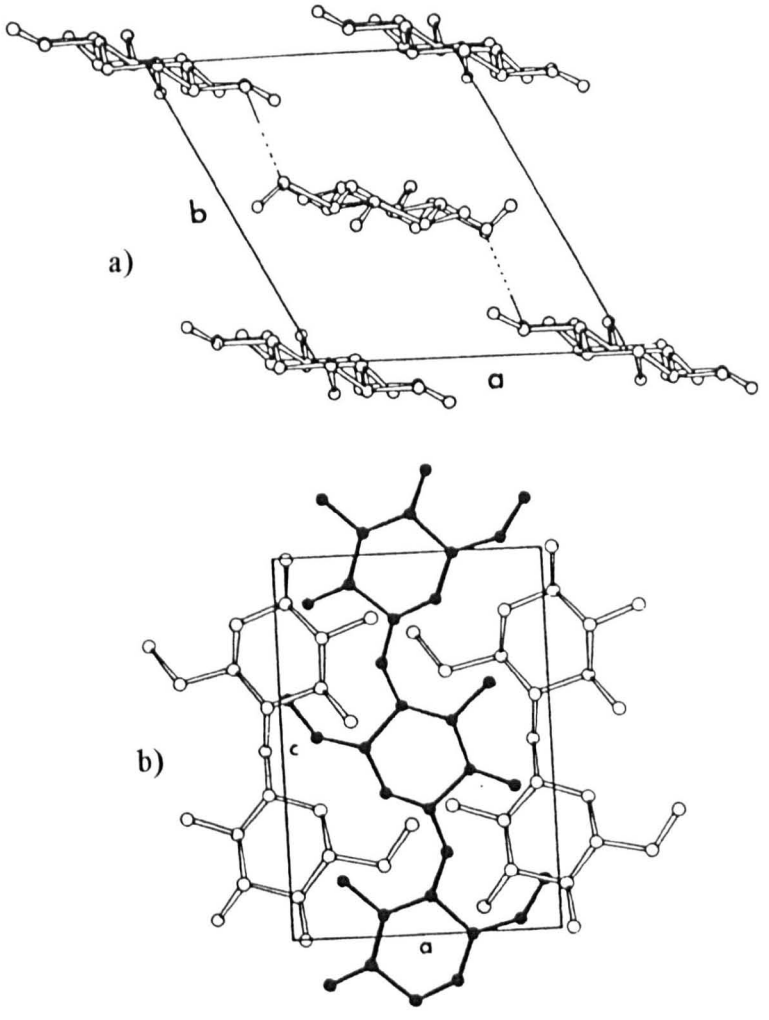

Figure 1.5 Unit cell structure of the crystal lattice of cellulose II. Dashed lines indicate hydrogen bonding between sheets; (a) perpendicular to the ab-plane (hydrogen bonding alone the 110-plane is shown) and (b) perpendicular to the ac-plane.

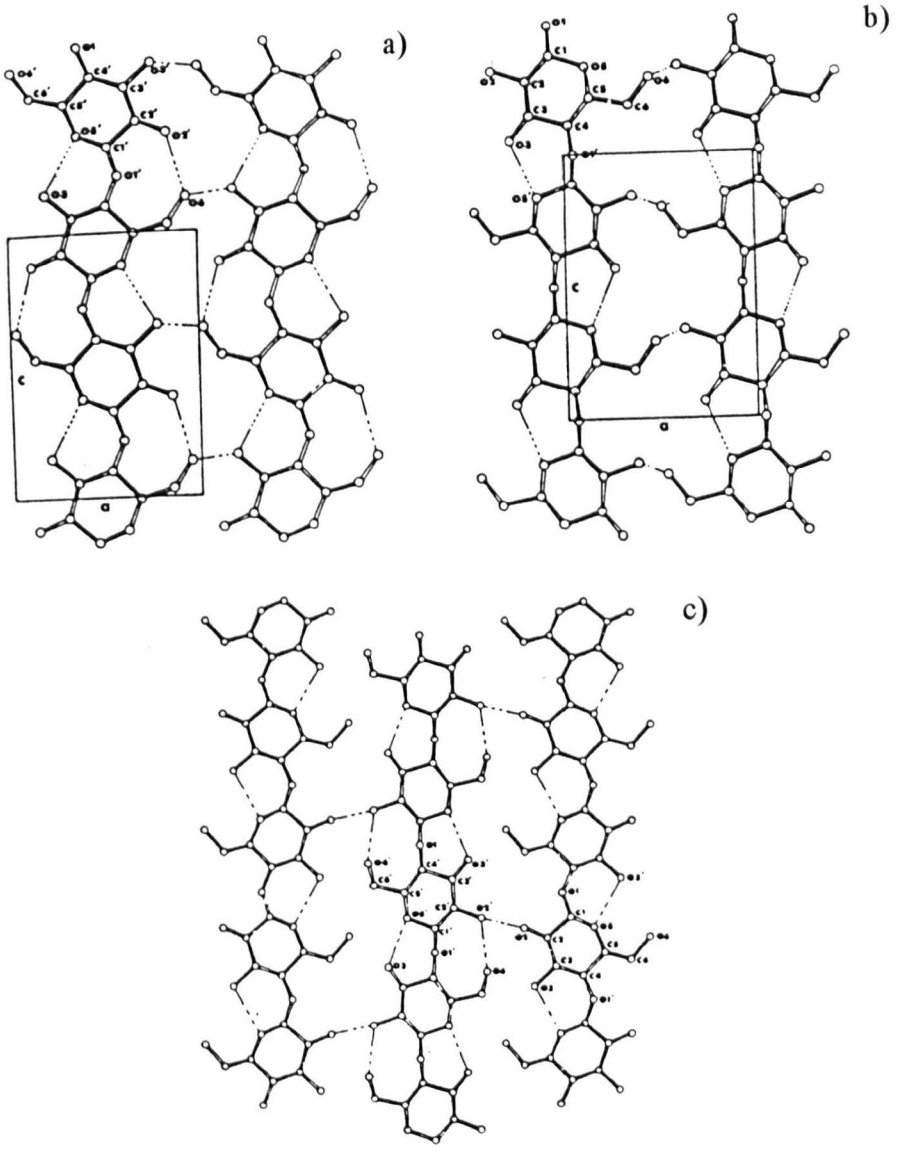

Figure 1.6 Hydrogen bonding network of the cellulose II structure; (a) perpendicular 002 plane for centre down chains, (b) in the 002-plane for centre up chains and (c) between antiparallel chains in the 101-plane.

1.4.2 The dimorphism of cellulose I

Diffraction analysis has found that cellulose from *Velonia*[45] or other algae contains more diffraction spots than those of the higher plants such as ramie.[48] The same phenomenon was observed when the diffraction diagrams for *Velonia* were compared to that of tunicin.[61] These observations can be explained by considering cellulose I as a composite of two distinct crystalline phases. This idea was first suggested in 1984 by Atalla and VanderHart from a study on native cellulose from various origins using high resolution ^{13}C solid-state NMR spectroscopy.[62,63] Their idea was based on peak multiplicities of the C1, C4 and C6 carbons of native celluloses that could only be explained as inequivalencies within the unit cell. They named these two crystalline modifications as cellulose I_α and I_β. According to their spectroscopic evidence (*i.e.* doublets at C1, C4 and C6) cellulose I_β has inequivalent successive glycosidic linkages along each chain (this also occurs for cellulose II). Although they did not suggest structures for these polymorphs, with the aid of spectral manipulation of various native celluloses, they presented solid-state NMR spectra of the I_α and I_β polymorphs (figure 1.7). They found that the I_α crystalline form was dominant in *Acetobacter* and *Velonia*, while I_β was dominant in cotton, ramie and pulp celluloses.

Cellulose I_β has subsequently been found to be more stable than the I_α form.[64,65] The $I_\alpha \rightarrow I_\beta$ conversion has been studied in detail with solid-state NMR by Debzi *et al.*[66] using various annealing techniques (*i.e.* using different temperatures and solvents). They found that in excess of 260 °C was required and that polar solvents were more efficient for the conversion process. Electron diffraction and infrared techniques have also been used to investigate the transformation of I_α to I_β.[67] IR bands were identified at 3240 and 750 cm^{-1} for I_α, and 3270 and 710 cm^{-1} for I_β.

Sugiyama *et al.*[68] published the structures of the two crystalline phases (figure 1.8). Their study using electron diffraction indicated that the I_α has a P1 triclinic structure with one cellulose chain per unit cell and the I_β has a monoclinic $P2_1$ structure with two chains per unit cell. Although the two phase structures of cellulose I is controversial, Wada *et al.* provided further evidence using X-ray diffraction in 1993.[69]

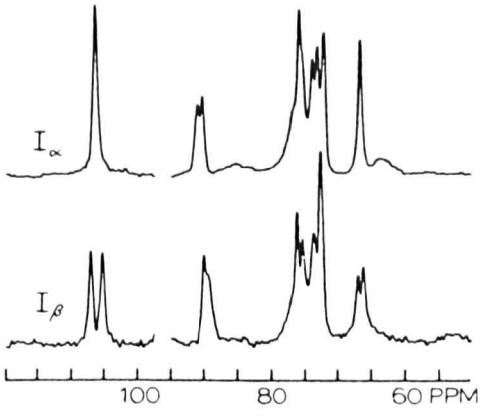

Figure 1.7 Solid-state ^{13}C NMR spectra of the two polymorphs of cellulose I.

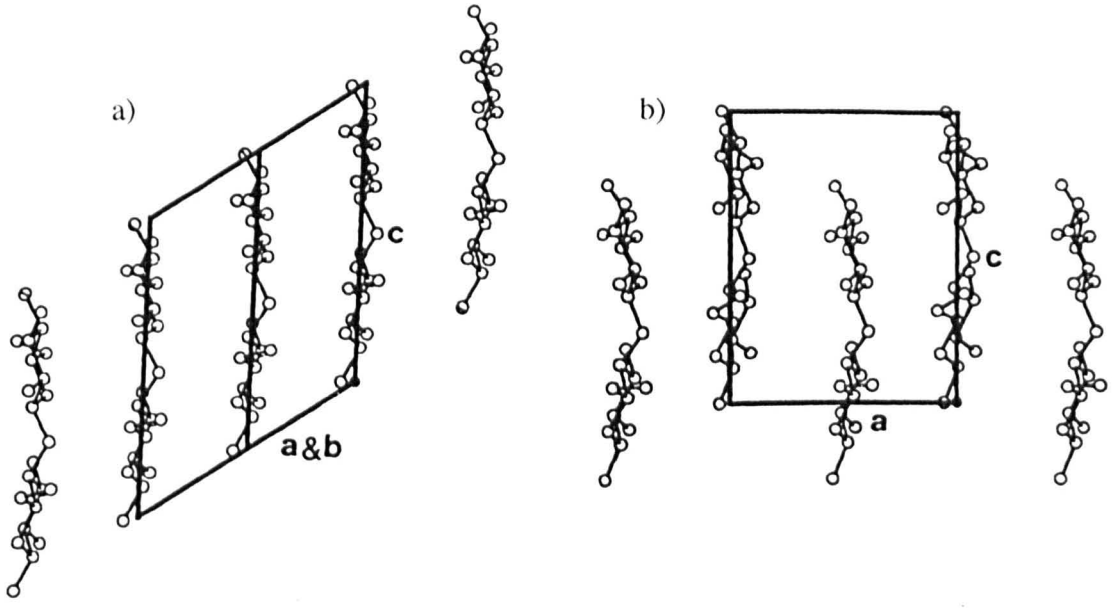

Figure 1.8 Unit cell structure of; (a) cellulose I_α and (b) cellulose I_β.

1.4.3 Crystallinity of cellulose

Solid-state NMR spectra of cellulose reveal that the C4 and C6 peaks have broad wings upfield to their sharp components (figure 1.9). It is anticipated that crystalline regions of solids will give narrow components while noncrystalline or paracrystalline regions will give broad resonances.[70] However, the intensity ratios of the broad and crystalline peaks suggest a crystallinity[71] of 55-60 % for cotton and ramie which is less than the 80-96 % obtained from other techniques such as X-ray diffraction and solvent absorption studies.[72,73] Earl and VanderHart[71] concluded that the broad regions are attributed to anhydroglucose units on the surface of elementary fibres and not from noncrystalline regions. VanderHart and Atalla[63] also came to the same conclusion by comparing the C4 and C6 broad wings of CPMAS spectra of cotton linters, *Acetobacter xylinum* cellulose and *Velonia ventricosa* cellulose scaled in their relative intensities along the crystal surface area. They assumed typical lateral crystallite dimensions in these three materials as 3.5 × 3.5 nm,[74] 6 × 6 nm[75] and 10 × 20 nm[76] respectively.

Marcel *et al.* found that the broad peaks can be increased in intensity at the expense of the narrow peaks by ball-milling cellulose samples.[77] This can be attributed to an increase in surface area of each sample and an assumption that the pattern of hydrogen bonding is different in the surface and interior regions. A decrease in crystallinity is also responsible for the broadening of these peaks.

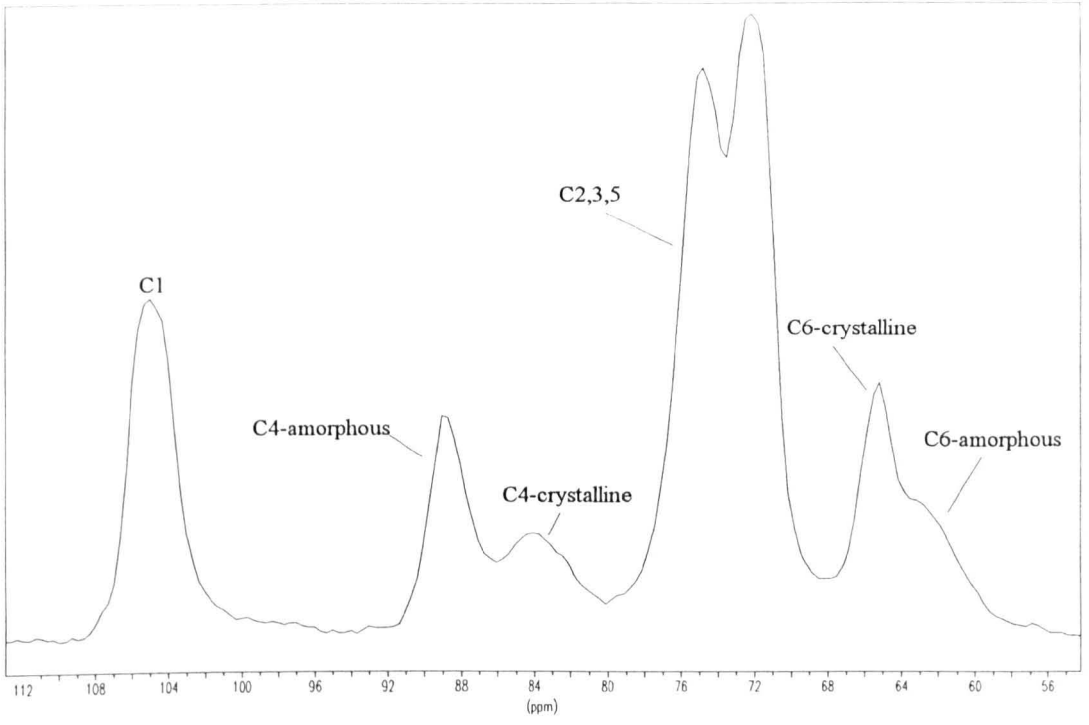

Figure 1.9 Solid-state ^{13}C NMR spectrum (CPMAS) of cellulose I.

1.4.4 Ultrastructure of cellulose

Nägeli and Schwendener[78] were the first to propose a structural concept for cellulose fibres in 1865. Their idea postulated the so called "micelle" theory in which the substrate was held together by glue-like substances. This model was later modified by Hengstenberg and Mark,[79] and Seifritz[80] during the late 1920's.

The "fringe-micellar" structural concept (figure 1.10) was developed after acceptance of the high polymer nature of cellulose.[81,82] According to this model, the micelles are crystalline domains embedded in an amorphous matrix. Because of their length the chain molecules pass alternatively through several crystallites.[83] This concept conformed with diffuse reflections obtained from X-ray diffraction patterns typical for paracrystalline

materials. However, it did not sufficiently take into account the fibrillar nature of fibrous substrates.

Fibrous substrates have been shown by light microscopy to be built from fibrillar elements known as macrofibrils. These macrofibrils vary in dimension from several microns to a few tenths of a micron. After the electron microscope was developed at the end of the 1930's these microfibrils were found to be aggregates of still much thinner fibrillar units with cross dimensions of between 3 to 20 nm. Basic fibrillar elements are known as elementary fibrils. It was later discovered that these elementary fibrils were composed of elementary crystallites.[84]

On the basis of this information further modifications of the fibre structure model emerged during the 1940's and 1950's. Hess,[85,86] Kratky,[87] Frey-Wyssling[88] and their co-workers developed the fringed fibril structure (figure 1.11). According to their concept the fibre is formed from a network of many cellulose molecules which are linked together in repeating lengths along their chains. Strands of elementary crystallites are held together by parts of the long molecules reaching from one crystallite to the next through less ordered interlinking regions.

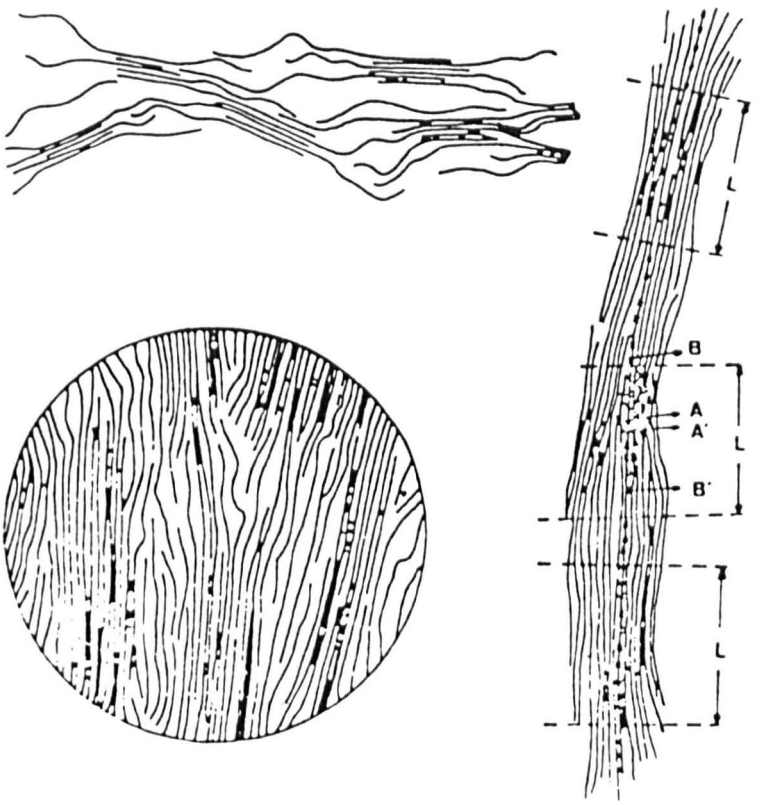

Figure 1.10 The "fringe-micellar" structural concept of cellulose.

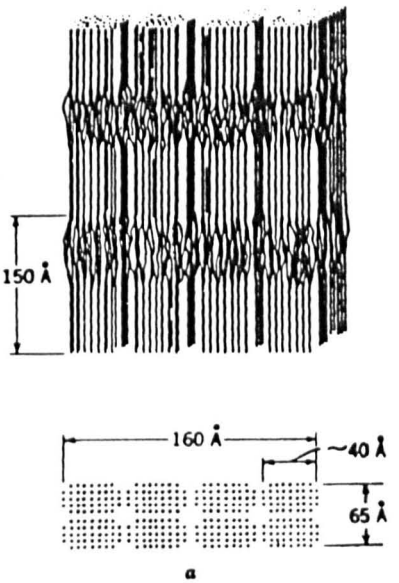

Figure 1.11 The "fringed fibril" structure of cellulose.

Hearl[89] proposed a somewhat different model of the fringed fibril structure in 1963. In this model the fibrils are considered to be long imperfect crystals that transverse the fibre structure. The long chain molecules composing the elementary fibrils diverge from the fibrillar surface in irregular distances becoming part of neighbouring fibrils, and forming less-ordered interlinking regions.

Krässig[90] developed the model that best fits the experimental observations. This model (figure 1.12) consists of fibres composed of elementary fibrils, *i.e.* strings of elementary crystallites, associated in a more or less random manner into aggregations, and interlinked in to a fibrillar network by isolated segments of fibrils fringing from one aggregation to neighbouring ones. The internal cohesion is made up by the transition of the long cellulose molecules from crystallite to crystallite (represented by small rectangles) in the elementary fibrils.

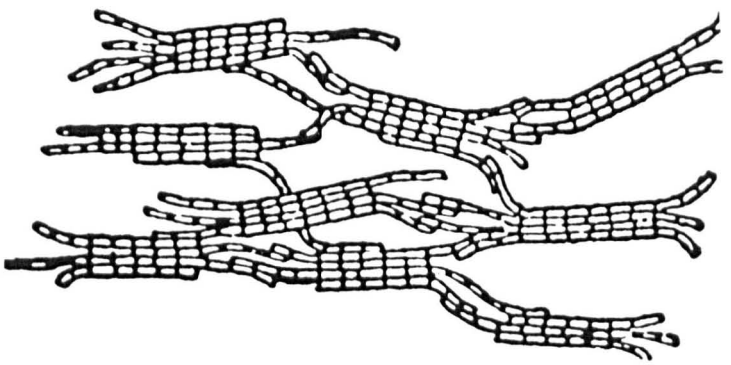

Figure 1.12 The structure of cellulose according to Krässig.

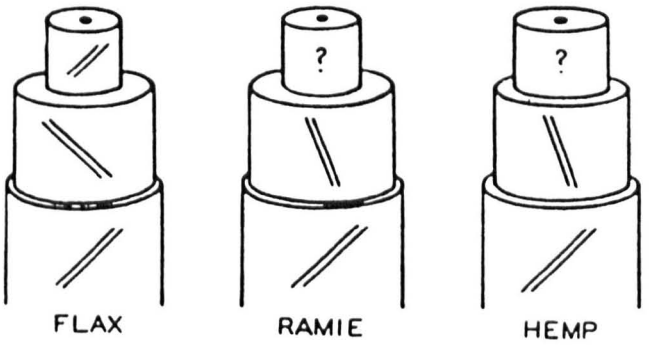

Figure 1.13 Schematic representation of the orientation of fibrils in the different cell walls of fibres from three different origins.

1.4.5 Cell walls structure of native celluloses

During the first stage, the living protoplasm produces a primary wall (P). The substance between adjacent primary cell walls is known as the intercellular layer (I) or lamella. After these layers are created the secondary cell walls are formed onto the inside of the primary walls. According to Kerr and Bailey, normal wood cells consist of P and S walls, and the S layer composed of a thin outer layer (S1), a relatively thick middle layer (S2) and an inner layer (S3).[91] The central channel of the cell, known as the lumen, is narrow but not completely filled. This structure of cellulose fibres is still commonly accepted since it has been confirmed by subsequent investigations using electron microscopy.

Figure 1.13 shows a schematic diagram of the orientation of fibrils in the different cell wall layers of various fibres. This diagram also shows the change of microfibril orientation when going from the primary to the secondary layers.[92] The exact orientation of the fibrillar elements is dependent on the source of the cellulose and has a distinct

influence on the swelling behaviour and thus many of the physical and chemical properties of the fibre. The cell wall thickness is also dependent on the specific source of the cellulose fibre. The cellulose extraction process chosen has an important bearing on the strength of the outer cell walls, thus influencing the fibre properties.

Channels, pores and voids are of great importance on the chemical reactivity and swelling ability of cellulose and these internal accessible surfaces can vary widely among various celluloses.

1.5 Polymer solutions

The solubility of a polymer is determined by the change of the free energy ΔG_m during mixing with a solvent:

$$\Delta G_m = \Delta H_m - T\Delta S_m$$

Dissolution occurs provided that ΔG_m (Gibbs free energy of mixing) remains negative. ΔS_m (entropy of mixing) is always positive but usually has a much smaller value for a polymer than low molecular mass solutes. Primarily, the value of ΔH_m determines whether or not a polymer is soluble in a particular solvent. The highest solubility is observed when the solvent molecules and the monomer units are similar, *i.e.* $\Delta H_m < 0$. If ΔH_m is strongly positive then it will no longer compensate for the small negative value of $-T\Delta S_m$ and the polymer will not be soluble since ΔG_m becomes positive. Clearly, the solubility of the polymer increases with temperature.

The conformation of long chain molecules is that of a random coil with root mean square end to end distance of $\langle r^2 \rangle^{1/2}$. Good solvents will promote contact with the polymer, the coil will expand and thus increase the value $\langle r^2 \rangle^{1/2}$. When the solvent quality decreases the coils expel solvent molecules by contracting, *i.e.* $\langle r^2 \rangle^{1/2}$ decreases. The conformation of a polymer chain in solution is continuously changing because of rotation about bonds between atoms. Some conformations will be more stable than others and thus more likely to occur. The solvent chosen can have drastic effects on the most stable conformations and thus have a profound effect on $\langle r^2 \rangle^{1/2}$.

The polymer coil can be forced to contract by lowering the temperature or decreasing the quality of the solvent until the θ-temperature or θ-solution condition is reached. Under θ-conditions coil expansion because of intermolecular excluded volume effect and coil contraction because of attraction between non-neighbouring segments in the same chain cancel out.

Polymer solutions are viscous because of the strong solvation of polymer chains, producing expanding coils with a larger hydrodynamic volume than the bare chains. During flow such expanded coils are exposed to a greater proportion of the velocity gradient, which results in a larger transfer of impulse to and from the surrounding solvent, which flows with a different rate. If the coils are large then the viscosity of the solution increases. At high flow rates orientation of larger chains in the flow direction will occur resulting in an anisotropic solution. Such liquid crystalline solutions have a lower overall viscosity. Since the viscosity of polymer solutions depends on flow rates these systems behave as non-Newtonian liquids.

Flory[93] and Huggins[94] independently developed the theoretical basis for the understanding of statistical thermodynamics of polymer solutions. Their model consisted of a distribution of monomer segments and solvent molecules at random over the sites of

a liquid lattice (figure 1.14). The restrictions are that non-terminal segments must be connected to two other polymer segments and that each lattice site must be occupied with only one monomer segment or one solvent molecule. The entropy of the solution is found to be:

$$S_{12} = k \ln \Omega_{12}$$

where k is the Boltzmann's constant, and Ω_{12} is the number of ways in which N_2 chains of P segments each and N_1 solvent molecules can be placed in the lattice. The entropy of mixing of the polymer and solvent becomes:

$$\Delta S_m = S_{12} - S_1 - S_2 = k \ln \Omega_{12} - k \ln \Omega_2$$

This yields:

$$\Delta S_m = -k(N_1 \ln \Phi_1 + N_2 \ln \Phi_2)$$

where: $N_1 + PN_2 = N$ = total number of lattice sites

$\Phi_1 = N_1 / N$ = volume fraction of solvent

$\Phi_2 = PN_2 / N$ = volume fraction of the polymer

Since Φ_1 and Φ_2 are less than one, ΔS_m will always be positive. The energy of mixing of a polymer and a solvent is given by:

$$\Delta U_m = U_{12} - U_1 - U_2 = N \Phi_1 \Phi_2 z \Delta u \qquad \text{equ. 1.1}$$

where U is the energy content and z is the coordination number of the lattice. Δu is given by:

$$\Delta u = u_{12} - \tfrac{1}{2}u_{11} - \tfrac{1}{2}u_{22}$$

where $\frac{1}{2}u_{11}$ is the interaction energy between pairs of solvent molecules, $\frac{1}{2}u_{22}$ between pairs of monomer segments and u_{12} between monomer segments and solvent molecules.

By substituting the following Flory-Huggins interaction parameter:

$$\chi = \frac{z}{kT}\Delta u$$

we obtain:

$$\Delta U_m = kTN\Phi_1\Phi_2\chi \qquad \text{equ. 1.2}$$

Finally the free energy of mixing the two components is given by:

$$\Delta F_m = \Delta U_m - T\Delta S_m = kT[N_1 \ln \Phi_1 + N_2 \ln \Phi_2 + N\Phi_1\Phi_2\chi] \qquad \text{equ.1.3}$$

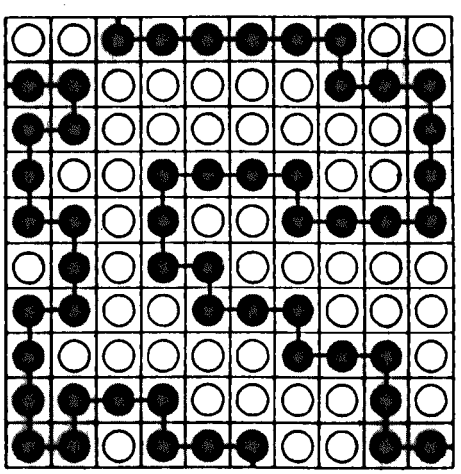

Figure 1.14 Lattice model for a polymer (• is a monomer segment and o is a solvent molecule).

1.6 The swelling and dissolution of cellulose

Cellulose is the most abundant renewable organic material in the world but nevertheless has not reached its potential in many areas of application, since natural cellulose is unsuitable for many uses. Therefore, it would be beneficial to dissolve cellulose and then regenerate it into the desired product from solution. However, the dissolving step is often hazardous or expensive. This is particularly true for the viscose industry where pollution control places increasing restraints on the process.[95] The properties of the regenerated cellulose material are of course important but not a sufficient prerequisite for the new technology. Other than pollution constraints, the feasibility of recycling the chemicals and economy of the operation are decisive criteria for selecting a process.

For the purpose of dissolution, cellulose can act as an acid or base and can form complexes and derivatives. The remaining part of this section gives examples of various solvents used to dissolve and swell cellulose.

1.6.1 Derivatizing solvents

Derivatizing systems exert their solvent actions by forming covalent but unstable ethers or esters of cellulose which then decompose often by a change in pH or by switching from an aprotic to a protic system to regenerate cellulose. An example of a derivatizing system is the viscose process that uses cellulose xanthogenate as the spinning solution. Problems can arise with derivatizing systems because of possible side reactions between the active agent and the solvent acting as the reaction medium. A mixture of N_2O_4 / dimethylformamide will give good cellulose solutions and good fibres but vacuum distillation is required to prevent the HNO_3 / DMF complex from decomposing.

DMSO / paraformaldehyde is also not a commercially feasible solvent system since the paraformaldehyde needs to be dried before being reused.

1.6.2 Nonderivatizing solvents

This category of cellulose solvents (*i.e.* when cellulose acts as an acid or base) dissolves the polymer by intermolecular interactions only, such as the formation of hydrogen bonds.

An example of a nonderivatizing solvent is aqueous sodium hydroxide.[96] In this case cellulose acts as an acid and the concentration of NaOH needed for maximum swelling of the polymer is not the same as that needed for dissolution. About 18 % NaOH is required for cellulose to dissolve while 8-10 % results in maximum swelling.[97] Other inorganic bases such as KOH and LiOH can also swell and dissolve cellulose. However, these alkaline systems are not able to dissolve high DP cellulose of commercial interest and there are problems with recovering and recycling of the reagent. Temperature also plays a major role in the dissolution of cellulose with these solvents; cold conditions give maximum swelling and dissolution.

Liquid ammonia is able to swell cellulose to such a degree that other volatile materials such as carbon tetrachloride remain trapped in the swollen cellulose microstructure after the ammonia has evaporated. Cellulose has been reported[98] to dissolve in liquid ammonia when certain inorganic salts such as NaI, $NaNO_3$, NaCNS, NH_4I and NH_4CNS are used as additives. Only a narrow range of NH_3 / salt / H_2O ratios will dissolve cellulose.

Some organic bases are known to dissolve cellulose. 16.5 % methylamine in DMSO was reported by Scherer and Phillip[99] to dissolve cellulose under cold anhydrous conditions. However, solutions of cellulose were insufficiently concentrated for commercial consideration. Amine oxides are presently the most important class of organic bases that gives cellulose solutions. Courtaulds PLC uses N-methylmorpholine-N-oxide (NMMO) as a solvent for preparing cellulosic spinning solutions. Amine oxides, especially NMMO, has been one of the central themes of the research in the present study and these compounds will be discussed in more detail in section 1.7.

Certain acids dissolve cellulose rapidly at room temperature and give excellent solutions.[100] 78 % phosphoric acid, 68 % nitric acid, 42 % hydrochloric acid or 70 % sulphuric acid are known to dissolve cellulose but the recovery and recycling of concentrated acids are the limiting economical factors.

1.6.3 Complex formation with cellulose

Complexes can be formed with cuprammonium but problems occur with pollution since it is difficult to completely recover the metallic effluent contaminants. Also, the fibre properties are inferior to those of the viscose process. Petrov[101] reported dissolving cellophane films with a DP of 300 to 600 with *bis*-(β-γ-dihydroxypropyl)-disulfide at 110 °C. However, this solvent is unable to dissolve wood pulps directly.

Dimethylacetamide with LiCl has been shown to dissolve cellulose.[102] Only LiCl and no other lithium salt, such as LiBr, $LiNO_3$, *etc.*, will work. The Li^+ ion is thought to be complexed between the carbonyl and nitrogen electrons of dimethylacetamide. This releases Cl^- to act as a base towards cellulose hydroxyl group hydrogens.

1.7 The use of amine oxides as solvents for cellulose

Amine oxides are considered to the best of present knowledge as nontoxic and the problems of recovering the reagent from an aqueous spinning bath have been solved.[103] Fibres obtained using amine oxides are superior to normal-grade viscose and compete successfully with cotton and polyester.[104] This type of solvent has also been successful in preparing cellulose-copolymer blends, such as with nylon as the copolymer component.[105-107] Figure 1.15 shows a schematic diagram of fibre production using the cellulose-NMMO process.[108]

However, not all amine oxides are able to dissolve cellulose. Armstrong *et al.* published five criteria for an amine oxide to have the capability for cellulose dissolution.[109] These five criteria are:

1. The amine oxide must be a tertiary amine oxide.
2. With the exception of triethylamine-N-oxide and N,N-dimethylethanolamine-N-oxide, the amine oxide must have a cyclic structure.
3. The cyclic position of the molecule must have a width of 5.15 Å.
4. The molecule must have a strong N→O dipole capable of disrupting the hydrogen bond within the cellulose structure.
5. A critical amount of water is necessary for dissolution at a reasonable temperature.

Armstrong and McCorsley also published a list of amine oxides that were found experimentally to be either able or unable to dissolve cellulose.

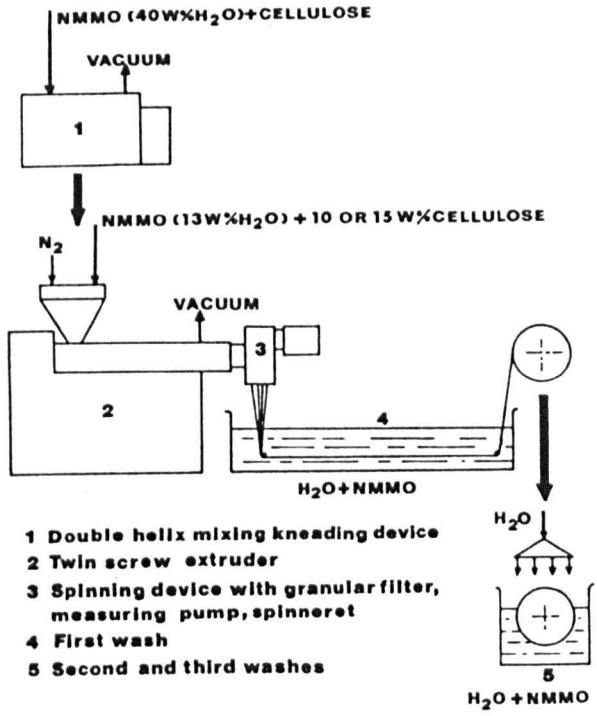

Figure 1.15 The NMMO process.

1.7.1 Theory of cellulose dissolution in amine oxides

The amine oxide / water system has been shown by NMR to give true cellulose solutions above the melting point of the solvent.[110] Unlike derivatizing solvent systems where the chemical reaction occurring between cellulose and the active agent is clearly known, with nonderivatizing solvent systems the polymer-solvent interaction is less clearly understood. One of the reasons for this is the problem of acquiring quantitative data on intermolecular interactions between cellulose and the solvent. One possible theory proposed by Kabrelian is that NMMO has the ability to act as a wedge and penetrates into the ordered regions of the fibre structure before the polymer chains become completely separated.[111]

Other theoretical considerations on the mode of action of nonderivatizing solvents have been published by various authors. An acid-base theory of the interaction between cellulose and the aqueous phase in addition to the nonaqueous solvent was proposed by Turbak *et al.*[95] Schleicher *et al.*[112] considered a cellulose-nonaqueous solvent interaction where the hydrogen as well as the oxygen atom of an OH-group could be involved with different functional groups or different components of the solvent system. Berger *et al.* suggested a "cryptoionic" theory of dissolution that combines the acid-base concept with hydrogen bonding to enhance the strength of the polymer-solvent interaction.[113] These authors also emphasised the dominant role of the OH-group in the C6 position (see section 1.7.2), showing that, for example, a xylan where the CH_2OH group is missing, does not dissolve at all in this class of organic solvents.

Yakimanskii *et al.* suggested that the solvating power of certain amine oxides is determined by a certain set of parameters of electronic structure, each of which may be responsible for a certain contribution to the total energy of interaction of the solvent with cellulose.[114] They based all their conclusions on theoretical calculations. As an example they compared the dissolving TEAO with the non-dissolving TMAO (see figure 1.1). The former amine oxide was found to have a greater positive charge on the nitrogen atom and a lower energy of the LUMO (lowest unoccupied molecular orbital). According to Yakimanskii *et al.*, this indicated a more pronounced electron-acceptor property for TEAO compared to TMAO. They also stated those amine oxides that dissolve cellulose have energies of hydrogen bonds with OH-groups greater than 6 kJ mol^{-1}, and the angle formed by the hydrogen bond vector relative to the N→O bond is between 154° and 155°. Their calculations also showed that monohydrates of each amine oxide studied, both solvents and nonsolvents, have a greater dipole moment along the N→O bond than the corresponding anhydrous amine oxide. This would strengthen the interaction with cellulose and could be a possible explanation for the necessity of a small amount of water needed for dissolution of cellulose by amine oxides.

1.7.2 Importance of primary hydroxyls (C6)

Bochek *et al.* studied the solubility of cellulose acetate (CA) with various degrees of substitution (DS) and tritylcellulose (Tr-Cell) using NMMO and dimethylformamide (DMF) as solvents.[115] They found that Tr-Cell substituted at the primary hydroxyl groups was soluble in DMF but completely insoluble in NMMO. They also found that cellulose acetate with a DS greater than 2.6 was also insoluble in NMMO but soluble in DMF. The opposite case occurred for cellulose acetate with a DS less than 2.6. Bochek *et al.* concluded that the interaction between the solvent molecules with the cellulose primary hydroxyl groups is important for dissolution in NMMO and the secondary hydroxyl groups important for dissolution in DMF. They estimated that 30-40 % of primary hydroxyl groups were required for dissolution in NMMO to take place. Berger *et al.* also came to the conclusion that the primary hydroxyls play the main role in the dissolution of cellulose in amine oxides.[113]

A rheological investigation was also published by Bochek *et al.*[115] They showed that the viscosity of solutions of CA in NMMO increased with a decrease in DS, solutions of unsubstituted cellulose being the most viscous. All samples of cellulose and cellulose derivatives had approximately equal DP. In their opinion the presence of hydroxyl groups effects the mobility and behaviour of the molecules of cellulose and its derivatives in amine oxide solutions.

A dielectric absorption study on cellulose treated with NMMO was undertaken by Borisova *et al.*[116] They observed an absorption peak at 70 °C for cellulose dissolved in NMMO which they attributed to the reorientation of the primary hydroxyl groups of cellulose. They concluded that during dissolution the NMMO molecules initially formed a complex with cellulose primary hydroxyl groups. They claimed that this gave further evidence that hydrogen bonds involving these hydroxyl groups are broken during

dissolution. Their work also involved using triphenylmethyl cellulose as a model compound. This compound lacks any primary hydroxyl groups and does not dissolve at all in amine oxides. An intimate solution of this compound with NMMO was prepared using DMF as a solvent. They found that no peak occurs at 70 °C, showing, in their opinion, that the primary hydroxyl groups appear to be decisive for dissolution of cellulose in NMMO. However, they also stated that NMMO may also form complexes with secondary hydroxyl groups.

1.7.3 Hydrate forms of NMMO

The dissolution of cellulose in amine oxide solutions is only possible in a narrow range of conditions.[117] The limited area of the phase diagram is a critical function of the water-cellulose ratio. Chanzy *et al.* demonstrated that NMMO forms a monohydrate and a hydrate of five molecules of water per two NMMO molecules.[118] Their phase diagram showed the upper temperature limit for dissolution was about 150 °C, above which rapid and dangerously uncontrollable decomposition of the NMMO occurs. They also demonstrated that control of water concentration was very important. It appeared that no further driving force for NMMO to interact with the cellulose OH-groups occurred when two molecules of water were already present to interact with the N→O bond. However, some water needs to be present to enable the solvent system to work. Turbak suggested the small amount of water helps to activate and open the cellulose internal areas and pores that have been closed during initial pulping operations.[119]

An X-ray diffraction study on anhydrous and monohydrate NMMO was completed by Maia *et al.*[120] They found that the morpholine ring adopted an almost perfect chair conformation and the methyl group is equatorial in both cases. Van der Waals forces were found to hold the crystal structure of anhydrous NMMO molecules together.

However, the monohydrate was determined to be held together by a network of hydrogen bonds resulting in a ribbon like structure with only weak interactions between neighbouring ribbons. They concluded that this segregation between the hydrophobic and hydrophilic moieties enhances the ability of NMMO molecules to complex to other molecules.

A similar study on the structure of NMMO : $2.5H_2O$ revealed that the N→O oxygen can be an acceptor of two hydrogen bonds.[121] Maia and Perez concluded that the ratio of water molecules bonded to NMMO must be less than two to avoid saturation of the hydrogen bonding capability of the N→O bond to cellulose.[121] The strengths of the H-O-H...O-N hydrogen bond for the two hydrates forms of NMMO was calculated by Harmon *et al.* using vapour pressure measurements.[122] Hydrates containing 2.5 and 1 mole of water per mole of NMMO were calculated to form H-bond strengths of 15.83 and 12.01 kcal mol^{-1} respectively. They concluded that the failure of the higher hydrate to dissolve cellulose may arise because water is more firmly bound to NMMO at higher H_2O content, rather than because the N→O oxygen is saturated with hydrogen bonds.

Chanzy *et al.* also studied the crystal structure of the complex of NMMO with trans-1,2-cyclohexanediol (TCH) as a cellulose model compound.[123] Their results suggested that the TCH molecules are linked through two hydrogen bonds to the N→O oxygen of two separate NMMO molecules. They also concluded that NMMO would not interact with the hydroxyl groups of the same glucose unit as a result of steric hindrance. Their final conclusion was that an NMMO molecule could be envisaged to interact with the primary hydroxyls of one cellulose glucose unit and either the OH2 or OH3 of an adjacent glucose unit.

1.7.4 Flory-Huggins interaction parameter for the cellulose / NMMO / water system

Chanzy *et al.* obtained a value for the Flory-Huggins interaction parameter for the cellulose / NMMO / water system by measuring the depression of the melting point with increasing polymer concentration.[124] The ability of cellulose to depress the melting point of this system is regarded as confirming the strong interaction of cellulose with NMMO. In this case an unusually large negative interaction parameter of -3 was obtained. Only rarely does a Flory-Huggins interaction parameter exceed -1. Chanzy *et al.* explained their unusual result by the suggestion that dissolution of cellulose with NMMO is brought about by cleavage of hydrogen bonds between cellulose chains and formation of stronger H-bonds between solvent and polymer.

The Flory-Huggins interaction parameter for the same system was also measured by Iovleva *et al.*[125] using a similar method to Chanzy *et al.* This research group obtained a value of -20. They concluded that the Flory-Huggins theory of the depression of melting points is insufficiently correct, since this hypothesis becomes very approximate in the case of polar polymers with rigid chains capable of strong interactions with the solvent.

Bochek *et al.*[126] suggested that these anomalously large negative values estimated from melting point depression by Chanzy and Iovleva *et al.* may be an artefact caused by the ability of highly concentrated cellulose solutions in NMMO to supercool. By measuring the degree of swelling of cellulose in NMMO they calculated an interaction parameter of 0.35-0.40 for cellulose in anhydrous NMMO and 0.5 for cellulose in NMMO monohydrate. They stated that the difference between these values can be attributed to an improvement in the thermodynamic quality of the solvent with decreasing water content.

1.7.5 Anisotropic solutions of cellulose in NMMO

Amine oxide solutions of cellulose have been found to be anisotropic under certain interconnected conditions.[124,127-131] These conditions are temperature, water, cellulose concentration and the DP of the cellulose. The anisotropic behaviour of these solutions can be easily detected by the occurrence of birefringence (*i.e.* from a pattern of bright and dark areas) with a polarising microscope. A rheological study of cellulose in a mixture of NMMO and water found that the transition between the isotropic and anisotropic phases produced a change of viscosity of the solution.[132]

It has been shown that highly oriented films with the cellulose II structure are formed from liquid crystalline solutions with comparable mechanical properties with high tenacity *Rayon* or *Fortisan.* No orientation was found in cellulose films formed from isotropic solutions. Anisotropic NMMO solutions of some other derivatised[133] and underivatised[127] polysaccharides have also been shown to be anisotropic under certain conditions, and upon regeneration gave well-oriented films or fibres. Chanzy *et al.* also concluded that the flexibility of the polysaccharide was an important factor in the dissolution of a given polysaccharide in NMMO, *i.e.* dextran which can take up many conformations is more soluble than rigid cellulose of the same DP.[127] They also found that the stiffness of the polysaccharide chains is an important factor for solutions to become anisotropic. Although dextran is more soluble than cellulose because of its flexibility, only isotropic solution of this polysaccharide in NMMO can be formed.

1.7.6 Degradation of amine oxides and cellulose during fibre production

Antioxidants such as propylgallate or magnesium sulphate can help reduce depolymerization of cellulose during the NMMO process by catching oxygen that is released from the decomposition of NMMO.[108] At high temperatures cellulose is degraded from oxidation at the reducing end and rupture of the glycosidic bond.[134]

1.8 Conformational study and spectra of 1,2-dimethoxyethane (DME), *bis*-(2-methoxyethyl)-ether (BMEE) and poly(ethylene oxide) (PEO)

There has been considerable recent interest in determining the conformational preferences of 1,2-dimethoxyethane (DME),[135-137] both as a guide to the molecular modelling[1-8] of the widely used (see below) poly(ethylene oxide) (PEO) and also because the rotameric distribution about the C-C bond seems to have considerably more *gauche* contributions than expected from simple methods of modelling. This also has implications for the modelling of related molecules, such as crown ethers, and even for the glycosidic bond. Therefore, this study was undertaken partly in order to elucidate likely conformations of the glycosidic bond in the ensuing work on cellulose dissolution. The dependence of the rotameric distributions on solvent is also central to understanding the widespread use of PEO and of block copolymers of PEO with, *e.g.* poly(propylene oxide) to create non-ionic micelles.

In this study we have sought to:

(i) amplify existing measurements on DME by extending the range of solvents in which it is studied, by a parallel study on the next highest oligomer, *bis*-(2-methoxyethyl)-ether (BMEE) and also by using samples of PEO itself, of relatively low molecular mass (structures of these compounds are shown in figure 1.16).

(ii) quantitate the link between bond conformations, deduced by NMR, and overall polymer conformations, deduced from the bulk properties of the polymer.

(iii) understand solvent effects better.

(iv) understand the special conformational variations at the chain ends.

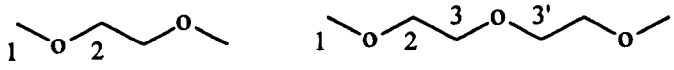

1,2-dimethoxyethane (DME) *bis*-(2-methoxyethyl)-ether (BMEE) poly(ethylene oxide) (PEO)

Figure 1.16 Compounds used in this work.

NMR is highly suited to the quantitative investigation of these rotameric states. The ^{13}C sidebands in the ^{1}H NMR spectra of DME and of PEO arise from an isotopomer in which the H degeneracy is partially removed, so that both of the $^{3}J_{HH}$ values may be deduced by subspectrum simulation. Much the same patterns occur in the main, ^{12}C isotopomer of BMEE. These coupling constants may be converted into rotameric proportions using a well-parameterized Karplus relationship[138,139] (see figure 1.17). Also the proton-coupled ^{13}C NMR spectra of DME and of BMEE permit the computerised extraction of all the $^{2}J_{CH}$ and $^{3}J_{CH}$ coupling constants, including the C-O-C-H couplings that enable study of the C-O bond. For this case the Karplus parameters are somewhat less certain, but can nevertheless be established with acceptable accuracy as described below. The corresponding $^{3}J_{CH}$ data can be extracted for normal PEO in solvents where it has adequate solubility. Also there are a few combinations of solvent and ether for which some polymer couplings, *e.g.* for endgroups, cannot be reliably interpreted because of inconvenient coincidences of multiplet components.

Some solvents also permit sufficient variation of temperature for the approximate extraction of ΔH as well as ΔG values. These imply that ΔS for the $g \leftrightarrow t$ transition can be significant.

DME and related model compounds have also been previously investigated by Raman spectroscopy,[140] electron diffraction,[141] IR,[142] molecular modelling[1-8] and by NMR

spectroscopy.[135,136,143,144] Tasaki and Abe[135] studied DME as a model compound of PEO with NMR spectroscopy in a range of solvents but their publication contained misinterpretations of ^{13}C spectra. Table 1.1 shows a comparison between the proportions of each conformation of DME in the gaseous phase calculated from molecular modelling by Smith *et al.*,[1] electron diffraction data by Astrup,[141] both at 273 K, and from NMR data by Inomata and Abe at 295 K.[136]

BMEE was first thought to be useful for obtaining ^{1}H-^{1}H NOE data; this data is not obtainable with DME and the polymer because of the equivalence of their CH_2 protons. However, it is now recognised that because of the second order nature of the spin system, the NOE data is fatally obscured by spin-tickling effects. However, BMEE is a useful model for PEO because this compound contains a central ether link that resembles those located in the polymer.

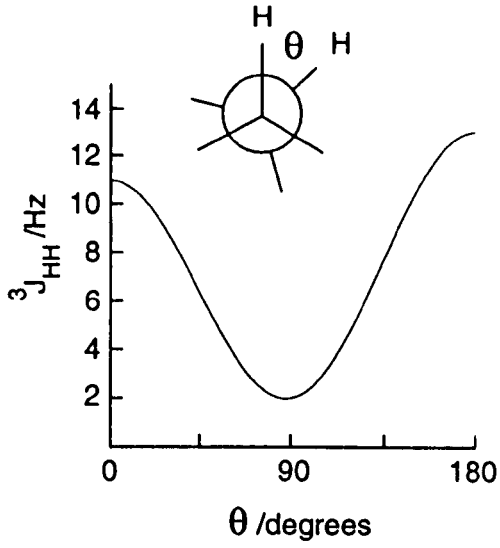

Figure 1.17 An example of a Karplus type curve.

Table 1.1 Relative proportion of each DME conformation in the gaseous phase calculated by computational calculations, NMR and electron diffraction data.

Conformation	Calculated by Smith *et al.*[a] %	Calculated by Inomata and Abe[b] %	Calculated by Astrup[c] %
ttt	16	12	13
tgt	25	46	23
$tg^{\pm}g^{\mp}$	46	27[d]	53[d]
$tg^{\pm}g^{\pm}$	3		
ttg	5	9	3
Other	5	6	8

[a] From computational calculations at 273 K (ref. 1)
[b] From NMR data and RIS calculations (see section 1.8.7) at 295 K (ref. 136)
[c] From electron diffraction data at 273 K (ref. 141)
[d] Includes both tgg conformations

1.8.1 Commercial uses for poly(ethylene oxide) (PEO)

Poly(ethylene oxide) is commercially available in a wide range of molecular weights, from 200 to several millions. The lower members (200-600) are liquids, the intermediate members (600-20,000) are waxy solids and the high molecular weight PEO's are tough thermoplastics. Low and high molecular weight PEO's have a wide variety of applications.

The non-ionic PEO's are soluble in water and are widely formulated in ointments. This allows the ointment to be readily washed off with water and these inert polymers do not interfere with the release of medication and can be applied to dry and moist skin with equal ease. PEO's of 1,000 to 4,000 molecular weight are used in suppository bases, the softening point being dependent on the relative amounts of the higher and lower molecular weight of polymer in the formulation. These polymers are also used as dry binders, in tablet coatings, and for the formulation and manufacture of compressed tablets. Formulation of cosmetics such as creams, cakes and powders, often includes PEO, for its water solubility permits easy removal of the materials.

In industry, these polymers are used as mould release agents and as pigment dispersants. PEO's are also used as spinning aids and dye dispersants in the textile industry. Other applications of PEO's include use as spreading agents in agricultural sprays, anti-static agents and plasticisers for starch adhesives and for cellulose. Postage stamps can be prevented from curling if a small amount of polymer is added to the adhesive.

High molecular weight PEO has the property to reduce frictional drag of flowing water. This is known as the "Toms" effect. The throughput of water in a fireman's hose can be doubled when the polymer is present at a concentration of between 10 and 50 ppm. The polymer changes only the flow characteristic and not the fire-fighting properties of water.

PEO can also be painted on the hull of a ship or a torpedo to reduce the drag of the water.

1.8.2 ^{1}H Spectra of 1,2-dimethoxyethane (DME)

The proton spectrum of DME contains two main peaks, which correspond to the methoxy and methylene groups. Although the spectrum appears not to contain any coupling information, a closer inspection proves this not to be the case. ^{13}C satellites appear at about 70 Hz on each side of the methylene resonance and encode the ^{3}J coupling information between protons across the C-C bond. This occurs because the proton equivalence of the methylene groups is removed when one is attached to a ^{13}C nucleus neighbouring a ^{12}C nucleus, thus producing an AA'BB' spin system. The methylene ^{13}C satellite spectrum consists of five resolved peaks (figure 1.18) although there are others that cannot usually be seen because of the limitations of resolution. If these five lines are numbered from 1 to 5 then the following simultaneous equations[143] give a good approximation of the $^{3}J_{HH}$ coupling constants:

$$^{3}J_{ab}+{}^{3}J_{ab'}=n_1-n_5 \qquad \text{equ. 1.3 (a)}$$

$$^{3}J_{ab}-{}^{3}J_{ab'}=n_2-n_4 \qquad \text{equ. 1.3 (b)}$$

The relevant rotamers for this compound are shown in figure 1.19. Our first assumption is the same as Tasaki and Abe, that the *trans* and *gauche* couplings are identical for all solvents.[135] The second assumption is that the *gauche* couplings are the same at 60° and 300° and that each contributes 50 % of the total *gauche* rotamer. From the temperature dependence and least squares fit they calculated *trans* and *gauche* couplings to be 11.4 Hz and 2.3 Hz respectively. These figures seem sensible for this type of compound, so the present study has used them directly.

If 11.4 Hz and 2.3 Hz are the couplings for the pure *gauche* and *trans* conformers respectively, the percentage of *gauche* rotamer about the C-C bond can be calculated as follows:

$$^3J_{ab} = [1-(g^+ + g^-)](2.3) + g^+(11.4) + g^-(2.3)$$

$$\text{Percentage of } g^+ = \frac{^3J_{ab} - 2.3}{9.1} \qquad \text{equ. 1.4 (a)}$$

$$^3J_{ab'} = [1-(g^+ + g^-)](11.4) + g^+(2.3) + g^-(2.3)$$

$$\text{Percentage of } g^- = \frac{11.4 - 9.1g^+ - ^3J_{ab'}}{9.1} \qquad \text{equ. 1.4 (b)}$$

Therefore the total percentage of *gauche* rotamer about the C-C bond is the sum of g^+ and g^-.

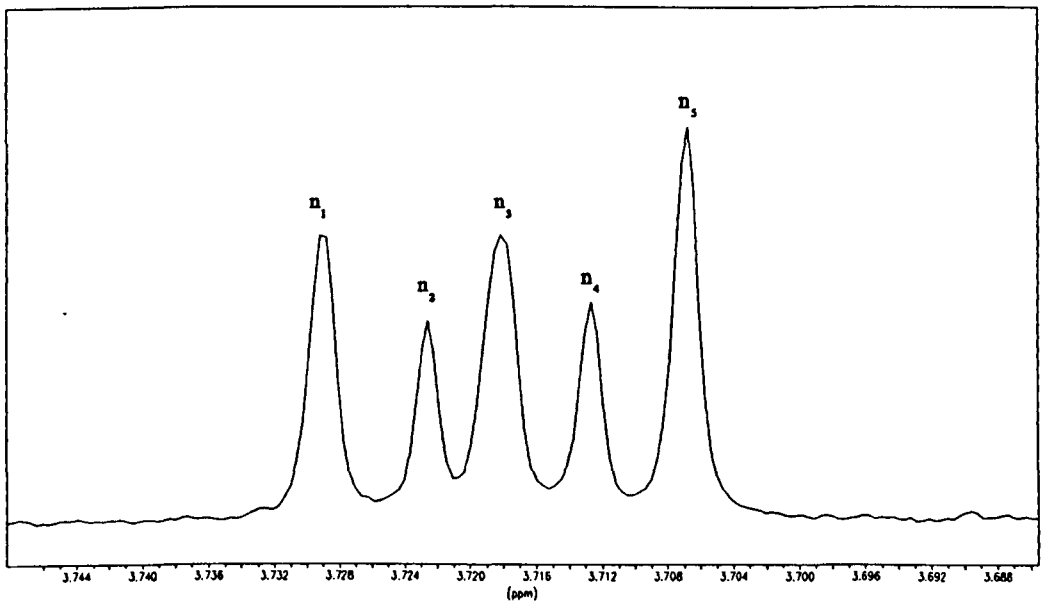

Figure 1.18 Portion of a proton spectrum showing one part of the carbon satellites of DME in D_2O.

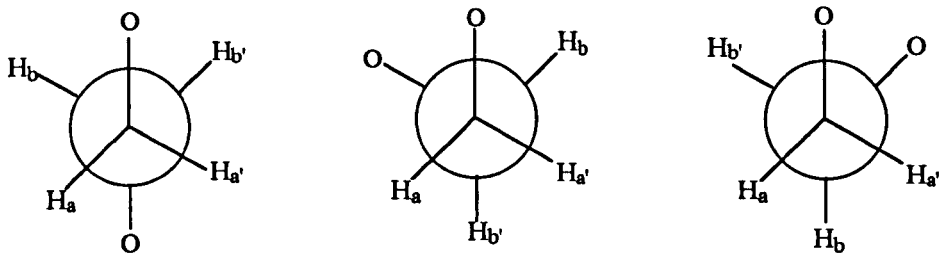

$^3J_{ab} = {}^3J_{g-}$
$^3J_{ab'} = {}^3J_t$

$^3J_{ab} = {}^3J_t$
$^3J_{ab'} = {}^3J_{g+}$

$^3J_{ab} = {}^3J_{g+}$
$^3J_{ab'} = {}^3J_{g-}$

Figure 1.19 Relevant rotamers for the analysis of proton spectra of DME (bold type indicates backbone configuration).

1.8.3 ^{13}C Spectra of 1,2-dimethoxyethane (DME)

To obtain information about the rotamer distribution across the C-O bond, proton-coupled ^{13}C spectra (figure 1.20) need to be examined. The relevant conformations are shown in figure 1.21. Both of the *gauche* rotamers will place the methoxy carbon nucleus *trans* to one of the methylene protons. The magnitude of the $^3J_{CH}$ coupling then discloses the distribution of *trans* and *gauche* rotamers about the C-O bond.

Tasaki and Abe expected to obtain triplets from the $^3J_{CH}$ couplings of the methoxy carbon nucleus from two identical methylene protons. We now know this is not the case, for in reality a quintet is obtained with smaller broad peaks on either side that are modulated by the size of the $^3J_{HH}$ couplings. Although Tasaki and Abe corrected their errors in a later publication, their measurements were not based on iterated fittings of the couplings.[136]

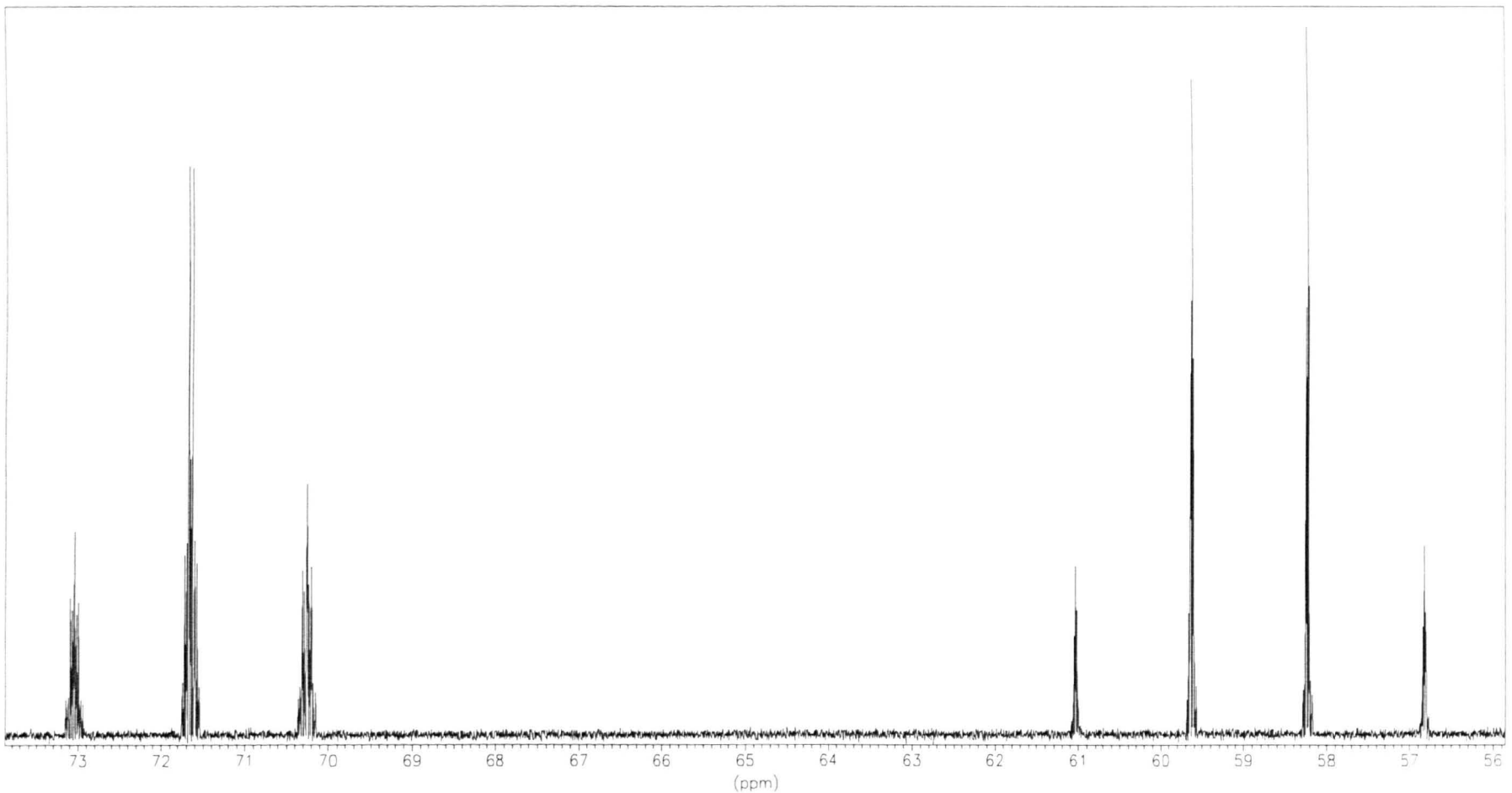

Figure 1.20 Fully proton-coupled ^{13}C spectrum of DME in $CDCl_3$ at 295K.

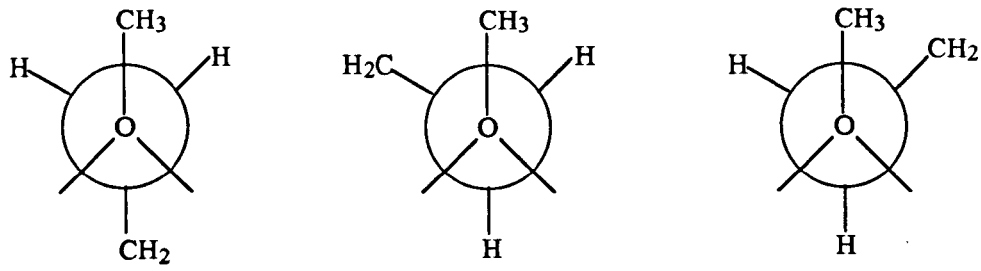

t $^3J_{C1H2} = {}^3J_{g+} + {}^3J_{g-}$

g$^+$ $^3J_{C1H2} = {}^3J_{g-} + {}^3J_t$

g$^-$ $^3J_{C1H2} = {}^3J_{g+} + {}^3J_t$

Figure 1.21 Relevant rotamers for the analysis of carbon spectra of DME (bold type indicates backbone configuration).

Each of the four equal splittings of the quintet is approximately half of the $^3J_{CH}$ coupling, and an exact value can be obtained with the use of iterative software. The system is formally AA'BB'X, but when modelled as A_4X, satisfactory fits to the experimental data were obtained. The quintet is produced instead of the expected triplet because each methylene proton pair has coincidentally the same identical chemical shifts and thus forms a strongly coupled system. Therefore, the protons act as if they were in fast exchange with each other and so five lines are observed with approximately half the triplet couplings expected if this strong coupling is ignored. In theory, the broader outer lines that are modulated by the $^3J_{HH}$ couplings could provide a method to check data from ^{13}C satellite spectra, but in practice this would be very difficult using iterative software as noisy ^{13}C spectra are usually obtained.

An accurate determination of the average bond angles and thus the proportion of *trans* and *gauche* rotamers would require a Karplus curve that takes into account the coupled nuclei, the coupling pathway and substituents about these atoms. This information is presently not fully available but one parameter that is useful in this situation is the $^3J_{CH}$ coupling between the methylene carbon nearest to the methyl protons. The methyl group

is freely rotating and so must give a $^3J_{CH}$ value which is the exact average of one *trans* and two *gauche* couplings. Since the *trans* coupling is experimentally five times that of the *gauche* coupling in all Karplus curves,[145] to a good approximation, the individual coupling constants for each rotamer (*i.e.* ^3J_g and ^3J_t) can be calculated as follows;

$$^3J_{CH_3OC} = (J_t + 2J_g)/3 = (J_t + \tfrac{2}{5}J_t)/3 = \tfrac{7}{15}J_t \qquad \text{equ. 1.5}$$

Thus, $J_t = \dfrac{^3J_{CH_3OC}}{7} \times 15$ and $J_g = J_t/5$

Using the ^3J_g and ^3J_t couplings calculated above, the proportion of the *gauche* rotamer about the C-O bond can be obtained as follows;

$$^3J_{CH} = fraction\ of\ trans \times {}^3J_g + (1 - fraction\ of\ trans) \times \frac{^3J_t + {}^3J_g}{2}$$

Thus, $fraction\ of\ gauche = 1 - \dfrac{Z - {}^3J_{COCH}}{Z - {}^3J_g}$ equ. 1.6

where, $Z = \dfrac{^3J_t + {}^3J_g}{2}$

1.8.4 ^{1}H Spectra of *bis*-(2-methoxyethyl)-ether (BMEE)

The methylene portion of the proton spectrum of BMEE (figure 1.22) is similar to the ^{13}C satellites of DME and thus the $^{3}J_{HH}$ couplings can be calculated in a similar manner to before. The AA'BB' system produces eight lines although some may be overlapping. In this case an approximate value for $^{3}J_{ab} + {}^{3}J_{ab'}$ is given by n_1-n_7 whereas $^{3}J_{ab} - {}^{3}J_{ab'}$ is given by n_3-n_6. As before, this data when compared to a Karplus type curve gives the proportion of the *trans* and *gauche* rotamers about the C-C bond.

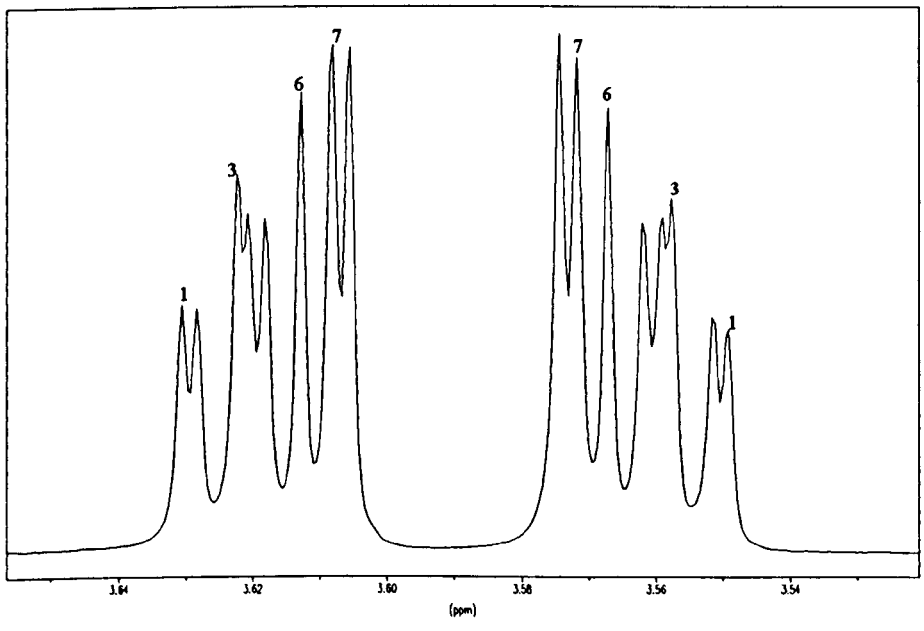

Figure 1.22 Portion of a proton spectrum of BMEE in D_2O showing the methylene resonances.

1.8.5 ^{13}C Spectra of *bis*-(2-methoxyethyl)-ether (BMEE)

The proton-coupled ^{13}C spectrum of BMEE (figure 1.23) produces three sets of multiplets. Whereas the methyl resonances of DME gave quintets, in this instance the proton equivalence of the methylene pair is absent so that triplets are obtained which can simply be interpreted. Each of the methylene resonances gives a series of complex multiplets so the $^3J_{CH}$ coupling information is best extracted using iterative software. The $^3J_{C1H2}$ value gives the rotamer distribution about the terminal C-O- bond while the $^3J_{C3H3'}$ value gives the distribution about the central -C-O- bond.

1.8.6 Proton and carbon spectra of PEO

The ^1H spectrum of PEO contains a single peak which corresponds to the methylene groups. As with DME, ^{13}C satellites appear at about 70 Hz on each side of the methylene resonance and encode the ^3J coupling information between protons across the C-C bond.

Fully proton-coupled ^{13}C spectra of PEO (figure 1.24) show a single triplet corresponding to the methylene group. Each component of the triplet produces a complex set of multiplets, so that coupling constants can only be extracted with the assistance of iterative software. As with DME and BMEE, information about the rotamer distribution across the C-O bond can be obtained from ^3J coupling constants.

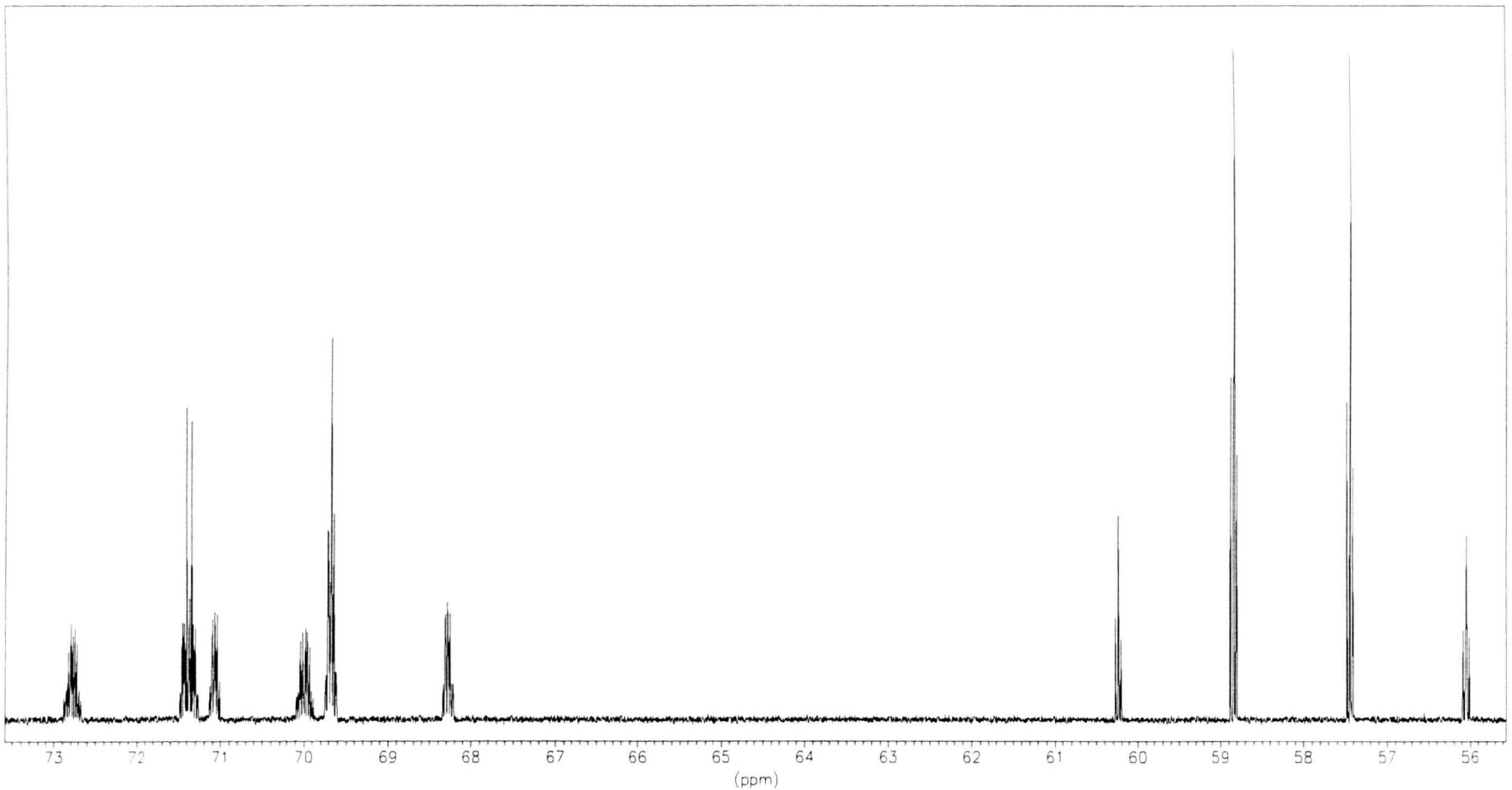

Figure 1.23 Fully proton-coupled ^{13}C spectrum of BMEE in DMSO at 295K.

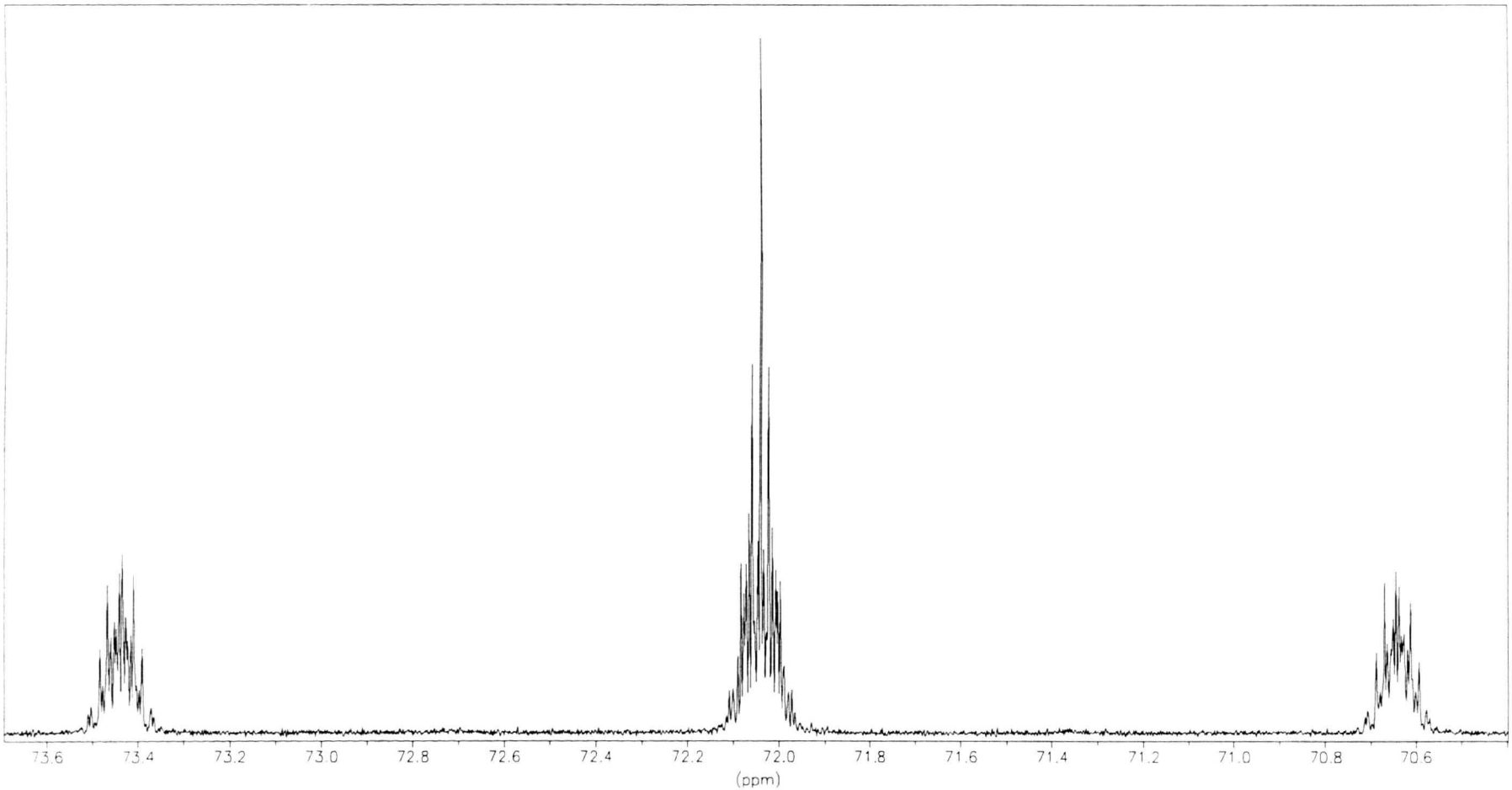

Figure 1.24 Fully proton-coupled ^{13}C spectrum of PEO 6000 in dioxan at 353 K.

1.8.7 Rotational isomeric state (RIS) analysis

The Rotational isomeric state (RIS) analysis[146] allows the proportion of each conformation of a polymer to be determined from experimental data. In this approximation, each polymer backbone bond is presumed to occur in any one of a small number of discrete rotational states that coincide with its potential minima. The conformation about a bond of a polymer chain is also dependent on the probability of occurrence of any rotational state about a given bond of its nearest neighbour. The source of the near neighbour interdependence of polymer conformation is the nonbonded interaction between groups separated by four bonds (*i.e.* the pentane effect). The resulting probabilities are expressed in the form of statistical weight matrices.

RIS analyses were first applied to poly(ethylene oxide) chains by Mark and Flory[147,148] in 1965. They formulated statistical weight matrices for bond rotations of various conformations about three successive bond pairs of the repeat unit of PEO. The three successive bond pairs are shown in figure 1.25, and table 1.2 lists calculated distances between nonbonded atoms and groups.[147]

A *gauche* rotation about the CH_2-O bond gives rise to interactions between methylene groups, and is given the statistical weight σ of one *gauche* state relative to the *trans* conformation. A *gauche* rotation about the CH_2-CH_2 bond decreases the distance between the attached oxygens from 0.367 to 0.284 nm, the latter distance is larger than twice the Van der Waals radius of the oxygen atom and so steric interactions are unimportant. As mentioned in section 1.3 the *gauche*-oxygen effect lowers the energy of the *gauche* state relative to the *trans* rotamer about the C-C bond. Therefore, the statistical weight factor σ' of one *gauche* state relative to the *trans* rotamer is assigned for rotations about this bond (the *trans* conformer is always arbitrarily assigned as unity for each case). In any case σ' must be greater than σ.

Gauche rotations about two successive bonds increase the possibility of interactions between pairs of groups separated by four bonds. If the *gauche* rotations are of the same sign then these groups occur on opposite sides of the plane. Although the distances between these groups are large enough to avoid strong repulsions, their interaction may be significant. This has been acknowledged by the addition of suppression factors α and γ for rotations of like sign about CH_2-CH_2-O or O-CH_2-CH_2 bond pairs and CH_2-O-CH_2 pairs, respectively.

If the *gauche* rotations about the CH_2-O-CH_2 bond pair are of opposite sign then severe repulsions occur, and hence the statistical weight factor is assigned the value zero. The repulsion is less severe for *gauche* rotations of opposite sign about a CH_2-CH_2-O or a O-CH_2-CH_2 bond pair and is assigned the suppression factor β.

The respective statistical weight factors can be combined with four-bond interactions, and thus statistical weight matrices for rotations about two consecutive bonds in the polyoxyethyene chain were derived by Mark and Flory as follows;

$$U_1 = \begin{bmatrix} 1 & \sigma & \sigma \\ 1 & \alpha\sigma & \beta\sigma \\ 1 & \beta\sigma & \alpha\sigma \end{bmatrix} \qquad U_2 = \begin{bmatrix} 1 & \sigma & \sigma \\ 1 & \gamma\sigma & 0 \\ 1 & 0 & \gamma\sigma \end{bmatrix} \qquad U_3 = \begin{bmatrix} 1 & \sigma' & \sigma' \\ 1 & \alpha\sigma' & \beta\sigma' \\ 1 & \beta\sigma' & \alpha\sigma' \end{bmatrix}$$

U_1, U_2 and U_3 signify rotations about the CH_2-CH_2-O, CH_2-O-CH_2 and O-CH_2-CH_2 bond pairs respectively, and the rotational states in the above matrices are in the order t, g^+ and g^-. Multiplication of these matrices in repeating sequence generates statistical weights for all configurations of the polyoxyethyene chain.

From the variation of stress, characteristic ratio and dipole moment of PEO, Mark and Flory deduced RIS factors of between 1.8 and 2.07 for σ and between 0.055 and 0.220 for σ'. Their suppression factor, β, ranged from 0.566 to 1 in a C-C-O portion. They also demonstrated that their RIS analysis of the polyoxyethyene chain was insensitive to the exact values chosen for α and γ.

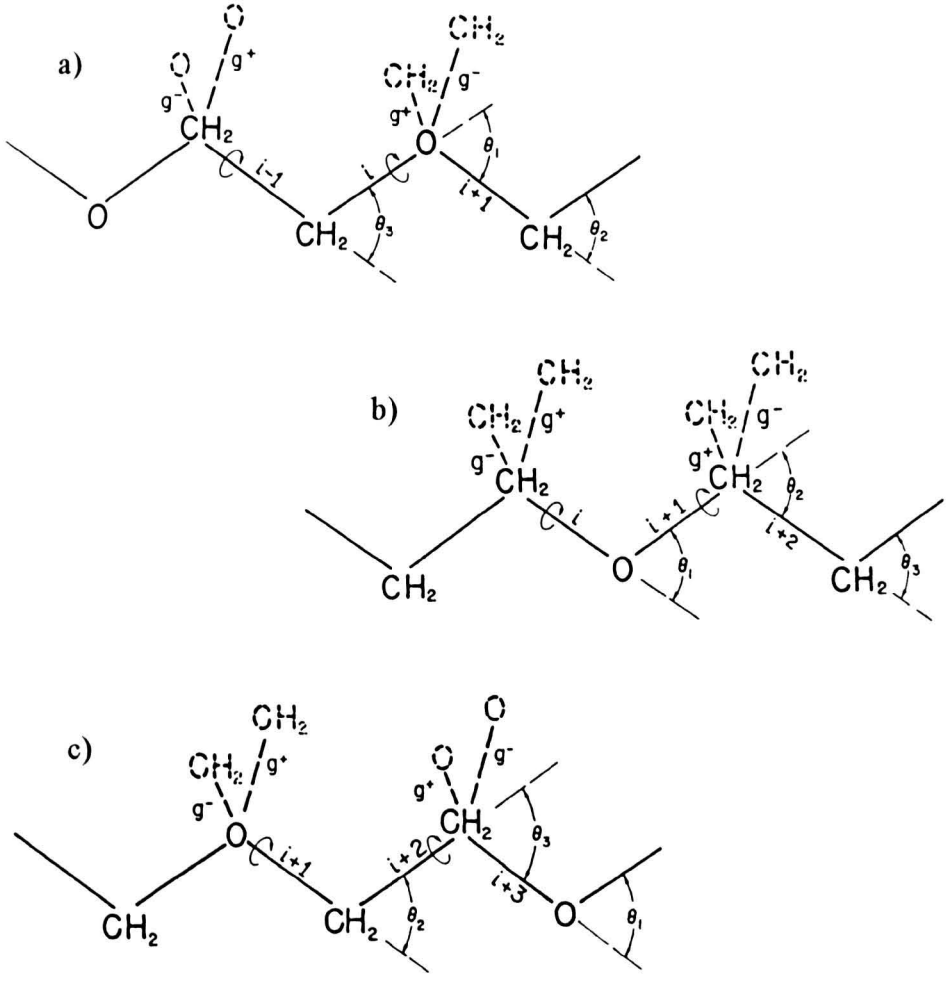

Figure 1.25 Rotational conformations about a) the CH_2-CH_2-O bond pairs, b) the CH_2-O-CH_2 bond pairs and c) the O-CH_2-CH_2 bond pairs. The *trans* rotamers are shown by solid lines and the 2 alternative *gauche* rotamers are shown by dashed lines.

Table 1.2 Distances between nonbonded atoms and groups.

Interacting atoms or groups	Number of bonds apart	Conformation	Distance nm	Statistical weight factor
$CH_2...CH_2$	3	t	0.370	1
	3	$g^{\pm}$	0.281	σ
O...O	3	t	0.367	1
	3	$g^{\pm}$	0.284	σ'
$CH_2...O$	4	$g^{\pm}g^{\pm}$	0.338	α
	4	$g^{\pm}g^{\mp}$	0.246	β
$CH_2...CH_2$	4	$g^{\pm}g^{\pm}$	0.334	γ
	4	$g^{\pm}g^{\mp}$	0.237	0

1.8.8 RIS analysis used in the present study

In this study, a simple RIS analysis was devised to disentangle the *gauche*-oxygen effect from the pentane effect, in the oligomers. This allows us to calculate the proportion of *gauche* rotamers about the C-C and C-O bonds if the interactions from the pentane effect are ignored, *i.e.* isolated bond probabilities.

Two matrices, one for DME and one for BMEE, were constructed as described below. The analysis in the present study made the same assumption as Flory, *i.e.* that *gauche* rotations of opposite sign about two consecutive bonds are forbidden (the pentane effect) and *gauche* rotations of the same sign are allowed for a CH_2-O-CH_2 segment. Pentane suppression factors, 'p_1' and 'p_2', used in this study were set to 0.8 and 0.5

respectively. The 'p_2' factor refers to *gg* rotations involving two consecutive C-O bonds (*i.e.* C-O-C segments), and amounts to a 100 % prohibition of g^+g^- and g^-g^+. The 'p_1' factor refers to rotations involving one C-C and one C-O bond (*i.e.* C-C-O or O-C-C segments). These are less strongly suppressed, according to Flory *et al.*, and we have used his suppression factor.

1.8.8.1 Matrix derived for DME

The matrix below shows the probabilities of each DME conformation when the following assumptions are made:

1. The basic probability of C-O being *gauche* (relative to *trans*) is y.
2. The basic probability of C-C being *gauche* (relative to *trans*) is x.
3. The pentane effect reduces the probability of *gg* about a C-C-O portion by 0.5, *i.e.* 'p_1'.

Matrix 1 derived for DME

C-O	C-C	C-O	Relative Probability
t	*t*	*t*	*1*
g	*t*	*t*	y
t	*g*	*t*	x
t	*t*	*g*	y
g	*g*	*t*	xyp_1
g	*t*	*g*	y^2
t	*g*	*g*	xyp_1
g	*g*	*g*	$xy^2p_1^2$

From the above matrix the following can be derived:

1. Total probability in the matrix above is $= 1 + x + 2y + 2xyp_1 + y^2 + xy^2p_1^2 = T$

2. Total probability of finding a *gauche* C-O bond $= \frac{2y + 2xyp_1 + 2xy^2p_1^2 + 2y^2}{2T}$

3. Total probability of finding a *gauche* C-C bond $= \frac{x + 2xyp_1 + xy^2p_1^2}{T}$

1.8.8.2 Matrix derived for BMEE

Two pentane reduction factors are required for the matrix derived for BMEE, *i.e.* 'p_1' for a C-C-O segment and 'p_2' for a C-O-C segment (see above). In the matrix below, '*a*' denotes the product of the corresponding values of column 1 and row 1, *e.g.* '*a*' in cell 2,2 is y^2 and '*a*' in cell 6,7 is xy^3p_1, *etc.*

The sum of all 64 cells in this matrix is denoted as TT. From the matrix below the following *gauche* probabilities can be determined:

1. *Gauche* probability of C-O_{outer} = $\sum$ rows 2, 5, 6, 8 + columns 4, 6, 7, 8 / 2TT
2. *Gauche* probability of C-O_{inner} = $\sum$ rows 4, 6, 7, 8 + columns 2, 5, 6, 8 / 2TT
3. *Gauche* probability of C-C = $\sum$ rows + columns 3, 5, 7, 8 / 2TT

Left and right in the matrix below refers to each of the two $CH_3OCH_2CH_2O$ portions of DMEE molecules.

Matrix 2 derived for BMEE

RIGHT

LEFT		1	2	3	4	5	6	7	8
		ttt	*gtt*	*tgt*	*ttg*	*ggt*	*gtg*	*tgg*	*ggg*
1	*ttt*	1	y	x	y	xyp_1	y^2	xyp_1	$xy^2p_1^2$
2	*gtt*	y	a	a	a	a	a	a	a
3	*tgt*	x	a	a	a	a	a	a	a
4	*ttg*	y	ap_2	a	a	ap_2	ap_2	a	ap_2
5	*ggt*	xyp_1	a	a	a	a	a	a	a
6	*gtg*	y^2	ap_2	a	a	ap_2	ap_2	a	ap_2
7	*tgg*	xyp_1	ap_2	a	a	ap_2	ap_2	a	ap_2
8	*ggg*	$xy^2p_1^2$	ap_2	a	a	ap_2	ap_2	a	ap_2

Hence there are 5 experimental values (*i.e.* conformations about 2 DME bonds and 3 BMEE bonds) and 2 unknowns (*i.e.* x and y). The unknown *gauche* probability factors were calculated in our RIS analysis by fitting them simultaneously to the experimental data obtained for both DME and BMEE iteratively, using EXCEL 4 in combination with SOLVER. The fitted values obtained for x and y, after normalisation (*i.e.* relative to the *trans* conformation set to unity), then lead to the isolated bond probabilities, σ and σ', for C-C and C-O bonds.

CHAPTER TWO

C-C and C-O Bond Conformations in 1,2-Dimethoxyethane (DME), *Bis*-(2-methoxyethyl)-ether (BMEE) and Poly(ethylene oxide) (PEO): Dependence on Solvent and Temperature

2.1 Introduction

The intention of this study was to investigate the conformational preferences for DME, BMEE and PEO under different conditions, *i.e.* dependence on solvent and temperature, using NMR methods (see section 1.8). Calculation of isolated bond probabilities about C-C and C-O bonds for PEO with an RIS analysis using NMR experimental data obtained from DME and BMEE (see figure 1.15) was also of interest.

2.2 Experimental

All NMR spectra were recorded using a Bruker ACP 400 spectrometer, and analysed iteratively using Bruker's WIN-DAISY program. The proton-coupled ^{13}C spectra typically required overnight accumulation, even using gated ^{1}H pre-irradiation. The outer, and thereby simpler components of the main ^{13}C multiplets were selected for the analyses, which were based on an AA'BB' spin system (^{1}H) and AA'BB'X (^{13}C). No $^{4}J_{CH}$ couplings were resolvable, and so they were not included in the simulations, although they are probably responsible for some line broadenings.

WIN-DAISY can either calculate a spectrum from a given set of coupling constants and chemical shifts, or fits a set of chosen parameters to an existing spectrum by iteration. In the iterative mode WIN-DAISY can only fit coupling constants to a given spectrum if these parameters are roughly known beforehand. Therefore, before

any iteration could be initiated, several simulations had to be performed while adjusting the ^2J and ^3J values until these couplings were near to their true values. Equation 1.3 gave good approximations of the $^3J_{HH}$ coupling constants, and subsequent iterations of spectra then produced more precise values. WIN-DAISY also requires an upper and lower limit of each parameter to be iterated, but in practice, especially for proton-coupled ^{13}C spectra, this bandwidth cannot be too wide, *i.e.* no more than ±10 % of the actual value for each parameter. For ^1H spectra the iterations typically took less than a minute and proton-coupled ^{13}C iterations lasted from 20 minutes for DME and BMEE spectra to 10 hours for the polymer. Examples of fits for each type of multiplet iterated are shown in figure 2.1 (a-h). The estimated errors in ^3J are ±0.1 Hz.

DME was obtained from Sigma Chemicals and DMEE and PEO (Mn = 600 and 6000) from Aldrich; all were used without further purification. The concentrations for the variable solvent data were 2 % w/w, with 5 % for the variable temperature experiments. Internal TSP (3-trimethylsilyl-2,2,3,3-tetrapropionic acid sodium salt) was used as the shift reference for D_2O and TMS (tetramethylsilane) for all other solvents.

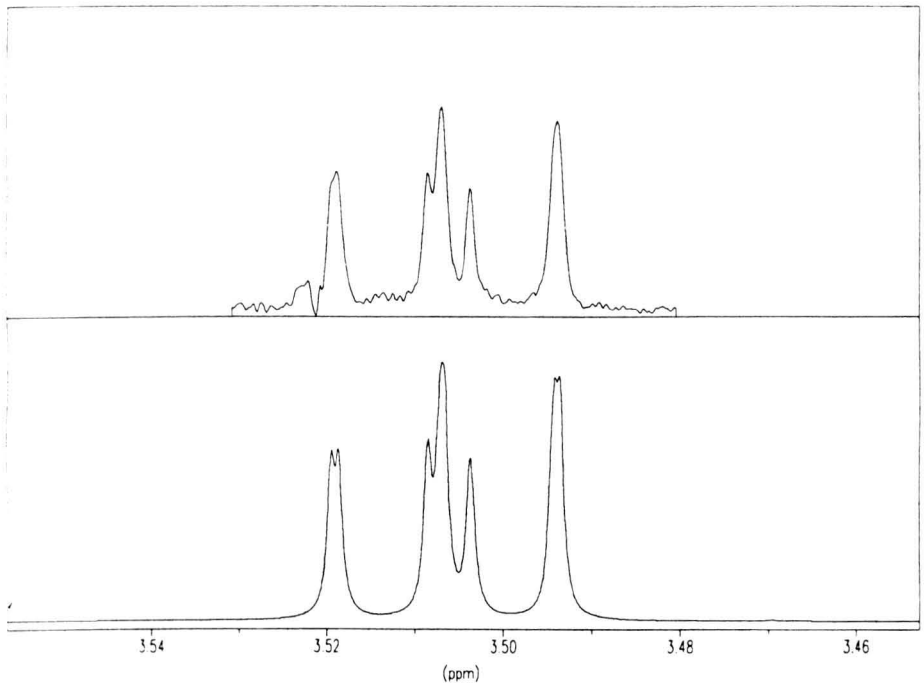

Figure 2.1 (a) (Upper trace) Portion of a proton spectrum of DME in DMSO-d_6 at 320 K showing one carbon satellite component. (Lower trace) Iterated simulation of the same component using WIN-DAISY.

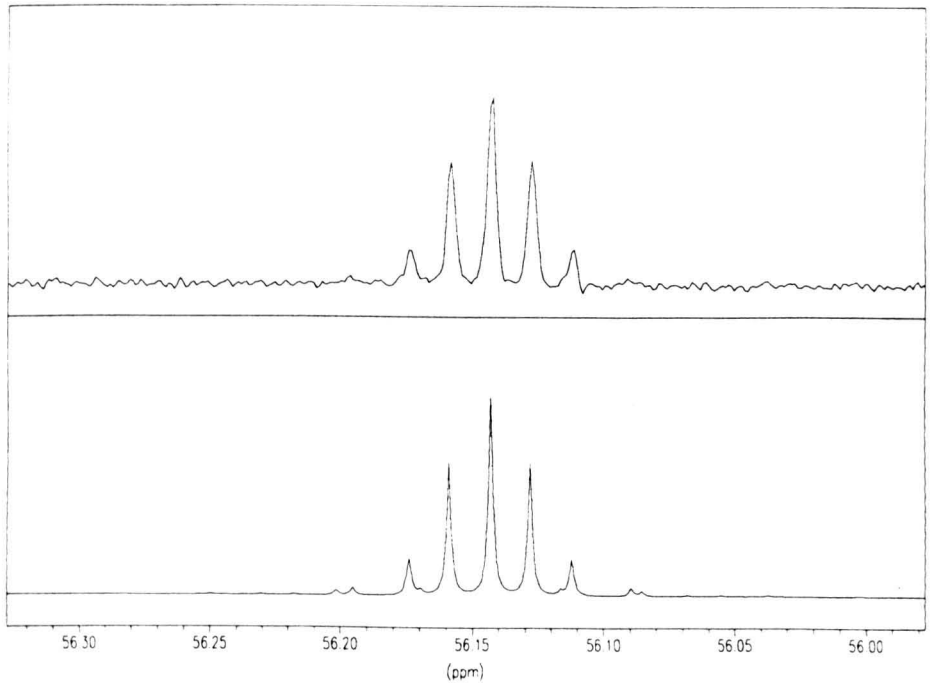

Figure 2.1 (b) (Upper trace) Left-hand outer component of a fully proton-coupled ^{13}C NMR quartet of the CH_3 group of DME in DMSO-d_6 at 295 K. (Lower trace) Iterated simulation of the same component using WIN-DAISY.

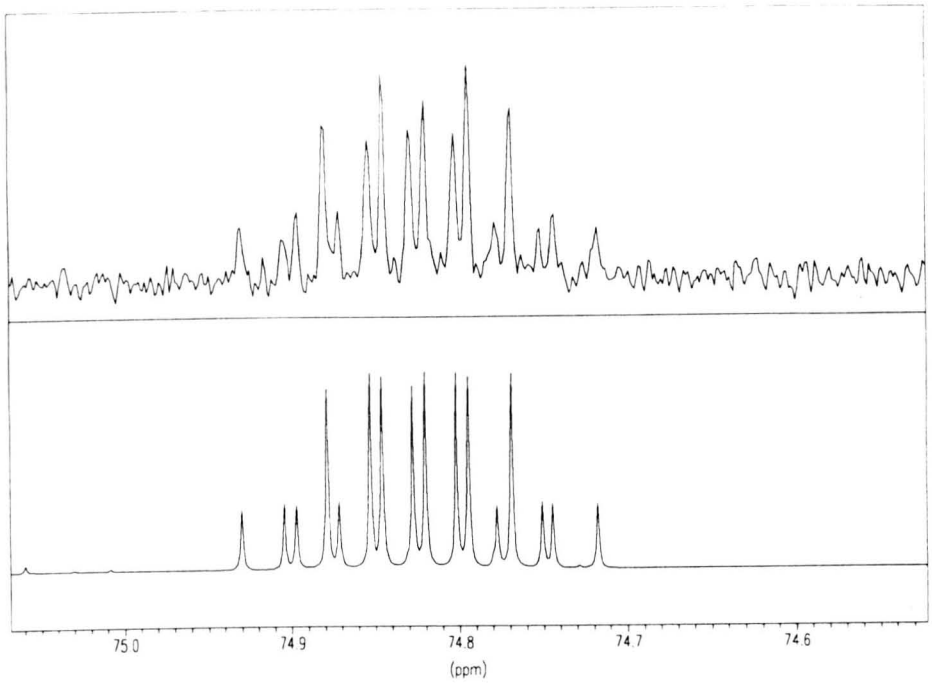

Figure 2.1 (c) (Upper trace) Left-hand outer component of a fully proton-coupled ^{13}C NMR triplet of the CH_2 group of DME in cyclohexane-d_{12} at 295 K. (Lower trace) Iterated simulation of the same component using WIN-DAISY.

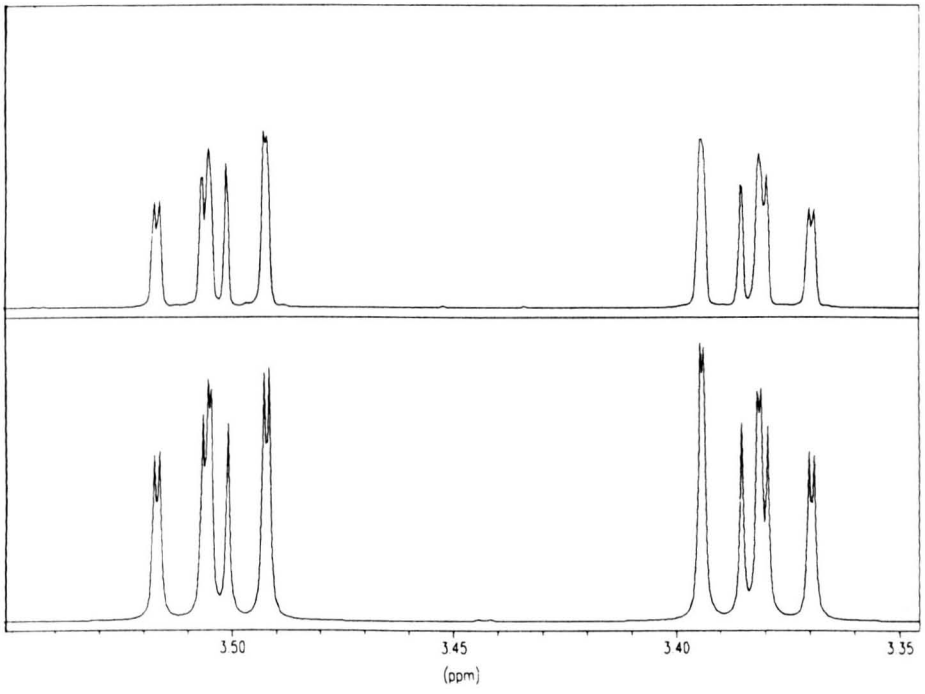

Figure 2.1 (d) (Upper trace) Portion of a proton spectrum showing the CH_2 groups of BMEE in benzene-d_6 at 295 K. (Lower trace) Iterated simulation of the same components using WIN-DAISY.

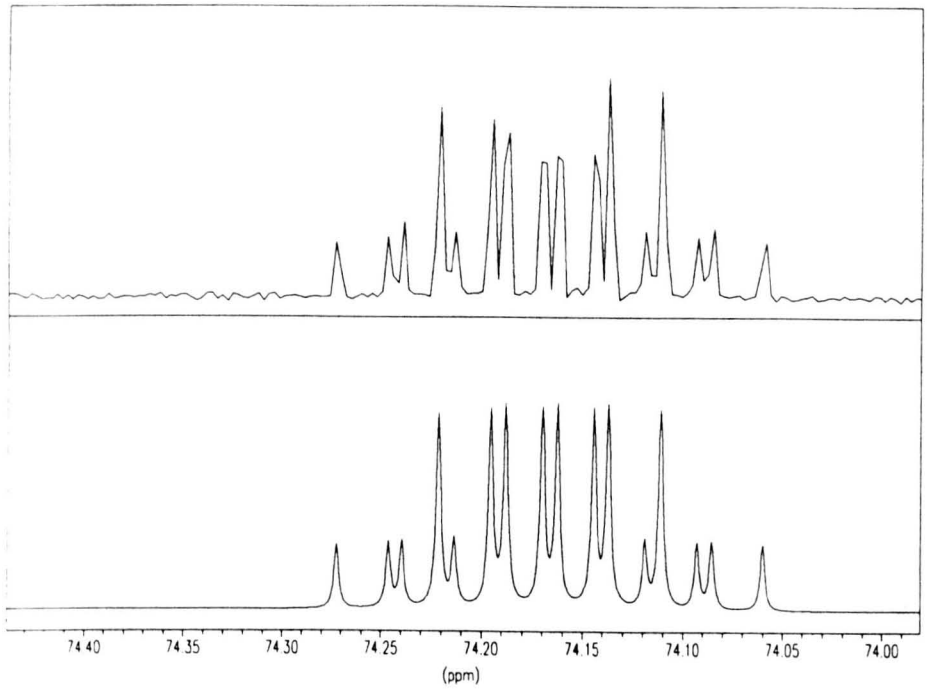

Figure 2.1 (e) (Upper trace) Left-hand outer component of a fully proton-coupled ^{13}C NMR triplet of the $C(2)H_2$ group of BMEE in DMSO-d_6 at 350 K. (Lower trace) Iterated simulation of the same component using WIN-DAISY.

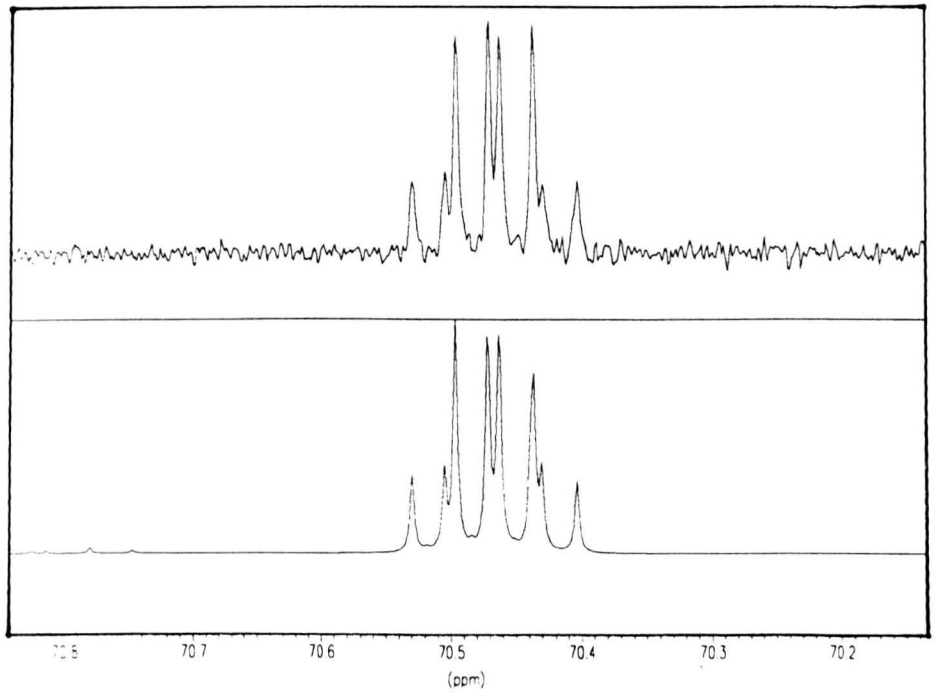

Figure 2.1 (f) (Upper trace) Left-hand outer component of a fully proton-coupled ^{13}C NMR triplet of the $C(3)H_2$ group of BMEE in dioxan-d_6 at 295 K. (Lower trace) Iterated simulation of the same component using WIN-DAISY.

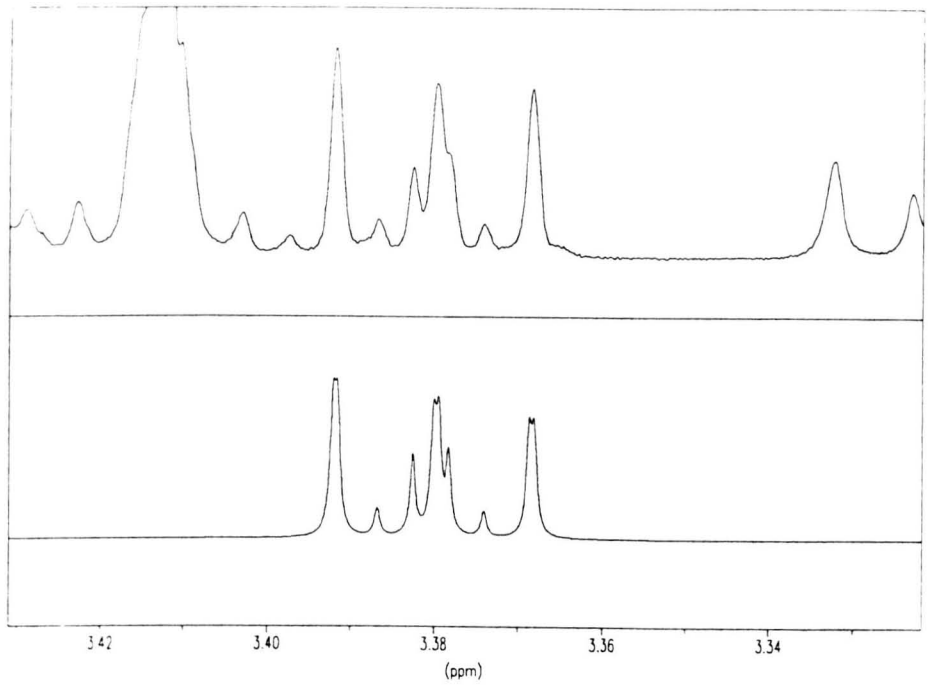

Figure 2.1 (g) (Upper trace) Portion of a proton spectrum showing one component of the endgroup resonance of PEO 6000 in benzene-d_6 at 295 K. (Lower trace) Iterated simulation of the same component using WIN-DAISY.

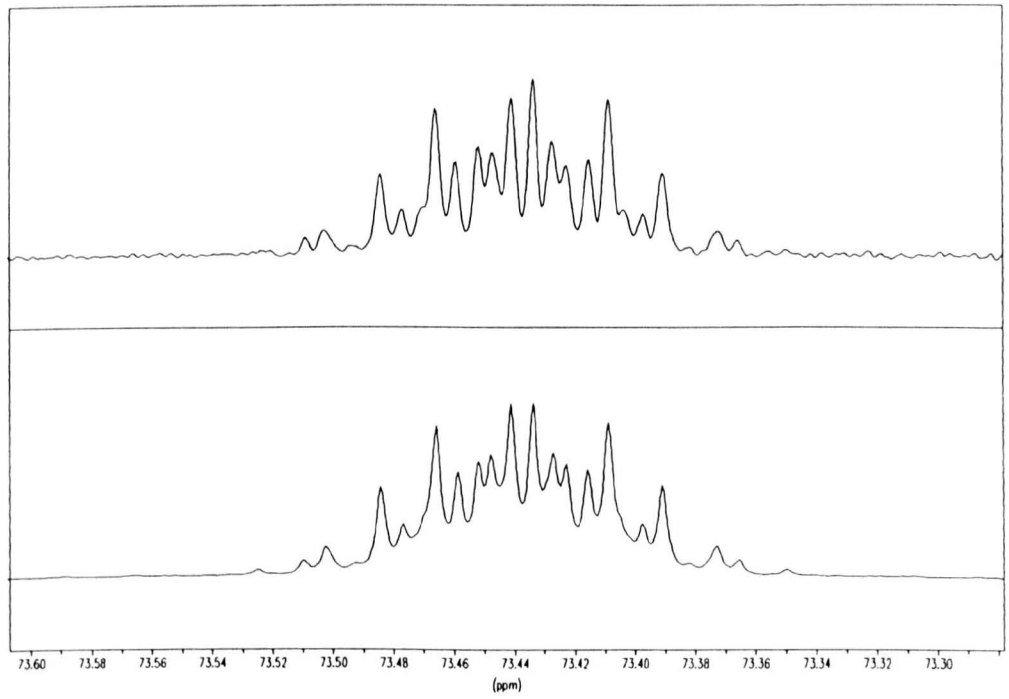

Figure 2.1 (h) (Upper trace) Left-hand component of a fully proton-coupled ^{13}C NMR triplet of PEO 6000 in dioxan-d_8 at 353 K. (Lower trace) Iterated simulation of the same component using WIN-DAISY.

2.3 Results

2.3.1 Variation with solvent

Table 2.1 summarises the ^3J couplings measured for the three ethers, in various solvents at 295 K. It also shows the total percentage of *gauche* rotamers for each bond, calculated *via* the Karplus relationship. As mentioned in section 1.8.2 the HCCH couplings were assumed to follow the relationship used by Tasaki and Abe, with $^3J_{HH(gauche)} = 2.3$ Hz and $^3J_{HH(trans)} = 11.4$ Hz in all solvents.[135] Thus their approximation that one averages any slight variation of these coupling contributions, between and within the three rotamers of a given bond was followed in this work.

No such Karplus relationship has been established for the $^3J_{CH}$ across methoxyl C-O bonds, except for HCOC couplings at the anomeric carbon in disaccharides, where $^3J_{CH(trans)} \sim 6.8$ Hz. Anderson[149] has deduced the relationship $^3J_{COCH} = 7.6 \cos^2 \phi - 1.7 \cos \phi + 1.6$ for methyl-cyclohexanes, but although the $\phi = 0°$ value used to derive this was well determined, the $\phi = 90°$ value was less fully parameterized.

As mentioned in section 1.8.3, one may note that $^3J_{(trans)} / {}^3J_{(gauche)} = 5.0$ in many different Karplus relationships.[145] The measurements in the present study included that of $^3J_{C(2)H(1)}$, with observed values ranging from 4.9 to 5.2 Hz and varying slightly with both solvent and temperature. Since these must be the average of one *trans* plus two *gauche* couplings, they can now be applied to our calculations (as discussed in section 1.8.3) to determine the proportions of each rotamer about the C-O bond. The observations in this work lead to Karplus relationships very similar to that deduced by Anderson (*e.g.* $J_t = 11.0$ and $J_g = 2.2$ in C_6D_{12}) but with slightly greater variation of J with ϕ, at both extremes, and a weak dependence on solvent.

Tables 2.2 and 2.3 show full data, including all coupling constants and chemical shifts obtained for DME and BMEE in each solvent. Table 2.4 records HCCH couplings for the terminal -OCH_2CH_2OH units (endgroups) of PEO 600 and 6000, where obtainable. The same table also shows the couplings obtained for central C-C groups for comparison. Because of the shift inequivalence of the methylene pairs in this terminal unit, their couplings may be observed directly rather than *via* the ^{13}C sidebands. This renders them detectable in at least some solvents.

2.3.2 Variation with position

The final part of table 2.1 shows the *gauche* probabilities deduced for isolated C-C and C-O bonds, by considering the five experimental values, in each solvent, found for both DME and BMEE, and then fitting these by our simple RIS calculation (see section 1.8.8). These isolated-bond probabilities correspond to Flory's standard RIS σ and σ' matrix elements. The calculation required a suitable assumption about the probability of any g^+g^- diad, *i.e.* about the size of the pentane effect, or equivalently of the RIS β or ω factor.* This probability was taken here to be the same as deduced by Mark and Flory[147], *i.e.* zero for C-O-C but 0.8 for C-C-O (section 1.8.7); our data did not convincingly support attempts to find a different fitted value. The calculation predicts, not surprisingly, that *gauche* rotamers occur more easily at the terminal C-O bonds than at the centre of the molecule. This is borne out by the data in table 2.1, within experimental error. As an example, the experimental values for dioxan solvent, at 295 K, with the fitted values in brackets alongside, are 82 [82] and 33 [31] for DME and 82 [82], 30 [31] and 27 [27] for BMEE, where the last figures refer to rotations about the inner C-O bonds.

* The RIS β factor was assigned the symbol ω in Mark and Flory's subsequent publications.

The relatively small variations of the *gauche* proportions between DME and BMEE suggest that PEO will not differ greatly in its rotameric populations, from those of the inner groups of BMEE. This is borne out by the PEO 600 and PEO 6000 couplings, given for the various solvents in table 2.1.

2.3.3 Variation with temperature

Table 2.5 shows $\Delta H^{\ominus}$ and $\Delta S^{\ominus}$ values for the $g \rightarrow t$ transition, deduced from the temperature variation of the five couplings in DME and BMEE, each in two solvents. The errors in these thermodynamic values may be substantial, because the variations of calculated population with temperature are quite sensitive to small and non-systematic errors in the measured couplings. Nevertheless, reasonable Van't Hoff plots are obtained, as exemplified in figure 2.2 (a-e). The values of $\Delta S^{\ominus}$ are also compared with those calculated statistically from the fraction at 1 / T = 0, *i.e.* deduced by setting all rotamer probabilities equal except for those forbidden by the pentane effect between carbon atoms. K (*i.e.* t / total g) and hence $\Delta G^{\ominus}$ led to $\Delta S^{\ominus}$ (statistical) when ΔH° (statistical) was set to zero.

The experimental $\Delta S^{\ominus}$ values are not highly reliable, but differ significantly in some cases from the statistical value.

Tables 2.6 to 2.10 show full data, including all coupling constants and chemical shifts obtained for DME, BMEE and PEO at various temperatures.

Table 2.1 Variation of ^3J couplings and rotamer probabilities with solvent at 295 K.

Bond	C_6D_6		Dioxan-d_8		DMSO-d_6		$CDCl_3$		D_2O	
	^3J (Hz)	% g	^3J (Hz)	% g	^3J (Hz)	% g	^3J (Hz)	% g	^3J (Hz)	% g
DME C-C[a]	6.10	84	6.10	82 (80)[h]	6.16	87 (85)[h]	6.27	94	6.42	98
	3.78		3.92		3.33		2.88		2.45	
DME C-O[b]	3.66	34	3.62	33 (39)	3.57	31 (38)	3.15	23	3.12	25
BMEE C-C[a]	6.10	83	6.14	82 (80)	6.21	88 (83)	6.25	90	6.40	99
	3.82		3.87		3.38		3.26		2.60	
BMEE, inner C-O[c]	3.35	26	3.36	27 (32)	3.11	21 (30)	3.11	21	2.71	14
BMEE, outer C-O[b]	3.60	31	3.51	30 (37)	3.48	29 (36)	3.12	21	2.99	21
PEO 600, central C-C[a]					6.10	87			6.62	97
					3.47				2.59	
PEO 6000, central C-C[a]	6.04	82	6.15	81 (80)	6.28	88 (81)	6.07	85	6.23	97
	3.97		3.99		3.37		3.68		2.55	
PEO 6000, central C-O[d]			(3.65)	(34)	(3.59)	(32)				
Isolated bond probabilities[e]										
C-C		42		41 (41)		44 (43)		46		49
C-O		17		16 (20)		15 (19)		12		11
α_1[f]		0		0		0		0.44		1.17
β_1[g]		0.10		0.37		0.76		0		0.18

[a] From $^3J_{HCCH}$
[b] From $^3J_{C(methyl)OCH}$
[c] From $^3J_{CO(central)CH}$
[d] From $^3J_{COCH}$
[e] % Probability of a single *gauche* rotamer, after RIS allowances, calculated from DME and BMEE data only
[f] Taft solvent H-bond donor parameter
[g] Taft solvent H-bond acceptor parameter
[h] Bracketed figures obtained at 353 K

Table 2.2 (a) Full ^{1}H data of DME in various solvents.

Solvent	Chemical shift (ppm)		Coupling constants (Hz)		% *gauche* about C-C bond
	CH_3	CH_2	$^3J_{ab}$	$^3J_{ab'}$	
C_6D_6	3.12	3.33	6.10	3.78	84
Dioxan-d_8	3.26	3.42	6.10	3.92	82
DMSO-d_6	3.24	3.43	6.16	3.33	87
$CDCl_3$	3.40	3.55	6.27	2.88	94
D_2O	3.37	3.60	6.42	2.45	98

Table 2.2 (b) Full ^{13}C data of DME in various solvents.

Solvent	Chemical shifts (ppm)		Coupling constants (Hz)					*trans* and *gauche* couplings[a] (Hz)		% *gauche* about C-O bond[b]
	CH_3	CH_2	$^1J_{C(1)H}$	$^1J_{C(2)H}$	$^2J_{C(2)H(3)}$	$^3J_{C(1)H(2)}$	$^3J_{C(2)H(1)}$	J_t	J_g	
C_6D_6	58.69	72.23	140.2	140.2	2.36	3.66	5.11	10.95	2.19	34
Dioxan-d_8	58.66	72.33	140.1	140.0	2.35	3.62	5.15	11.03	2.21	33
DMSO-d_6	57.95	70.97	140.5	140.5	2.26	3.57	5.12	10.97	2.19	31
$CDCl_3$	59.08	71.81	140.1	140.5	2.30	3.15	5.02	10.96	2.15	23
D_2O	60.74	73.53	142.7	143.0	1.97	3.12	4.88	10.45	2.09	25

[a] Obtained from $^3J_{C(2)H(1)}$
[b] Obtained from $^3J_{C(1)H(2)}$

Table 2.3 (a) Full ^{1}H data of BMEE in various solvents.

Solvent	Chemical shift (ppm)			Coupling constants (Hz)		% *gauche* about C-C bond
	CH(1)	CH(2)	CH(3)	$^3J_{ab}$	$^3J_{ab'}$	
C_6D_6	3.12	3.35	3.46	6.10	3.82	83
Dioxan-d_8	3.26	3.43	3.51	6.14	3.87	82
DMSO-d_6	3.24	3.42	3.50	6.21	3.38	88
$CDCl_3$	3.39	3.57	3.66	6.25	3.26	90
D_2O	3.26	3.53	3.44	6.40	2.60	99

Table 2.3 (b) Full ^{13}C data of BMEE in various solvents.

Solvent	Chemical shift (ppm)			Coupling constants (Hz)							
	C(1)H	C(2)H	C(3)H	$^1J_{C(1)H}$	$^1J_{C(2)H}$	$^1J_{C(3)H}$	$^2J_{C(2)H(3)}$	$^2J_{C(3)H(2)}$	$^3J_{C(1)H(2)}$	$^3J_{C(2)H(1)}$	$^3J_{C(3)H(3')}$
C_6D_6	58.67	72.38	70.92	140.2	139.6	140.5	2.51	2.23	3.60	5.18	3.35
Dioxan-d_8	57.65	71.50	70.93	140.2	140.3	140.5	2.27	2.38	3.51	5.14	3.36
DMSO-d_6	57.96	71.20	69.50	140.4	140.4	140.7	3.38	2.31	3.48	5.13	3.11
$CDCl_3$	59.04	71.92	70.56	140.9	141.0	140.8	2.39	2.23	3.12	5.14	3.11
D_2O	60.71	71.67	71.09	140.2	139.6	140.5	1.98	2.12	2.99	5.18	2.71

Table 2.3 (b) continued

Solvent	*trans* and *gauche* couplings (Hz)[a]		% *gauche* C-O, outer bond[b]	% *gauche* C-O, inner bond[c]
	J_t	J_g		
C_6D_6	11.10	2.22	31	26
Dioxan-d_8	11.01	2.20	30	27
DMSO-d_6	11.00	2.20	29	21
$CDCl_3$	11.01	2.20	21	21
D_2O	11.10	2.22	21	14

[a] Obtained from $^3J_{C(2)H(1)}$
[b] Obtained from $^3J_{C(1)H(2)}$
[c] Obtained from $^3J_{C(3)H(3')}$

Table 2.4 Variation of couplings and rotamer probability about the central and endgroup C-C bond of PEO with solvent at 295 K.

Bond	D_2O		DMSO-d_6		CD_3CN		MeOD		Acetone-d_6		Dioxan-d_8		C_6D_6	
	$^3J_{HH}$	% g	$^3J_{HH}$	% g	$^3J_{HH}$	% g	$^3J_{HH}$	% g	$^3J_{HH}$	% g	$^3J_{HH}$	% g	$^3J_{HH}$	% g
PEO 600, central C-C	6.62	97	6.10	87	6.21	89	6.20	90	6.02	85				
	2.59		3.47		3.27		3.22		3.71					
PEO 600, endgroup C-C	6.32	93	6.03	75	6.18	85	6.25	87	6.07	82				
	2.97		4.54		3.65		3.48		3.93					
PEO 6000, central C-C	6.23	97	6.28	88							6.15	81	6.04	82
	2.55		3.37								3.99		3.97	
PEO 6000, endgroup C-C	6.19	90	5.97	74							6.08	87	6.19	90
	3.23		4.68								3.51		3.23	

Table 2.5 Variation of $t \leftarrow g$ equilibria with temperature.

Ether	Solvent	Bond	$\Delta H^{\ominus}$ [a] (kJ mol^{-1})	$\Delta S^{\ominus}$ (JK^{-1} mol^{-1})	$\Delta S^{\ominus}$ (Statistical)[c]
DME	Toluene-d_8	C-C	3.35	-2.41	-5.76
DME	Toluene-d_8	C-O	-3.94	-6.87	-5.76
DME	C_6D_{12}	C-C	2.04	-3.84	-5.76
DME	C_6D_{12}	C-O	-2.83[b]	-4.78[b]	-5.76
BMEE	DMSO-d_6	C-C	4.99	0.85	-5.76
BMEE	DMSO-d_6	C-O (inner)	-4.65	-6.52	-2.39
BMEE	DMSO-d_6	C-O (outer)	-4.63	-8.50	-5.76
BMEE	C_6D_{12}	C-C	2.49	-2.37	-5.76
BMEE	C_6D_{12}	C-O (inner)	[b]	[b]	2.39
BMEE	C_6D_{12}	C-O (outer)	-2.49	-2.90	-5.76
PEO 6000	DMSO-d_6	C-C (main)	6.38	5.78	-5.76

[a] $K = t/g^{(+ \text{ and } -)}$

[b] Not reliably determined

[c] From RIS calculation (see section 2.3.3) only retaining the pentane effect

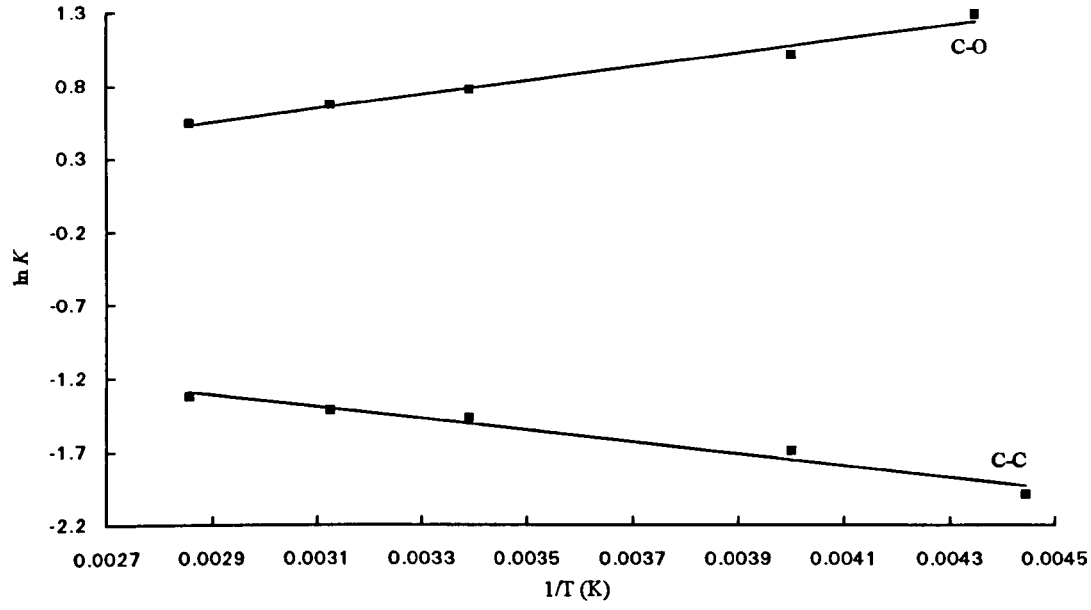

Figure 2.2 (a) Temperature dependence of K (= $t/g^{(+ \text{ and } -)}$) for two bonds of DME in toluene-d_8.

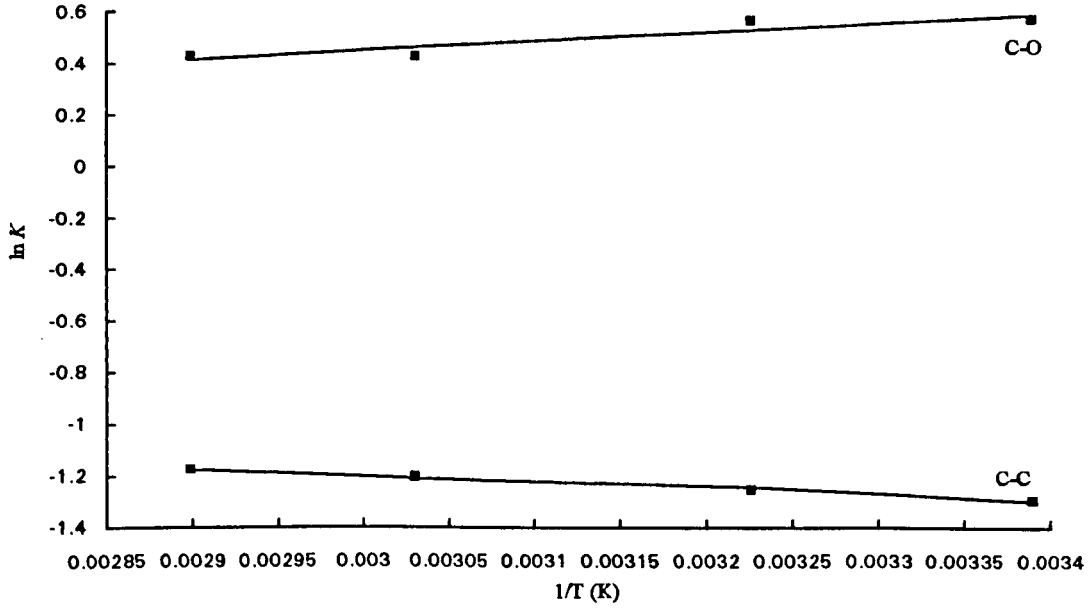

Figure 2.2 (b) Temperature dependence of K (= $t/g^{(+ \text{ and } -)}$) for two bonds of DME in C_6D_{12}.

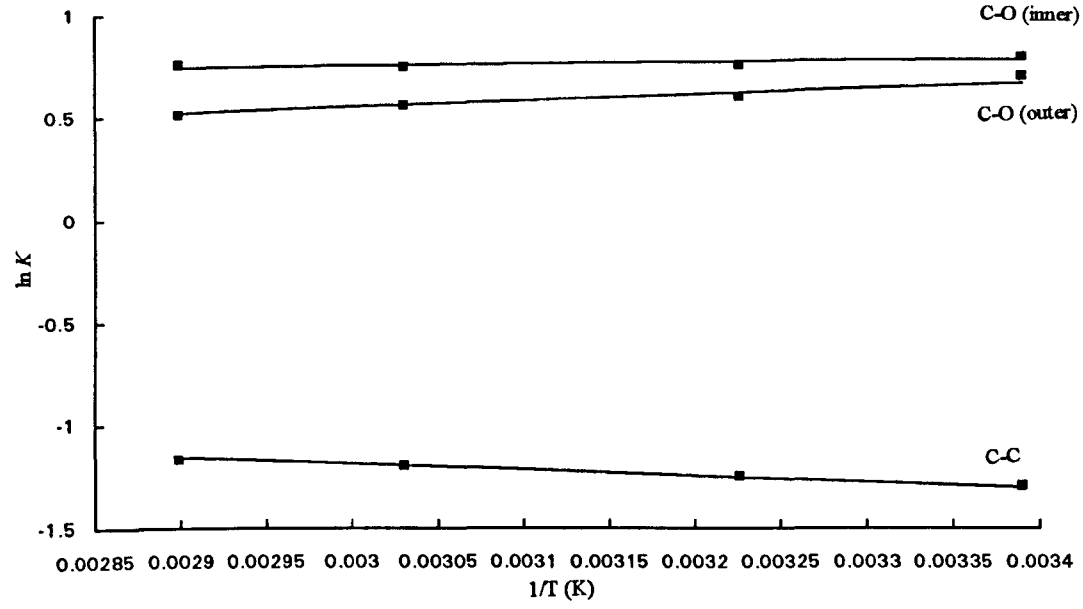

Figure 2.2 (c) Temperature dependence of K (= $t/g^{(+ \text{ and } -)}$) for three bonds of BMEE in C_6D_{12}.

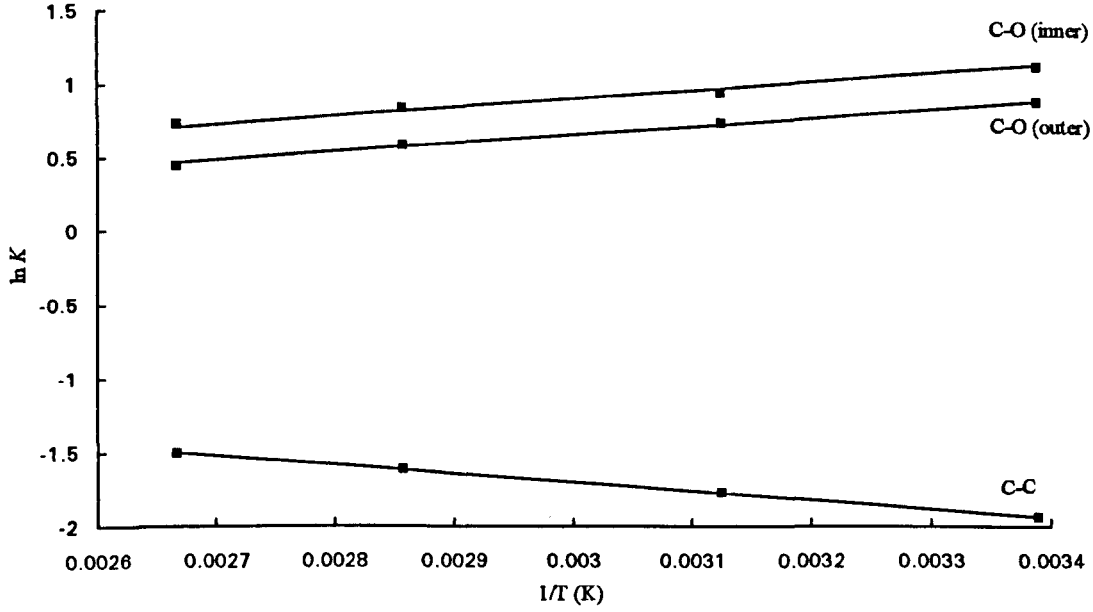

Figure 2.2 (d) Temperature dependence of K (= $t/g^{(+ \text{ and } -)}$) for three bonds of BMEE in DMSO-d_6.

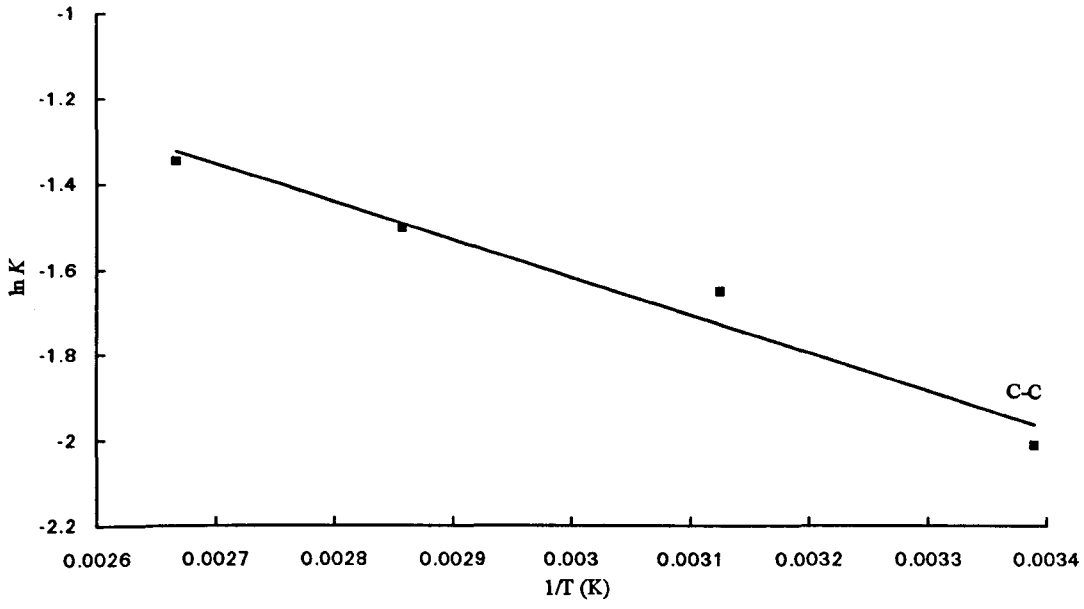

Figure 2.2 (e) Temperature dependence of K (= $t/g^{(+ \text{ and } -)}$) for C-C bonds of PEO 6000 in dioxan-d_8.

Table 2.6 (a) Full ^{1}H data of DME in toluene-d_8 at various temperatures.

Temperature K	Chemical shift (ppm)		Coupling constants (Hz)		% *gauche* about C-C bond
	CH_3	CH_2	$^3J_{ab}$	$^3J_{ab'}$	
350	3.16	3.35	6.01	4.21	79.0
320	3.15	3.33	6.01	4.07	81.5
295	3.13	3.32	6.11	4.00	81.3
250	3.10	3.28	6.07	3.71	84.5
230	3.09	3.26	6.16	3.40	88.0

Table 2.6 (b) Full ^{13}C data of DME in toluene-d_8 at various temperatures.

Temperature K	Chemical shifts (ppm)		Coupling constants (Hz)					*trans* and *gauche* couplings (Hz)[a]		% *gauche* about C-O bond[b]
	CH_3	CH_2	$^1J_{C(1)H}$	$^1J_{C(2)H}$	$^2J_{C(2)H(3)}$	$^3J_{C(1)H(2)}$	$^3J_{C(2)H(1)}$	J_t	J_g	
350	58.65	72.46	140.0	140.9	2.54	3.82	5.13	11.00	2.20	36.9
320	58.65	72.36	139.9	140.3	2.46	3.69	5.13	11.00	2.20	33.9
295	58.66	72.29	140.0	139.9	2.49	3.57	5.10	10.93	2.19	31.6
250	58.64	72.16	140.0	139.8	2.47	3.37	5.11	10.95	2.19	26.8
230	58.62	72.10	140.3	139.8	2.46	3.14	5.11	10.95	2.19	21.7

[a] Obtained from $^3J_{C(2)H(1)}$
[b] Obtained from $^3J_{C(1)H(2)}$

Table 2.7 (a) Full ^1H data of DME in C_6D_6 at various temperatures.

Temperature K	Chemical shift (ppm)		Coupling constants (Hz)		% *gauche* about C-C bond
	CH_3	CH_2	$^3J_{ab}$	$^3J_{ab'}$	
295	3.26	3.41	6.02	4.25	78.6
310	3.26	3.41	5.97	4.34	77.6
330	3.26	3.42	5.98	4.39	77.0
345	3.27	3.42	5.97	4.45	76.4

Table 2.7 (b) Full ^{13}C data of DME in C_6D_6at various temperatures.

Temperature K	Chemical shifts (ppm)		Coupling constants (Hz)					*trans* and *gauche* couplings (Hz)[a]		% *gauche* about C-O bond[b]
	CH_3	CH_2	$^1J_{C(1)H}$	$^1J_{C(2)H}$	$^2J_{C(2)H(3)}$	$^3J_{C(1)H(2)}$	$^3J_{C(2)H(1)}$	J_t	J_g	
295	58.86	72.78	139.7	139.7	2.58	3.81	5.16	11.06	2.21	36.2
310	58.86	72.82	139.8	139.7	2.59	3.82	5.16	11.06	2.21	36.3
330	58.85	72.87	140.0	139.7	2.60	3.95	5.14	11.01	2.20	39.6
345	58.85	72.92	140.0	139.7	2.58	3.95	5.14	11.01	2.20	39.5

[a] Obtained from $^3J_{C(2)H(1)}$
[b] Obtained from $^3J_{C(1)H(2)}$

Table 2.8 (a) Full ^1H data of BMEE in C_6D_{12} at various temperatures.

Temperature K	Chemical shift (ppm)			Coupling constants (Hz)		% *gauche* about C-C bond
	CH(1)	CH(2)	CH(3)	$^3J_{ab}$	$^3J_{ab'}$	
295	3.26	3.52	3.41	6.02	4.26	78.5
310	3.27	3.52	3.41	6.01	4.33	77.7
330	3.27	3.52	3.42	5.99	4.42	76.8
345	3.27	3.52	3.42	5.99	4.47	76.2

Table 2.8 (b) Full ^{13}C data of BMEE in C_6D_{12} at various temperatures.

Temperature K	Chemical shift (ppm)			Coupling constants (Hz)							
	C(1)H	C(2)H	C(3)H	$^1J_{C(1)H}$	$^1J_{C(2)H}$	$^1J_{C(3)H}$	$^2J_{C(2)H(3)}$	$^2J_{C(3)H(2)}$	$^3J_{C(1)H(2)}$	$^3J_{C(2)H(1)}$	$^3J_{C(3)H(3')}$
295	58.61	72.66	71.18	139.8	140.1	140.4	2.47	2.81	3.63	5.09	3.53
310	58.83	72.93	71.44	139.8	140.2	140.5	2.42	2.78	3.74	5.10	3.59
330	58.84	73.99	71.49	139.8	140.2	140.5	2.43	2.78	3.82	5.15	3.63
345	58.83	73.04	71.53	139.9	140.1	140.6	2.46	2.76	3.89	5.20	3.64

Table 2.8 (b) continued

Temperature K	*trans* and *gauche* couplings (Hz)[a]		% *gauche* C-O, outer bond[b]	% *gauche* C-O, inner bond[c]
	J_t	J_g		
295	10.90	2.18	33.2	31.1
310	10.94	2.19	35.5	32.1
330	11.03	2.20	36.5	32.2
345	11.12	2.22	37.5	32.0

[a] Obtained from $^3J_{C(2)H(1)}$
[b] Obtained from $^3J_{C(1)H(2)}$
[c] Obtained from $^3J_{C(3)H(3')}$

Table 2.9 (a) Full ^{1}H data of BMEE in DMSO-d_6 at various temperatures.

Temperature K	Chemical shift (ppm)			Coupling constants (Hz)		% *gauche* about C-C bond
	CH(1)	CH(2)	CH(3)	$^3J_{ab}$	$^3J_{ab'}$	
295	3.25	3.51	3.43	6.23	3.45	87.4
320	3.25	3.52	3.43	6.18	3.62	85.5
350	3.26	3.52	3.44	6.12	3.81	83.4
375	3.26	3.53	3.44	6.09	3.96	81.8

Table 2.9 (b) Full ^{13}C data of BMEE in DMSO-d_6 at various temperatures.

Temperature K	Chemical shift (ppm)			Coupling constants (Hz)							
	C(1)H	C(2)H	C(3)H	$^1J_{C(1)H}$	$^1J_{C(2)H}$	$^1J_{C(3)H}$	$^2J_{C(2)H(3)}$	$^2J_{C(3)H(2)}$	$^3J_{C(1)H(2)}$	$^3J_{C(2)H(1)}$	$^3J_{C(3)H(3')}$
295	58.07	71.40	69.71	140.6	140.3	140.5	2.28	2.44	3.48	5.10	3.27
320	58.10	71.48	69.78	140.5	140.5	140.5	2.27	2.48	3.61	5.11	3.43
350	58.13	71.59	69.88	140.5	140.5	140.8	3.34	2.48	3.75	5.09	3.51
375	58.14	71.68	69.97	140.3	140.5	140.1	2.34	2.50	3.88	5.08	3.59

Table 2.9 (b) continued

Temperature K	*trans* and *gauche* couplings (Hz)[a]		% *gauche* C-O, outer bond[b]	% *gauche* C-O, inner bond[c]
	J_t	J_g		
295	10.92	2.19	29.7	24.9
320	10.95	2.19	32.4	28.2
350	10.91	2.18	35.9	30.4
375	10.89	2.18	39.2	32.5

[a] Obtained from $^3J_{C(2)H(1)}$
[b] Obtained from $^3J_{C(1)H(2)}$
[c] Obtained from $^3J_{C(3)H(3')}$

Table 2.10 Full ^{1}H data of PEO 6000 in DMSO-d_6 at various temperatures.

Temperature K	Chemical shift (ppm)	Coupling constants (Hz)		% *gauche* about C-C bond
		$^3J_{ab}$	$^3J_{ab'}$	
295	3.51	6.28	3.37	88.2
320	3.51	6.11	3.76	83.9
350	3.52	6.08	3.96	81.8
375	3.53	5.90	4.18	79.3

2.4 Discussion

The rotamer populations in table 2.1 underline and extend earlier, corrected deductions for NMR measurements, which were not based on direct, iterative fitting of the couplings.[135] They show the smaller $^3J_{HH}$ coupling to be even smaller than previously measured, especially in D_2O. This means that the C-C bond can be as much as 98 % *gauche* in some solvents. The simple rotational isomeric state (RIS) analysis, described in section 1.8.8, emphasises this further by estimating the *gauche* probability for an isolated bond, *i.e.* by disentangling this from the pentane effect in the complete molecule, which itself tends to favour *trans* rotamers. In its absence, the total *gauche* probability about the C-O bond rises to between 22 % and 34 % at 295 K, and of course higher at 353 K. The calculation is certainly naive in assuming that the rotamer populations are determined solely by the rotational properties of individual bonds, plus a pentane effect. Nevertheless, it does reproduce a general trend of the DME plus BMEE data that the *gauche* probability increases at the outer C-O bonds.

The NMR data, particularly in benzene and dioxan, fit well with electron diffraction data (see table 1.1) on DME.[141] These gas-phase data should compare closely with the data in a non-polar solvent, such as benzene, and also with the dioxan data, because Abe and Inomata[137] have shown that the NMR couplings for gaseous DME extrapolate almost linearly with temperature from those in the liquid phase. The diffraction data points to dominance of the *tgt* and *tgg* conformations with the C-C bond 79 % *gauche* and the C-O bonds each 36 % on average, at 273 K. Our corresponding NMR values in dioxan at 295 K are 82 % and 33 %.

Our NMR data also fit well with the σ and σ' RIS parameters deduced thirty years ago in Flory's classical papers[147,148] (section 1.8.7) from the variation of stress,

characteristic ratio and dipole moment of PEO with temperature. Mark and Flory's σ' factor, the $g^{(+ \text{ or } -)} / t$ probability for the C-C bond alone, ranged from 1.8 to 2.07, at 60 °C in good solvents such as benzene (see section 1.8.7). The equivalent figures from our 80 °C data are 2.1 in dioxan and 2.8 in DMSO. For C-O rotations, *i.e.* for the σ factor, Mark and Flory quote 0.055-0.220 as an acceptable range of fits to 60 °C data, with most of their calculations giving figures towards the higher end of this range. Our 80 °C figures are 0.16 (dioxan) and 0.15 (DMSO). Thus our methylated monomer and dimer data strongly support Mark and Flory's earlier deduction of a substantial *gauche* rotameric population about both bond types, but predict it to be even larger in some solvents. These deductions are supported by our direct measurements on the non-terminal parts of PEO at 353 K in dioxan and DMSO, for these show very similar proportions of *gauche* rotamers to the average of those in BMEE. The extrapolation from oligomer to polymer is also supported in table 2.1 by the 295 K data on PEO.

The solution data also fits well with either *ab initio* or parameterised force field gas-phase calculations (table 1.1), for these predict around 79 % of *gauche* C-C and 27 % of *gauche* C-O rotamers at 273 K.[1] However, Smith *et al.* predict a rather lower probability of 20 % for C-O *gauche* in the liquid state. They attributed this drop to intermolecular competition for strong 1.5 CH...O electrostatic interactions. Our observations in, *e.g.* dioxan solution do not support this, although we do observe a comparably lower proportion of C-O *gauche* in H-bonding solvents.

The solvent influences listed in table 2.1 yield a regular countertrend, within experimental error. The proportion of *gauche* C-O bonds falls as that of *gauche* C-C bonds rises, even after allowance for the pentane effect. This may be because of the different local dipoles in the various subunit rotamers. For example, the *tgt* conformer might be favoured over *tgg* and *ttt*, perhaps because it best permits interaction with a

solvent molecule. However, this countertrend may also be a subtle influence of long-range excluded volume effects, in a polymer with such a high proportion of *gauche* bonds. A second trend is that the proportion of *gauche* C-O bonds correlates with the Taft H-bond donor (α_1) and acceptor (β_1) properties of the solvent,[150] with the donor properties having markedly the greater weighting. This explains why chloroform has such a strong influence. It is probably affecting the C-O bonds through the *gauche*-oxygen effect,[151] by H-bonding to the oxygen lone pairs. The weaker, additional influence of the solvent acceptor properties is only apparent in the other three solvents. Their Taft β_1 parameters are in the order DMSO > dioxan > benzene, which is the reverse of the % C-O *gauche* order. This may reflect the proposal from Smith *et al.*, noted above, that an acceptor solvent disrupts internal H-bonding in the ether. Earlier work proposed that the influence of the solvent on PEO was mediated by the solvent dielectric. Our data, using a wider range of solvents, does not fully support this analysis, but instead shifts the emphasis towards H-bonding by the solvent.

The conformations of the endgroups listed in table 2.4 show that water, DMSO-d_6, CD_3CN, methanol-d_4 and acetone-d_6 reduce the probability of the terminal C-C bond being *gauche*, whereas benzene-d_6 and dioxan-d_8 increase it. The differences between the inner and the terminal groups must very largely arise from the -OH group on the latter. It is probable that this forms H-bonds to water, DMSO-d_6, CD_3CN, methanol-d_4 or acetone-d_6 and that these have the effect of extending the group out from the polymer into the solvent. Benzene-d_6 and dioxan-d_8, on the other hand, may cause the chain end to turn inwards and H-bond to other parts of the polymer chain instead.

Contributions from $\Delta S^{\ominus}$ are often ignored in comparisons between experiment and theory. The observations in table 2.5 may show that some of the remaining

discrepancies arise because the non-statistical contributions to ΔS are not in fact negligible, especially in the case of the polymer.

Unfortunately, no ^1H shift pattern could be determined for either DME, BMEE or PEO in any solvent. However, the data in tables 2.6 and 2.7 show the methylene resonance of DME shifts downfield with increasing temperature. The same is observed for PEO (table 2.10). Since there is a lower proportion of *gauche* about the C-C bond at higher temperatures, the *trans* rotamer is likely to have a higher average chemical shift relative to *gauche*. Björling *et al.*[152] calculated the fraction of *gauche* about the C-C bond of PEO using the methylene chemical shift. In contrast to DME and PEO, the methylene resonance of BMEE shows surprisingly very little variance with temperature, suggesting that the *gauche* and *trans* rotamers for this molecule have similar shift positions. There is little influence on the ^1J and ^2J coupling constants of DME by the solvent, with the exception of D_2O.

As stated before, the $^3J_{HH}$ couplings for the *gauche* and *trans* rotamers (*i.e.* 2.3 Hz and 11.4 Hz respectively) used in our calculations were taken from the work of Abe and Tasaki and assumed to be the same in all solvents and temperatures. We acknowledge that our calculated *gauche* probabilities about the C-C bond in each case heavily relies on the values chosen for both ^3J_g and ^3J_t (*e.g.* a 0.1 Hz change in the ^3J_g coupling constant can induce a 1 % error in the calculation for each rotamer population). However, there is no other evidence presently available to suggest the use of different values for either ^3J_g or ^3J_t.

CHAPTER THREE

Optical Microscopy Study on the Interaction of Cellulose Fibres With Amine Oxides

3.1 Introduction

The purpose of the remaining part of this study was to investigate the interaction of cellulose with amine oxides. This chapter starts this investigation by recording the visible interaction (*e.g.* swelling, dissolution, *etc.*) between various cellulose fibres and amine oxides, with an optical microscope. Of particular interest were regions on each fibre where the interaction commences and to what extent swelling occurs during dissolution. The phenomenon of "ballooning" was also of interest. "Ballooning" refers to localised swelling that occasionally occurs in some cellulose fibres (see section 3.3.2.1).

3.2 Experimental

In this study an Olympus optical microscope fitted with a Linkam hot stage was used. Images were recorded using a Panasonic monochrome video camera connected to a video recorder. During the latter stages of this work, polarising filters were fitted to the microscope to give greater contrast and thus higher quality images.

Fibres were sandwiched between two cover slips with the amine oxide introduced to each sample by capillary action. The hot stage was then heated to the required temperature.

Below is a list of amine oxides used for this investigation. All were used in combination with water except PNO (concentrations w/w in parentheses):

1. N-methylmorpholine-N-oxide (NMMO) (78.55 %, 81.2 % and 83.6 %) donated by Courtaulds Research.
2. N-ethylmorpholine-N-oxide (NEMO) (90 %) synthesised in our laboratory as described below.
3. Trimethylamine-N-oxide (TMAO) (68 %) obtained from Aldrich Chemicals.
4. Pyridine-N-oxide (PNO) (100 %) obtained from Lancaster Chemicals.

NMMO is the only amine oxide in the above list that will dissolve cellulose; the others are non-solvents.

Four fibre types were used in this study; ramie, hard and softwood pulp, and Avicel microcrystalline cellulose. These were all donated by Courtaulds Research.

All experiments on ramie fibres were conducted at a temperature of 100 °C, unless otherwise stated. Experiments on pulp fibres were performed at 80 °C when NMMO concentrations of 83.6 % and 81.2 % was used. The temperature was raised to 100 °C when an NMMO concentration of 78.55 % was used, to reduce the time required for the analysis.

3.2.1 Synthesis of N-ethylmorpholine-N-oxide (NEMO)

NEMO was prepared by the oxidation of N-ethylmorpholine with 3-chloroperoxybenzoic acid (both obtained from Lancaster Chemicals). The procedure adopted was similar to that published by Cymerman-Craig and Purushothman.[153]

A solution of 1.0 M of 3-chloroperoxybenzoic acid in CH_2Cl_2 was added gradually to an ice cooled solution of 1.0 M of the amine in CH_2Cl_2. The reaction was left for about 3 hours, during which the solution was allowed to come to room temperature.

The solution was passed through a column of alkaline alumina (100 mesh and 20 times the weight of the starting materials). Traces of unreacted amine were removed by washing with CH_2Cl_2. An NEMO solution was then eluded from the column with a 1:3 mixture of methanol-CH_2Cl_2. After rotary evaporation of CH_2Cl_2 at about 60 °C, an azeotrope of NEMO-methanol remained. This mixture was successfully separated by adding benzene several times during the rotary evaporation procedure until the NEMO crystallised.

3.3 Results

A summary of data obtained from the optical microscopy experiments is shown in table 3.1. A full report of the various types of behaviours observed with ramie, wood-pulp and MCC fibres in various amine oxide solutions is described below. Photographs showing the behaviours of some cellulose fibres in different amine oxide solutions are shown in figures 3.1 to 3.8.

Table 3.1 Summary of data obtained from microscopy experiments on various cellulose fibres.

Fibre	Amine oxide (w/w in water)	Temperature °C	Dissolution time observed (mins)			Comments
			minimum	maximum	average	
Ramie	78.55 % NMMO	100				No visible change observed.
Ramie	78.55 % NMMO	125				Swelled up to 2.7 times their diameter without dissolution.
Ramie	81.2 % NMMO	100	<1	>15	7	Some fibres swelled uniformly (up to 6 times fibre diameter, ave = 2.5 times) before dissolution, others burst into fragments or became "zigzagged" before dissolution. Some also swelled without dissolution.
Ramie	83.6 % NMMO	100	1	6	2.5	Most fibres dissolved without swelling, but occasionally some 'zigzagging' and swelling did occur. Some fibres were also observed to burst into fragments before dissolution.
Ramie	83.6 % NMMO	80				Fibres swelled up to 5 times their diameter without dissolution.
Ramie	90 % NEMO[a]	100				Swelled by about 45 % across fibre axis during the first 15 minutes.
Ramie	68 % TMAO[a]	100				Swelled by about 45 % across fibre axis during the first 15 minutes.
Ramie	100 % PNO[a]	100				No change to the fibre was observed.
Soft-wood pulp	78.55 % NMMO	100	<1	25	12	"Ballooning" was most likely to occur in fibres that took longest to dissolve.
Soft-wood pulp	81.2 % NMMO	80	<1	25	8	"Ballooning" rarely observed. Most fibres split along the fibre length, drifted away and dissolved. When the temperature was raised to 100 °C, fibres dissolved in less than a minute.
Soft-wood pulp	83.6 % NMMO	80	<1	25	6.5	All fibres dissolved without any "ballooning."
Hard-wood pulp	78.55 % NMMO	100				Little change observed.
Hard-wood pulp	81.2 % NMMO	80	<1	10	3.7	"Ballooning" rarely observed.
Hard-wood pulp	83.6 % NMMO	80				Dissolves in less than a minute.
MCC	81.2 % NMMO	80	<1	8	4	No swelling observed, most fibres became thinner until their image became unobservable.

[a] Non-solvent for cellulose

3.3.1 Ramie fibres

3.3.1.1 78.55 % NMMO

With an NMMO concentration of 78.55 % at 100 °C no visible change was observed. When the temperature was raised to 125 °C, ramie fibres swelled up to 2.7 times their diameter without dissolution.

3.3.1.2 81.2 % NMMO

With an NMMO concentration of 81.2 % at 100 °C both swelling and dissolution of fibres were observed. Some fibres dissolved with little or no swelling, others swelled significantly before dissolving and others swelled without completely dissolving during the time allowed for each experiment (at least 20 minutes). Certain ramie fibres dissolved in less than one minute while others took more than 15 minutes (standard deviation = 4.3 mins). The average swelling observed was 2.5 times the fibre diameter, however, some swelled by as much as 6 times.

It has been known for some time that dislocation marks exist along certain fibres such as those observed with ramie.[154] These dislocation marks could be described as "weak points," and during the present study, swelling and dissolution of ramie fibres often commenced at these regions. Sometimes these "weak points" would cause the fibres to explode into tiny fragments before dissolving (figure 3.1). On other occasions ramie fibres were observed to break at these dislocation marks creating a "zigzag" pattern (figure 3.2). This "zigzagging" is probably caused by a contraction of the outer layers of the fibre. To the best of our knowledge "zigzagging" has not been previously observed, but a reduction in the length of regenerated fibres (cellulose II) was observed by Chanzy *et al.*[155] They suggested that this reduction of fibre length occurs because of 'relaxation of highly oriented cellulose molecules.' Alternatively, "zigzagging" could be caused by the introduction of bent glycosidic linkages in cellulose chains located on the outer layers

of the fibre, under the influence of solvent. These would have the effect of shortening the polymer chains in their long dimension and thus the resulting reduction of the fibre length causes it to break at the weakest points, most likely where dislocation marks occur.

Although most fibres start swelling at certain regions, occasionally some fibres swell uniformly before dissolving without "zigzagging" or fragmentation occurring (figure 3.3). Once swollen, the fibres appear to become thinner until their image fades away and becomes unobservable.* Sometimes, however, fibres swell but resist being completely dissolved during the given time for the experiment. No correlation could be deduced between the fibre diameter and the time required for dissolution or maximum swelling. However, "zigzagging" is less likely to occur with the thickest fibres, possibly because these fibres are more difficult to break than thinner ones.

3.3.1.3 83.6 % NMMO

An NMMO concentration of 83.6 % at 100 °C was generally observed to dissolve fibres without swelling (figure 3.4). The average dissolution time under these conditions was 2.5 minutes with a standard deviation of 1.6 mins. Occasionally some swelling and "zigzagging" did occur but infrequently. Most dissolution started at the "weak points" and spread to the rest of the fibre. As observed in experiments using an NMMO concentration of 81.2 %, these points would sometimes cause the fibre to burst into fragments before the fibre dissolved.

When a temperature of 80 °C was used, the fibres swelled by up to 5 times their diameter without dissolving.

* The image would fade either because of the occurrence of dissolution or because as the fibre swells its refractive index becomes equal to the surrounding solvent and thus be indistinguishable from the solution.

3.3.1.4 Non-solvents

Ramie fibres were observed to swell uniformly by about 45 % across the fibre axis when heated with 90 % NEMO (figure 3.5) or 68 % TMAO (not shown), at 100 °C. Most of the swelling occurred during the first 15 minutes of the experiment, and very little change occurred thereafter.

No swelling of ramie fibres was observed with PNO at 100 °C. As a comparison, no visible change was also observed when ramie fibres were heated to 90 °C in distilled water.

3.3.2 Softwood pulp fibres

3.3.2.1 78.55 % NMMO

At 100 °C softwood fibres took an average of 12 minutes to dissolve with a standard deviation of 7.8 mins. The "ballooning" effect was occasionally observed before dissolution occurred (figure 3.6). On one occasion a single fibre was observed to swell to about three times its diameter before dissolving. "Ballooning" was more likely to occur in fibres that took the longest to dissolve.

3.3.2.2 81.2 % NMMO

At 80 °C "ballooning" or swelling was rarely observed. The average dissolution time was 8 minutes with a standard deviation of 4 mins. Most fibres split along the fibre length, drifted away and dissolved (figure 3.7). When the temperature was set to 100 °C pulp fibres dissolved in less than a minute.

Loosening of intertwined fibrils occurred on some occasions before being dissolved, showing their twisted nature.

3.3.2.3 83.6 % NMMO

At 80 C no "ballooning" occurred and the average dissolve time was 6.5 minutes with a standard deviation of 3 mins.

3.3.3 Hardwood pulp fibres

Most experiments were carried out using 81.2 % NMMO at 80 C. "Ballooning" was rarely observed under these conditions. Most would split into fragments along the fibre length and dissolve. The average dissolution time was 3.7 minutes with a standard deviation of 2.6 mins.

When 83.6 % NMMO at 80 C was used no "ballooning" was observed, the fibres would simply break apart and dissolve in under a minute.

Little change was observed when an NMMO concentration of 78.55 % was used at a temperature of 100 C.

3.3.4 Microcrystalline cellulose (MCC)

MCC used in this work was the same as that used during the solid-state NMR experiments that will be discussed in chapter five. These fibres behaved in a similar fashion to pulp fibres. No swelling or "ballooning" was observed to occur. In 81.2 % NMMO at 80 C these fibres took an average of 4 minutes to dissolve, however some of them took up to 8 minutes to dissolve while others dissolved in less than a minute. In common with wood pulp, these fibres were often observed to split apart along the fibre length before dissolution. However, the images of most fibres would just fade until they

became unobservable, probably because of dissolution. Figure 3.8 shows a sequence of photographs of MCC dissolving in 81.2 % NMMO at 80 °C.

Parts of fibres were observed to flake off the surfaces and drift away. This is not surprising since MCC consist of small fibre particles and the cell walls would be less firmly held together.

3.5 Conclusion

Chanzy *et al.*[155] constructed a phase diagram showing the behaviours of ramie fibres at various temperatures and concentrations of amine oxides. They stated that the boundaries between swelling, dissolution preceding swelling, non-activity, *etc.* were not clear cut. The present investigation showed that the time required to dissolve cellulose fibres is very variable and thus we conclude that Chanzy *et al.* understated their observation.

The present study clearly shows that phase diagrams for fibres from various origins can be very different. Indeed, fibres of the same origin show different behaviours under identical conditions. Chanzy *et al.* suggested that the different ranges in their phase diagram may vary slightly with the crystallinity and morphology between cellulose samples. However, our study suggests that fibres from different origins can behave very differently. However, with all fibre types, there is a general trend that the average dissolution time increases with increasing concentration of NMMO.

One factor that may regulate the way the fibre dissolves or swells is the density and lignin content of the fibre outer walls.[156] Cell walls with a high lignin concentration have been found to disfavour the "ballooning" effect. A wall of greater strength would resist

dissolution, whereas a weak one would be more likely just to break apart. Greater retaining action of the cell outer walls, *i.e.* the P and S_1 layers (see section 1.4.9), would facilitate the "ballooning effect," and if these layers are removed then the fibre can swell uniformly.[156]

Other factors that could determine the swelling and dissolution behaviour of fibres are the number and nature of "weak points," the DP of the cellulose, microfibril width and the presence of voids, pores and channels. This study has shown that there is a large distribution of dissolution rates recorded for fibres of the same origin under identical conditions and thus these factors may be significantly different between samples. Understanding why some fibres dissolve before others could have important consequences for *Tencel* manufacturing since a quicker process would be desirable.

Ramie fibres require more time to dissolve than the other fibres under the same conditions, probably because this source of cellulose is more crystalline than wood pulps and thus more dense. Another important factor is that ramie has a much higher DP than wood pulp making it harder to dissolve.

One final point is the ability of NEMO and TMAO to swell ramie fibres while PNO has no effect. This indicates that the interaction between some amine oxides with cellulose is strong enough to swell the polymer but too weak for dissolution to occur. Possible explanations for these observations will be discussed later.

This chapter has shown that although some amine oxides such as NEMO and TMAO can swell cellulose fibres, they are unable to dissolve them. Also, PNO was shown to have no visible effect on cellulose whatsoever. The next chapter will describe and discuss some solution-state NMR experiments on soluble model compounds for cellulose. These experiments began with the measuring of ^1H chemical shifts of NMMO and NEMO when

titrated with water or a soluble model compound for cellulose to determine binding constants between these molecules. The remaining experiments were based on the measurement of ^{13}C chemical shifts of some soluble cellulose model compounds when dissolved in various solvent and non-solvent amine oxide solutions, with the view of gaining a better understanding on their interaction with this polymer.

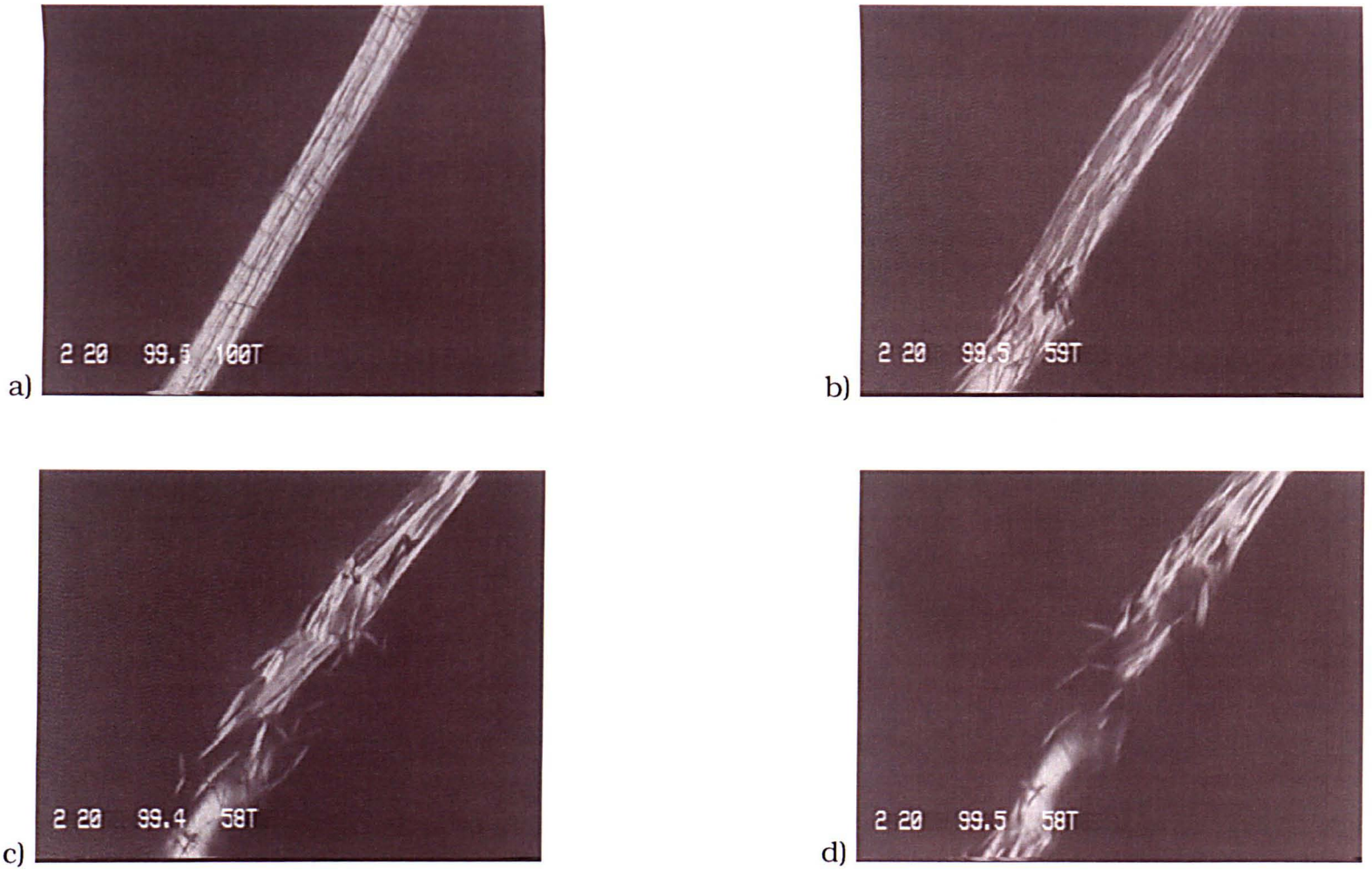

Figure 3.1 Ramie fibre in 81.2 % NMMO at 100 °C; a) initial b) after 1 minute c) after 2 minutes and d) after 2.5 minutes. (Scale is 10 microns per mm).

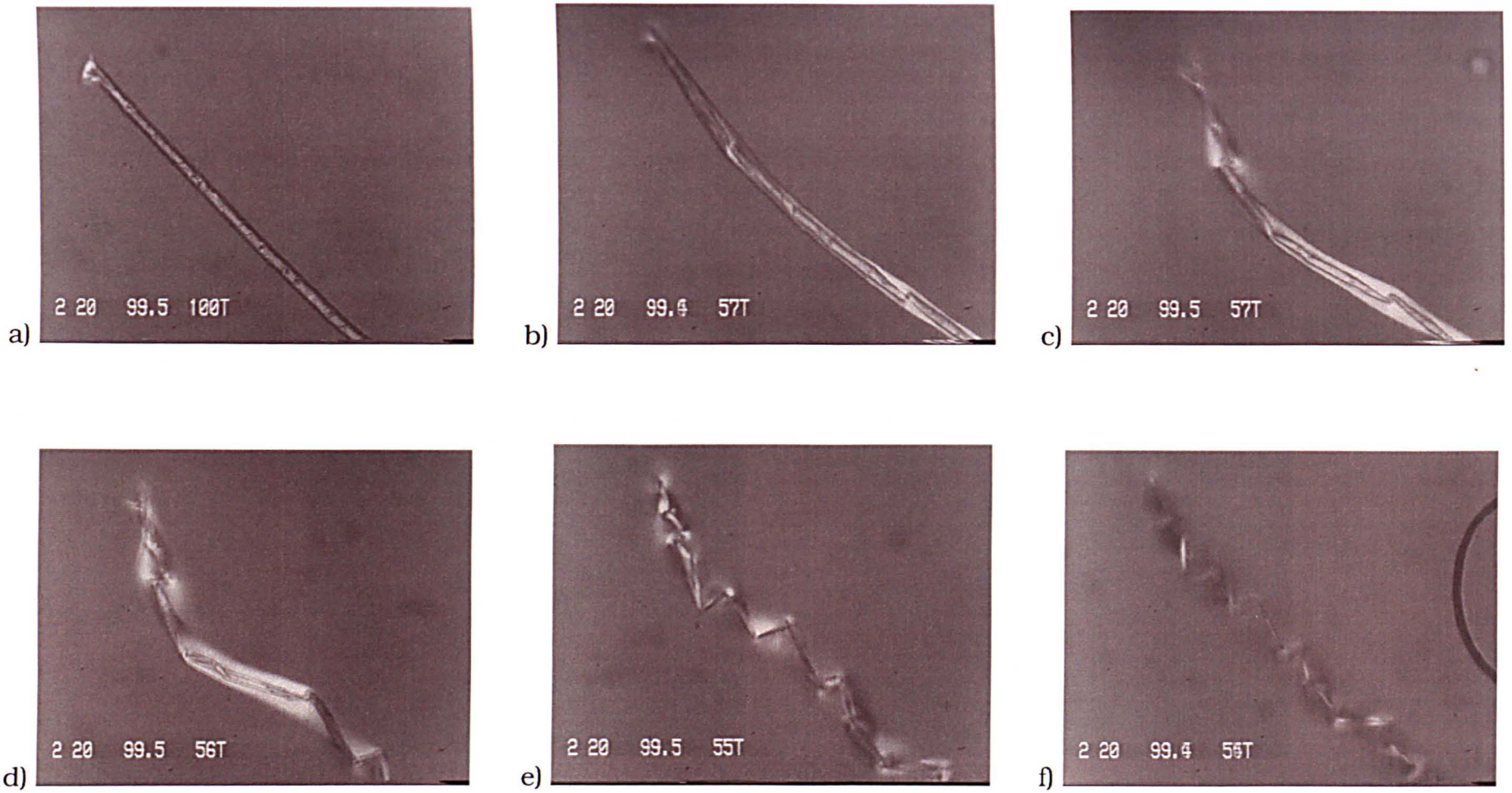

Figure 3.2 Ramie fibre in 81.2 % NMMO at 100 °C; a) initial b) after 3 minutes c) after 3.5 minutes d) after 4 minutes e) after 5 minutes and f) after 6 minutes. (Scale is 11 microns per mm).

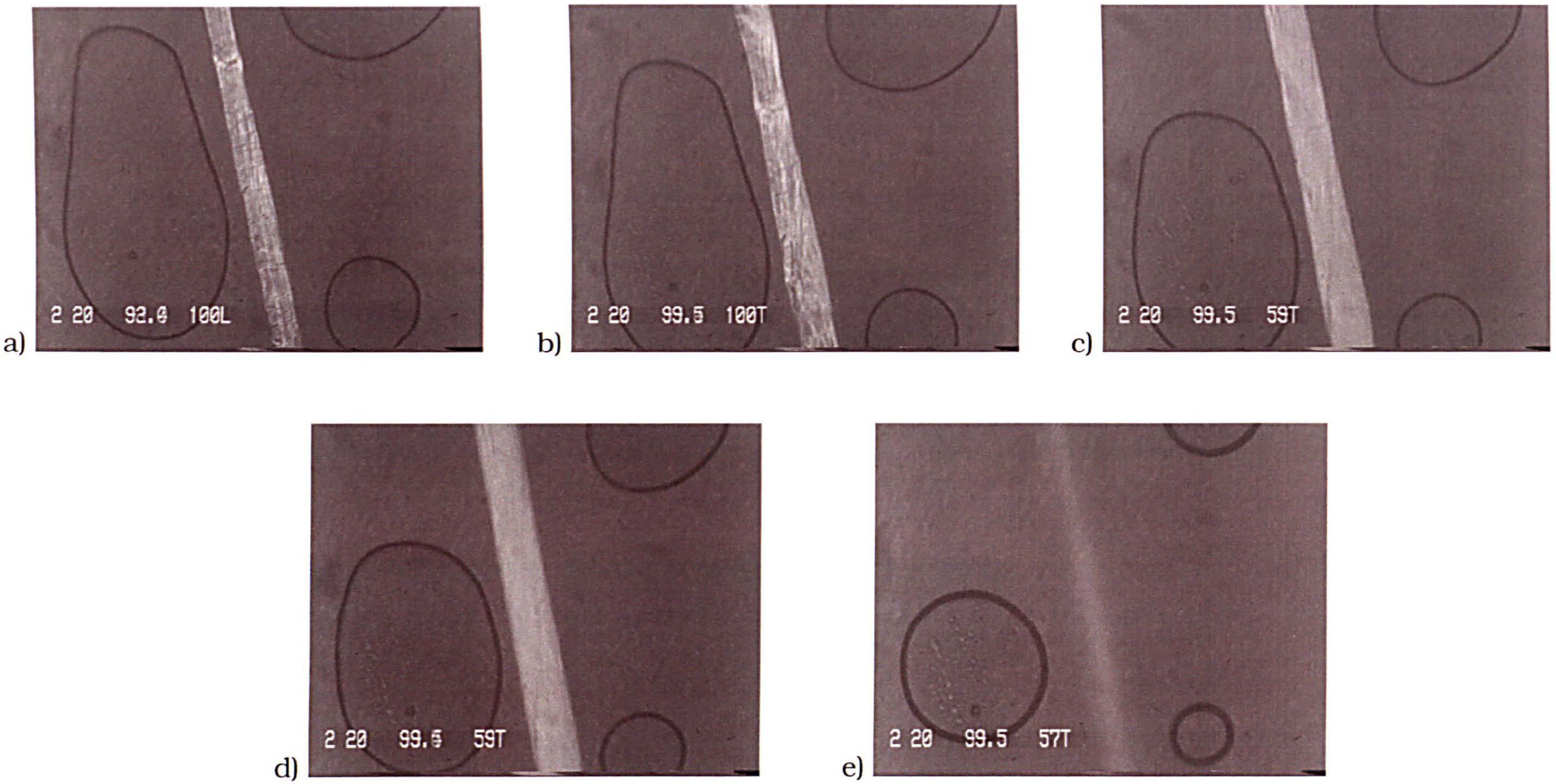

Figure 3.3 Ramie fibre in 81.2 % NMMO at 100 °C; a) initial b) after 0.5 minuute c) after 1 minute d) after 1.5 minutes and e) after 3 minutes. The circular objects are trapped pockets of air. (Scale is 11 microns per mm).

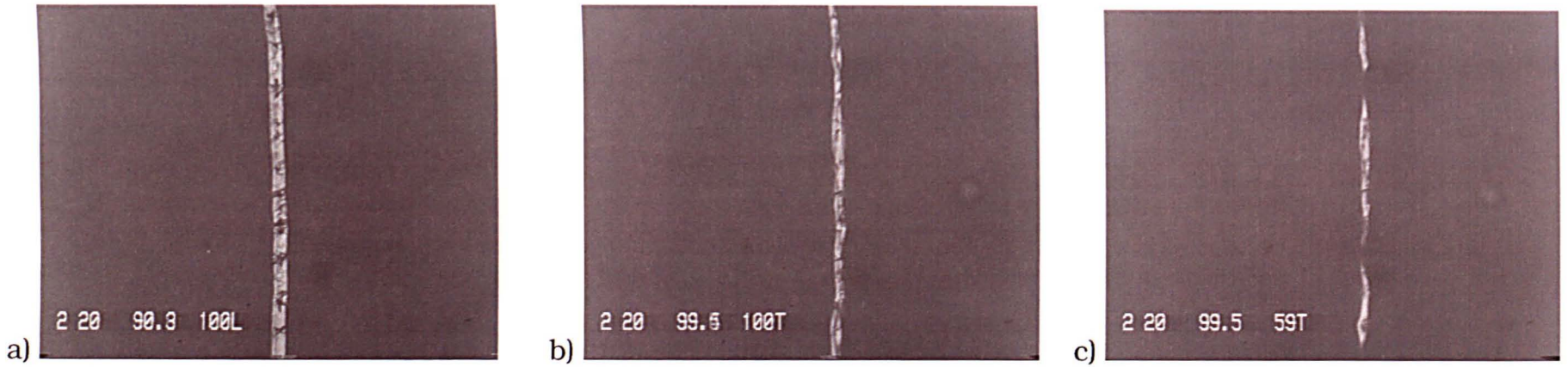

Figure 3.4 Ramie fibre in 83.6 % NMMO at 100 °C; a) initial b) after 0.5 minute and c) after 1 minute. (Scale is 11 microns per mm).

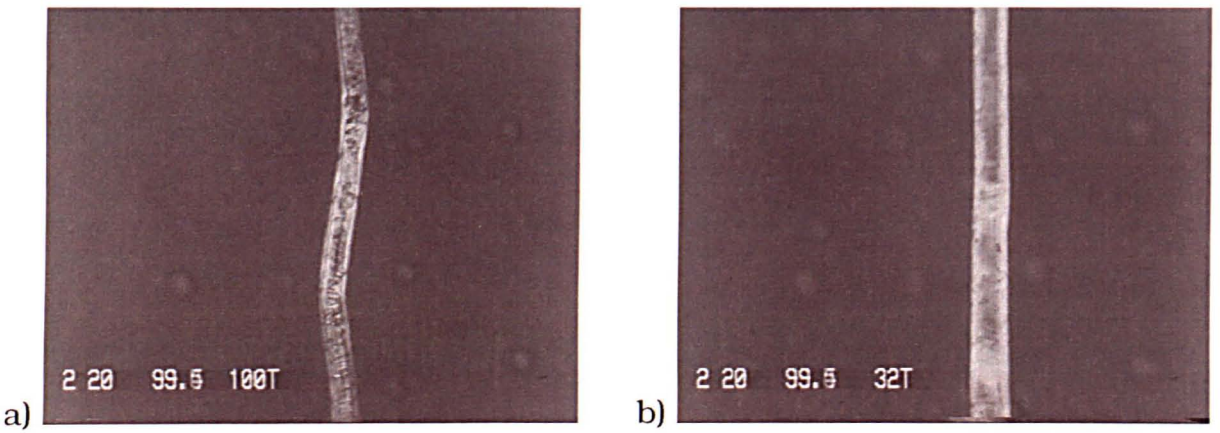

Figure 3.5 Ramie fibre in 90 % NEMO at 100 °C; a) inital and b) after 28 minutes. (Scale is 11 microns per mm).

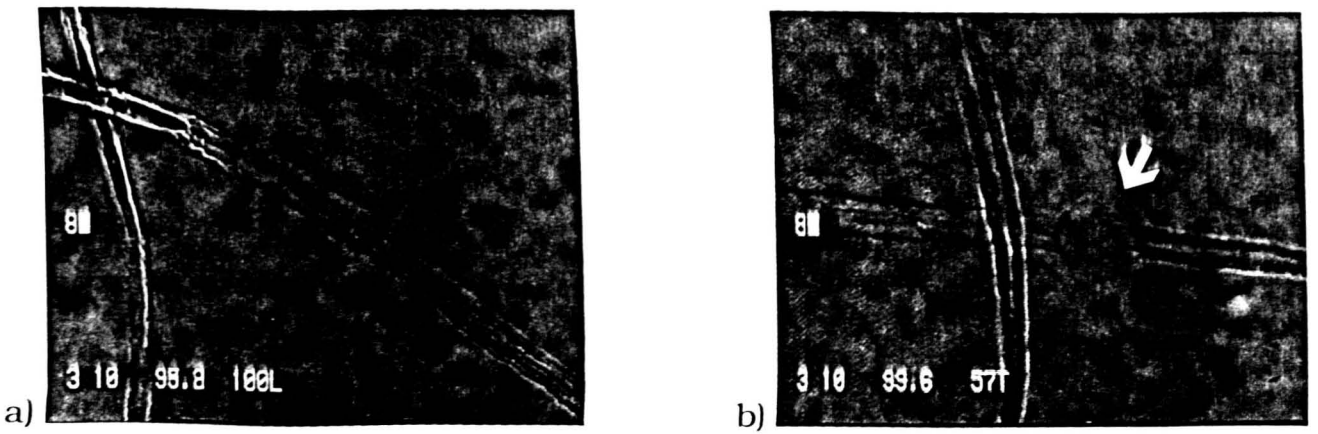

Figure 3.6 Softwood pulp fibre in 78.55 % NMMO at 80 °C; a) inital and b) after 3 minutes. (Scale is 4 microns per mm). Arrow indictates site of ballooning.

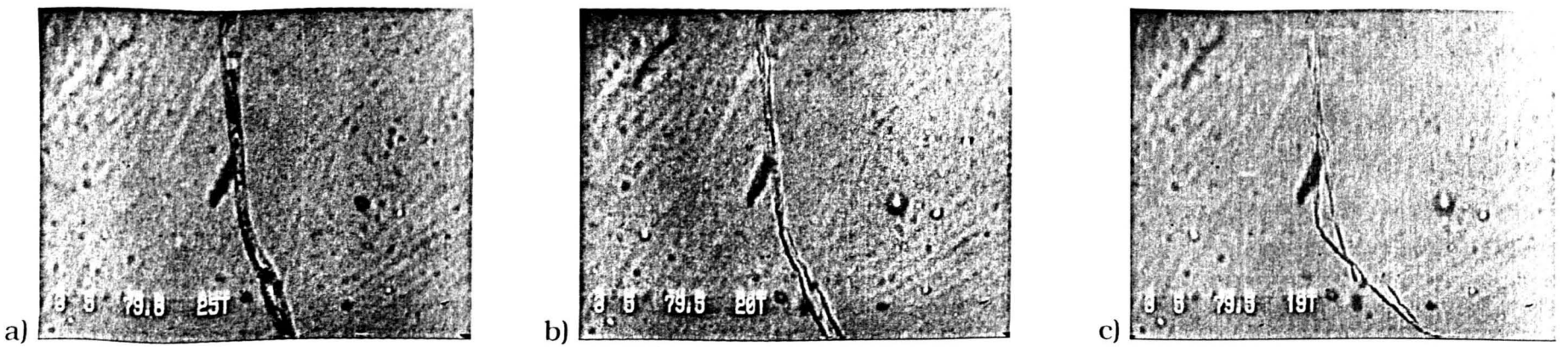

Figure 3.7 Softwood pulp fibre in 81.2 % NMMO at 80 °C; a) inital b) after 5 minutes and c) after 6 minutes. (Scale is 11 microns per mm).

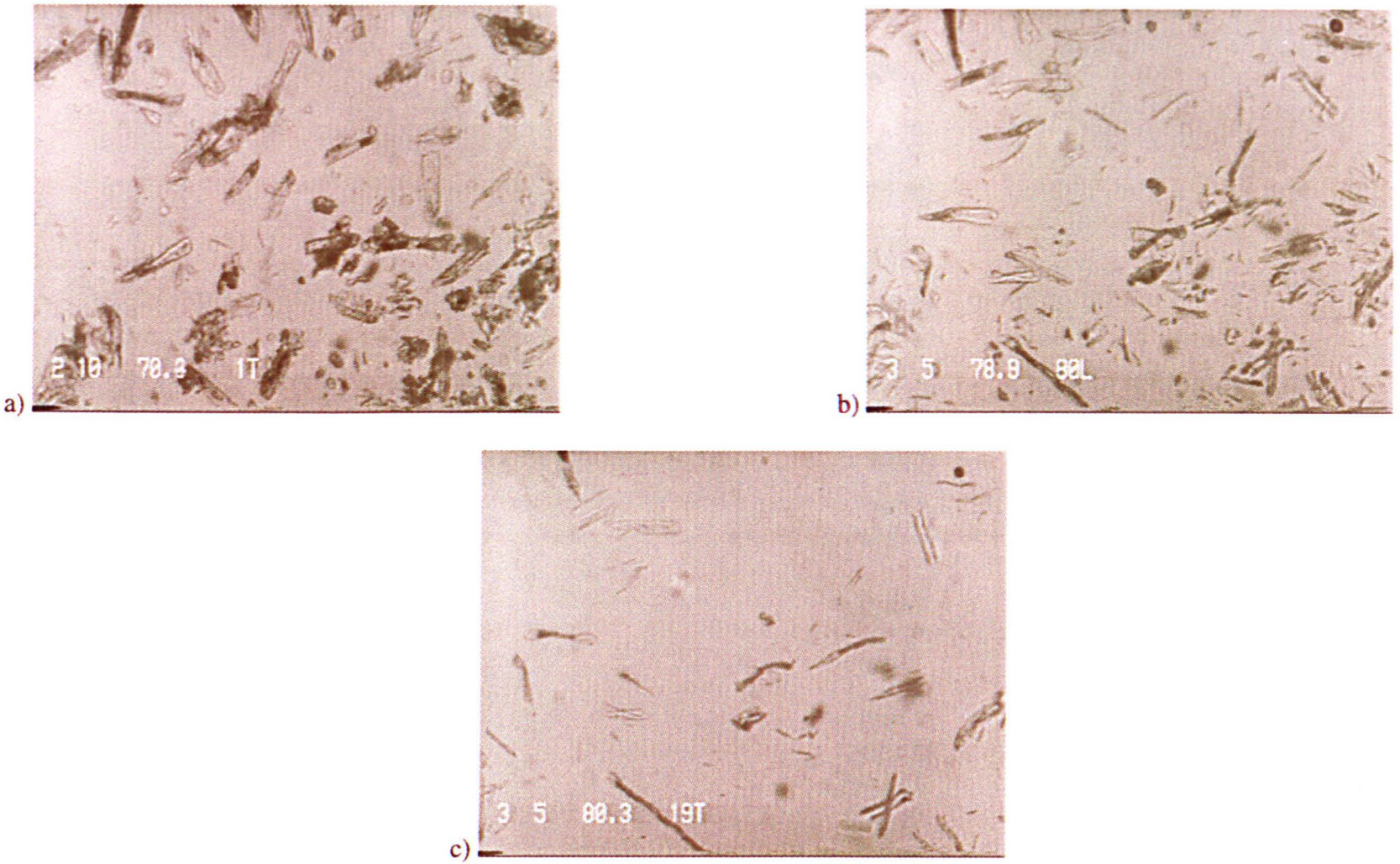

Figure 3.8 MCC in 81.2 % NMMO at 80 °C; a) initial b) after 1 minute and c) after 3 minutes. (Scale is 8 microns per mm).

CHAPTER FOUR

An Investigation of the Interaction of Amine Oxides With Cellulose Using Solution-State NMR Spectroscopy

4.1 Introduction

This chapter describes various ^{1}H and ^{13}C solution-state NMR experiments aimed at evaluating the interactions between amine oxides and cellulose. The intent was to obtain an insight on why some amine oxides dissolve cellulose while others do not. By comparing data obtained from both solvents and non-solvents for cellulose we hope to gain a better understanding of the dissolution of cellulose in certain amine oxides.

The first section of this chapter describes the determination of binding constants for NMMO with water and also with methyl-β-D-glucopyranoside as a soluble model compound of cellulose. The binding constants, K, were obtained by measuring ^{1}H NMR chemical shifts of NMMO on addition of water or methyl-β-D-glucopyranoside in varying amounts, and then fitting this data to an equation as described below. As a comparison, these experiments were also repeated with the non-solvent NEMO (N-ethylmorpholine-N-oxide) in place of NMMO. The purpose of these experiments was to determine how well NEMO binds to water and methyl-β-D-glucopyranoside, relative to NMMO. The relative ^{1}H shifts of NMMO may also help to reveal the active site of amine oxides.

Some NOE-difference experiments using NMMO / H_2O and NMMO / methyl-β-D-glucopyranoside samples were also run with the same hope of detecting the location on the amine oxide structure where water or saccharide molecules interact.

The second section of this chapter describes various ^{13}C solution-state NMR experiments, carried out with the purpose of gaining some information on how amine oxides interact with cellulose molecules during dissolution of this polymer. These experiments began by measuring carbon chemical shifts of cellobiose (a soluble model compound for cellulose) dissolved in various concentrations of NMMO solution. A comparison was then made between these shifts and the ones of cellobiose in pure water, *i.e.* the $\Delta\delta$ values. Our expectation was that these shifts would indicate the locations of interaction between NMMO and cellobiose.

The structures of cellobiose and methyl-β-D-cellobioside in the solid-state, according to Pizza and Eaton, are comparable to the approximate oligomers of mercerised and native cellulose respectively.[157] Pizza and Eaton also showed that these two saccharides can exist in several stable conformations. Their computational analysis revealed that the "fixing" of the most stable conformations are predominantly dependent on hydrogen bonding.

Carbon nT_1 values were measured using the same samples of cellobiose in various concentrations of NMMO as described above. These experiments were aimed at obtaining some information on the overall and the internal motions of cellobiose molecules in NMMO solutions compared with those in pure water. The nT_1 values obtained for C6 relative to the ring carbons as the concentration of NMMO increases may give some information on the local motions about the C5-C6 bond. If these data indicate an increase in the rotational freedom of the C5-C6 bond then this may suggest a hydrogen bond-breaking interaction between NMMO and cellobiose in this region of the molecule.

During the latter part of this study experiments were run using methyl-β-D-cellobioside as a soluble model compound for cellulose. This compound was used because, in

common with cellulose, it does not have a reducing end. These experiments involved measuring ^{13}C chemical shifts of methyl-β-D-cellobioside dissolved in various amine oxide solutions. Amine oxides that are solvents for cellulose as well as those reported to be non-solvents were used. Our expectation was that the non-solvents would cause smaller shifts and that the relative shifts might reveal the sites of interaction. To obtain spectra at a reasonable temperature all amine oxides in this study were used in aqueous solution.

Experiments were also run on methyl-β-D-cellobioside using sodium hydroxide solution as the solvent. The purpose of using a strong base, such as sodium hydroxide, was to determine if the carbon shifts observed for methyl-β-D-cellobioside arise simply from the basicity of the solvents or alternatively from a unique interaction between the amine oxides and the saccharide molecules.

4.2 Determination of binding constants for amine oxides (NMMO and NEMO) with water and methyl-β-D-glucopyranoside as a soluble model compound of cellulose

4.2.1 Experimental

4.2.1.1 Binding constant experiments between NMMO (or NEMO) and water

NMMO and NEMO were dried in a vacuum desiccator over phosphorus pentoxide. The vacuum was created with a rotary pump which was left running overnight. Some research groups have stated that sublimation[118] was required to prepare anhydrous NMMO, however, drying in a desiccator was found to be sufficient in our laboratory. DMSO-d_6 used in this work was dried for several days with 4Å molecular sieves.

Samples for NMR spectroscopy were prepared by dissolving about 20 mg of NMMO or NEMO in 0.6 ml of DMSO-d_6. Proton spectra were obtained on the initial samples and then with the addition of distilled water in steps of 1 µl to a maximum of 6 µl, then in steps of 2 µl to a maximum of 10 µl, and then one final addition of 4 µl making an overall water content of 14 µl for the last sample. In each case the mixture was shaken and allowed to equilibrate for a few minutes before scanning. The temperature was maintained at 295 K throughout the experiment and 16 transients with 64 k of data points were collected for each run.

During preliminary experiments the solvent peak of DMSO at 2.50 ppm was used as the absolute shift reference. However, subsequent experiments showed that the chemical shift of this peak was sensitive to the presence of both water and methyl-β-D-glucopyranoside. Although this sensitivity was small, the errors introduced into the calculation of binding constants were very significant. Therefore, DSS (2,2-dimethyl-2-silapentane-5-sulphonic acid sodium salt) dried in a desiccator over phosphorus

pentoxide was used as an internal shift reference at 0 ppm. DSS was chosen as the shift reference because it is a solid and thus easier to dry than a liquid such as TMS. During all titrations it was very important to keep the amount of unavoidable extraneous water* to a minimum for an accurate determination of the binding constants.

4.2.1.2 Binding constant experiments between NMMO (or NEMO) and methyl-β-D-glucopyranoside

For these experiments NMMO, NEMO and methyl-β-D-glucopyranoside were all dried in a vacuum desiccator as previously described above. In this case five separate samples were used in contrast to the water titration where only one sample was used in each case while increasing the amount of water. Samples with methyl-β-D-glucopyranoside / NMMO mole ratios of 0.94, 1.47, 2.03, 3.11 and 4.49 were used. For the methyl-β-D-glucopyranoside / NEMO titration mole ratios of 1.02, 1.57. 2.07, 4.02 and 5.83 were used. As before, the temperature was maintained at 295 K throughout the experiment and 32 transients with 64 k of data points were collected for each run. DSS was used as an internal shift reference at 0 ppm.

4.2.1.3 NOE difference experiments

Various samples of NMMO / water and NMMO / methyl-β-D-glucopyranoside were prepared. The solvent used for each sample was either DMSO-d_6 or $CDCl_3$. The β–anomer of methyl-D-glucopyranoside was used for most experiments, however, the α-anomer was also used to separate some overlapping peaks. NOE difference experiments were performed using a standard pulse sequence containing a 180° composite refocusing pulse. Typically, overnight accumulations were required to obtain adequate subtractions.

* Extraneous water refers to the small amount of water that remained after drying the amine oxides and the DMSO, and also to atmospheric water that contaminated each sample during preparation.

4.2.2 Derivation of an equation for the determination of binding constants of NMMO with water and methyl-β-D-glucopyranoside

If K is the equilibrium constant of binding for a 1:1 complex between NMMO and water (or methyl-β-D-glucopyranoside) then the following equations (symbols defined below) can be derived;

g = total molar concentration of water or glucose

G = concentration of unbound water (mol dm^{-3})

n = total molar concentration of NMMO

N = concentration of unbound NMMO (mol dm^{-3})

$\Delta\delta_{GN}$ = shift of bound NMMO with water or glucose forming a 1:1 complex

GN = concentration of bound water or glucose with NMMO (mol dm^{-3})

$\Delta\delta_{calc}$ = calculated shift for each NMMO peak

K = equilibrium binding constant ($mol^{-1}dm^3$)

$$\frac{GN}{G.N} = K \qquad \text{equ. 4.1}$$

$$G + GN = g \qquad \text{equ. 4.2}$$

$$N + GN = n \qquad \text{equ. 4.3}$$

$$\Delta\delta_{calc} = \frac{GN.\Delta\delta_{GN}}{N + GN} = \frac{GN.\Delta\delta_{GN}}{n} \qquad \text{equ. 4.4}$$

Now to eliminate GN:

From equ. 4.1 $$GN = K.G.N \qquad \text{equ. 4.5}$$

From equ. 4.2 $$G + K.G.N = g = G(1 + K.N) \qquad \text{equ. 4.6}$$

From equ. 4.3 $$N + K.G.N = n = N(1 + K.G) \qquad \text{equ. 4.7}$$

From equ. 4.4 $$\Delta\delta_{calc} = \frac{GN.\Delta\delta_{GN}}{n} = \frac{K.G.N.\Delta\delta_{GN}}{n} \qquad \text{equ. 4.8}$$

Now to eliminate G:

From equ. 4.6-4.7 $G - N = g - n$

Therefore, $G = N + g - n$

From equ. 4.8 $$\Delta\delta_{calc} = \frac{K.N.\Delta\delta_{GN}(N+g-n)}{n} \qquad \text{equ. 4.9}$$

Now to obtain and expression for N:

From equ. 4.6 $g.N = G.N + K.G.N^2$

From equ. 4.7 $n.G = G.N + K.N.G^2$

Therefore, $g.N - n.G = K.G.N(N-G)$

$[G = N + g - n]$

Therefore, $g.N - n.N - n.g + n^2 = K(N+g-n)N(n-g)$

The left-hand part of the above equation can be simplified to:

$$g(N-n) - n(N-n) = (n-g)(n-N)$$

Therefore, $n - N = K.N(N+g-n)$

Therefore, $n - N = K.N^2 + K.N.g - K.N.n$

Therefore, $N^2 + N(g - n + \frac{1}{K}) - \frac{n}{K} = 0$

Therefore, $$N = \frac{(n-g-\frac{1}{K}) + \sqrt{(g-n+\frac{1}{K})^2 + 4\frac{n}{K}}}{2} \qquad \text{equ. 4.10}$$

Microsoft EXCEL 4 with SOLVER can be applied to fit values for $\Delta\delta_{GN}$ and K iteratively to the experimental data using equations 4.9 and 4.10.

The above equations can also be applied to data obtained from other amine oxides, *i.e.* NEMO, that are non-solvents for cellulose. [Note that they only apply strictly to the formation of 1:1 complexes. Although the mole ratio of water (or methyl-β-D-glucopyranoside) to NMMO (or NEMO) exceeds unity during the titration, our assumption is that this excess is solvated by the solvent and that only 1:1 complexes are formed. However, if any other complexes were significant, this would almost certainly lead to peculiar non-fits, *e.g.* curves reversing in direction].

4.2.3 Results

A spectrum of anhydrous NMMO in DMSO-d_6 (0.3 mol dm^{-3}) is shown in figure 4.1. Even with the great care taken to keep the components of each sample dry, a small amount of extraneous water can clearly be seen. Figures 4.2 and 4.3 show fits of $\Delta\delta_{GN}$ and K to experimental data for titrations of NMMO in DMSO-d_6 with water and methyl-β-D-glucopyranoside respectively. For each titration these values were simultaneously fitted to the experimental data so that a single value for K was obtained and each peak gave a separate value for $\Delta\delta_{GN}$ (table 4.1). The errors in the calculated values for $\Delta\delta_{GN}$ and K are estimated to be about ±5 % for all experiments.

A spectrum of NEMO in DMSO-d_6 (0.3 mol dm^{-3}) is shown in figure 4.4, and $\Delta\delta_{GN}$ and K values fitted for titrations involving this amine oxide are shown in table 4.2. All the experimental data obtained from NEMO peaks were also fitted simultaneously to equation 4.9 (see figures 4.5 and 4.6) as described above.

A small adjustment was made to the experimental data obtained for both amine oxides titrated with water. The purpose of this adjustment was to take account of proton shifts that occurred by the presence of extraneous water in each sample at the beginning of

each titration. The amount of extraneous water was fitted concurrently with $\Delta\delta$ values and K to each amine oxide peak simultaneously. Our model calculated an extraneous water content of about 0.01 mol dm^{-3}. This agrees well with the integrals measured for the water peak recorded for each sample of amine oxide in DMSO-d_6, relative to the concentration of added water.

This type of adjustment was not possible when titrating with methyl-β-D-glucopyranoside because there are now two different components (*i.e.* water and the saccharide) interacting with the amine oxides giving rise to shifts in the proton resonances. Extraneous water in this case would be responsible for greater errors in $\Delta\delta$ values during the early stages of the titration. Therefore, as the amine oxide is titrated with methyl-β-D-glucopyranoside any extraneous water bound to the amine oxide during the latter stages will be replaced by sugar molecules and thus the presence of water becomes less important since this saccharide is now heavily in excess. At lower methyl-β-D-glucopyranoside concentrations the extraneous water would compete more effectively than at higher concentrations for binding to the amine oxide molecules and so an additional shift will be observed. As the titration progresses, methyl-β-D-glucopyranoside molecules will replace extraneous water molecules bound to NMMO and so the $\Delta\delta$ values observed will mainly be from amine oxide molecules bound to the sugar molecules. For this reason the lowest mole ratio of methyl-β-D-glucopyranoside / NMMO (or NEMO) chosen was about unity, and points at ratios lower than this were disregarded for the fitting process.

Titrations using solvents other than DMSO-d_6 were also investigated. However, solvents such as acetic acid-d_4, $CDCl_3$, CD_3CN and acetone-d_6 did not allow adequate solubility of all components of each sample. Titrations were also carried out in methanol-d_4, however, very small $\Delta\delta$ values were recorded. Although DMSO-d_6 is a polar solvent and will compete with either water or methyl-β-D-glucopyranoside for

binding to the amine oxides, this becomes unimportant since the main purpose was to compare the K values between the different titrations.

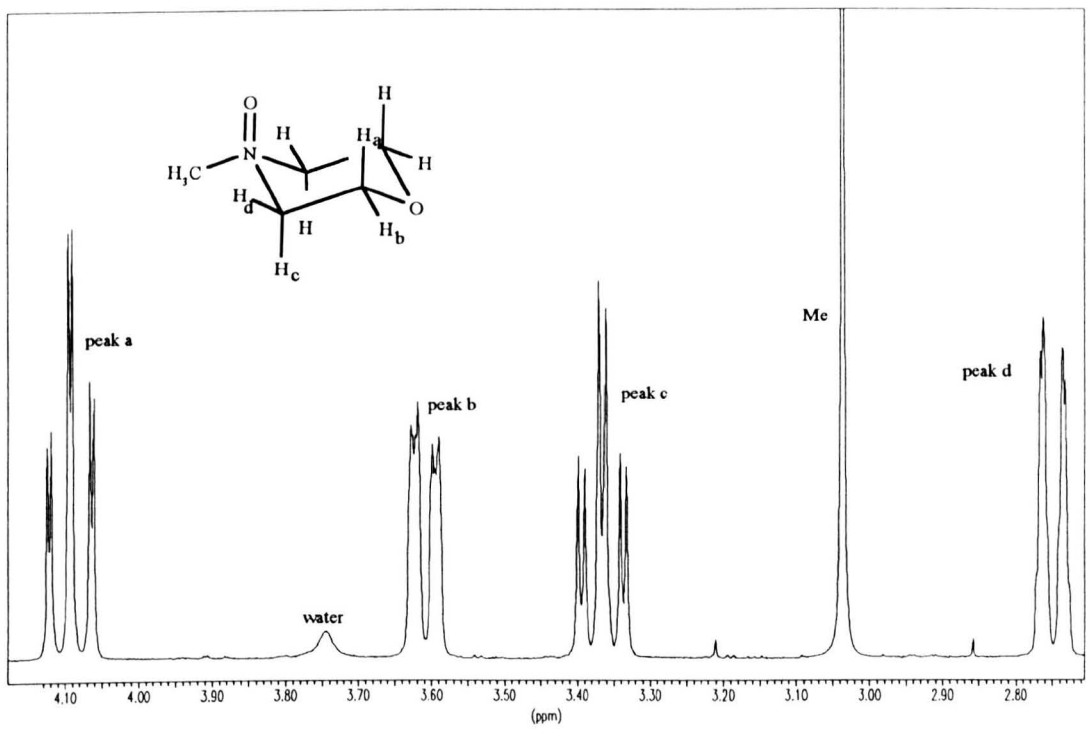

Figure 4.1 ^{1}H spectrum of NMMO in DMSO-d_6 (0.3 mol dm^{-3}).

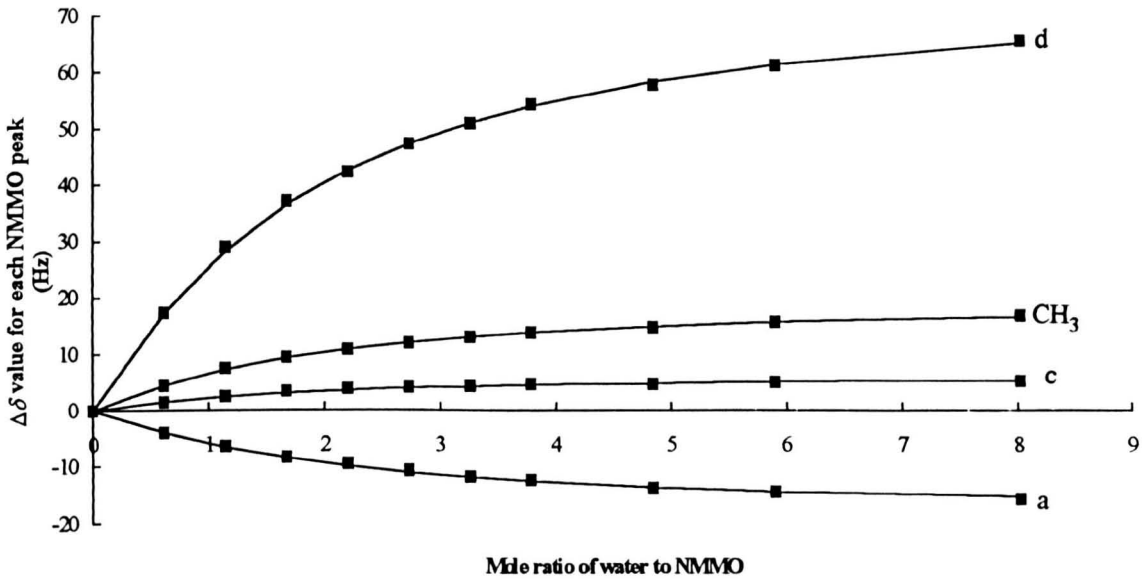

Figure 4.2 Fits obtained for experimental data for the titration of NMMO in DMSO-d_6 with water. Spectrometer operating frequency for ^{1}H was 400.13 Mz. a, c, d and Me refer to the position of the protons in the molecule (see figure 4.1).

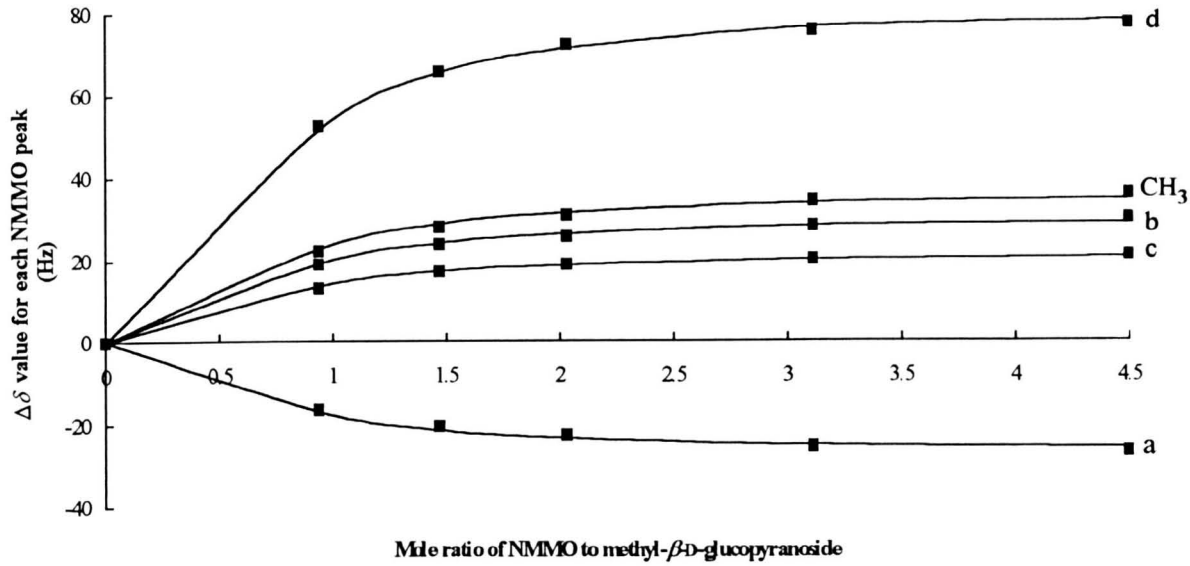

Figure 4.3 Fits obtained for experimental data for the titration of NMMO in DMSO-d_6 with methyl-β-D-glucopyranoside. Spectrometer operating frequency for ^{1}H was 400.13 Mz. a, b, c, d and Me refer to the position of the protons in the molecule (see figure 4.1). Each curve is spline fitted.

Table 4.1 Fitted data for the titration of NMMO in DMSO-d_6 with water and methyl-β-D-glucopyranoside. Spectrometer operating frequency for ^{1}H was 400.13 Mz.

titrant	$\Delta\delta_{GN}$ (Hz) peak a	$\Delta\delta_{GN}$ (Hz) peak b	$\Delta\delta_{GN}$ (Hz) peak c	$\Delta\delta_{GN}$ (Hz) peak d	$\Delta\delta_{GN}$ (Hz) CH_3	K $mol^{-1}dm^3$
Water	-18.08	N/A	6.45	77.04	19.70	2.71
methyl-β-D-glucopyranoside	-26.85	30.23	21.46	81.72	36.07	39.21

N/A not available because of overlaps with water

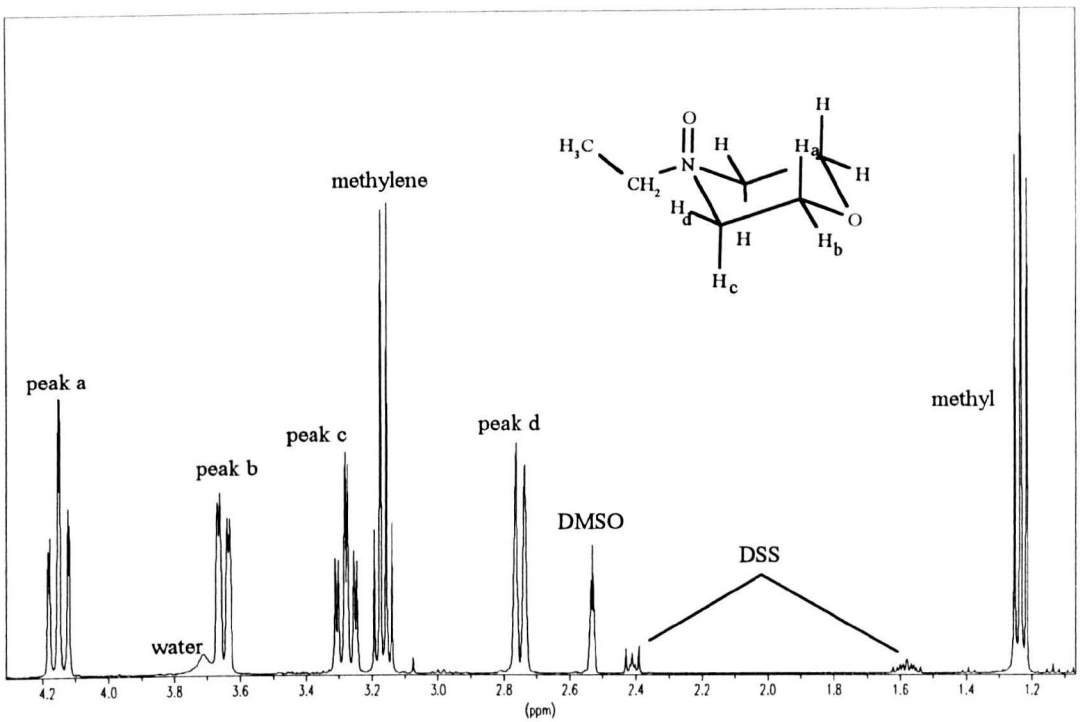

Figure 4.4 ^{1}H spectrum of NEMO in DMSO-d_6 (0.3 mol dm^{-3}).

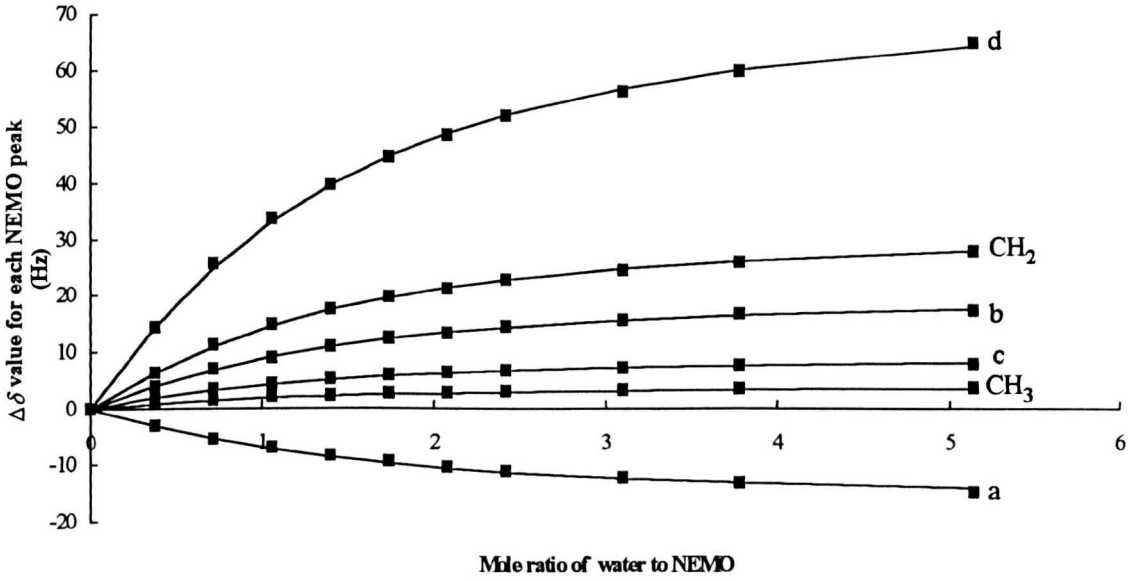

Figure 4.5 Fits obtained for experimental data for the titration of NEMO in DMSO-d_6 with water. Spectrometer operating frequency for ^{1}H was 400.13 Mz. a, b, c, d, CH_2 and Me refer to the position of the protons in the molecule (see figure 4.4).

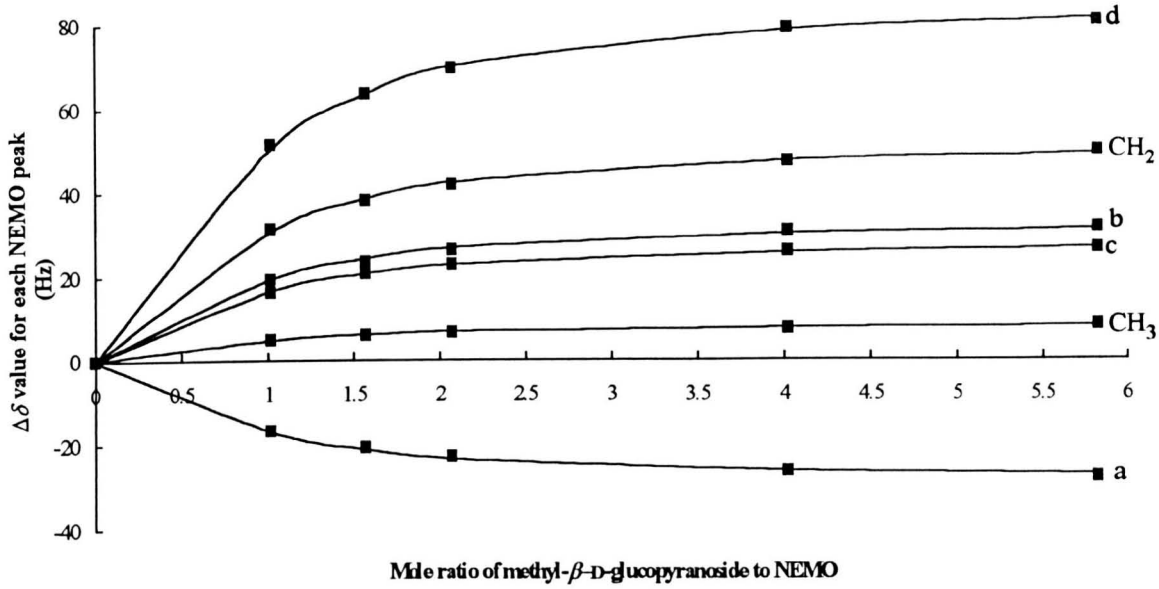

Figure 4.6 Fits obtained for experimental data for the titration of NEMO in DMSO-d_6 with methyl-β-D-glucopyranoside. Spectrometer operating frequency for ^{1}H was 400.13 Mz. a, b, c, d, CH_2 and Me refer to the position of the protons in the molecule (see figure 4.4). Each curve is spline fitted.

Table 4.2 Fitted data for the titration of NEMO in DMSO-d_6 with water and methyl-β-D-glucopyranoside. Spectrometer operating frequency for ^{1}H was 400.13 Mz.

titrant	$\Delta\delta_{GN}$ (Hz) **peak a**	$\Delta\delta_{GN}$ (Hz) **peak b**	$\Delta\delta_{GN}$ (Hz) **peak c**	$\Delta\delta_{GN}$ (Hz) **peak d**	$\Delta\delta_{GN}$ (Hz) **CH_2**	$\Delta\delta_{GN}$ (Hz) **CH_3**	***K*** $mol^{-1}dm^3$
Water	-16.74	20.64	9.54	75.86	32.95	4.07	4.55
methyl-β-D-glucopyranoside	-28.93	33.01	28.21	86.45	52.31	8.39	23.80

4.2.4 Discussion

The binding constant calculated for the binding of water to NMMO (2.71 mol^{-1} dm^3) is about half that obtained for water to NEMO (4.55 mol^{-1} dm^3). This demonstrates that the non-solvent NEMO binds better to water than does NMMO. This may help to explain the inability of NEMO to dissolve cellulose since the N→O bond of this amine oxide may become less available for binding to this polymer for dissolution to occur.

The binding constant calculated for the binding of methyl-β-D-glucopyranoside to NMMO (39.21 mol^{-1} dm^3) is about 50 % greater than that obtained for the same saccharide to NEMO (23.80 mol^{-1} dm^3). This gives some evidence that NMMO has a greater ability to bind to cellulose than does NEMO. These results together suggest that the non-solvent has a preference for binding to water whereas NMMO has a preference to bind with cellulose, sufficiently to become a solvent for this polymer. Although the evidence from this study suggests that both NMMO and NEMO can bind to cellulose, the binding must be above a certain strength to break the H-bonds between adjacent chains of cellulose. Possible reasons why the binding of NMMO to methyl-β-D-glucopyranoside is stronger than NEMO to the same saccharide will be discussed in section 4.4.

The proton shifts of NMMO molecules, recorded in both the titrations, are greatest for peaks **a**, **d** and CH_3. This indicates that, as previously believed (section 1.7), the interaction of water and methyl-β-D-glucopyranoside occurs in the region of the N→O group of amine oxides since **a**, **d** and CH_3 are positioned on the same side of the molecule as this bond. The reason why peak **a** should have a negative shift is unclear at present. The shifts obtained from peaks **b** and **c** are much smaller compared to those from other regions of the molecule. This indicates that the chemical shifts obtained because of the interaction of the N→O bond of NMMO molecules with water or

methyl-β-D-glucopyranoside molecules decrease with the spatial distance between this region and the protons on the amine oxide molecules. NEMO also shows a pattern of proton shifts similar to NMMO with the exception that CH_3 gives a much smaller shift. This is most likely because the CH_3 group of NEMO is further away from the N→O region than in NMMO. However, the closeness of the CH_2 group (absent in NMMO molecules) to the N→O bond of NEMO gives rise to a relatively large shift of the resonance from these protons.

Although proton shifts are observed for these two amine oxides with water or methyl-β-D-glucopyranoside, the mechanism and nature of the interactions between these species are not completely understood. The shifts are most probably caused by the interaction between species having OH-groups and the amine oxide. A possible reason why relatively small shifts are observed for NMMO titrated with water in methanol (see section 4.2.3) could be because large shifts have already occurred from the interaction of OH of this solvent with the amine oxide before the titration has commenced. Since methanol is present in much greater quantities than water added during the titration, the N→O bond may have become fully involved with binding of the OH-groups of solvent molecules and thus become unable to interact with any other species added to the sample containing OH-groups.

As mentioned in section 4.2.2 the equation derived to calculate K assumes that the binding occurs between an equal molar ratio between NMMO (or NEMO) and water (or methyl-β-D-glucopyranoside). Since the experimental data fit so well to equation 4.9 we can conclude that our original assumption of the formation of only 1:1 complexes was indeed valid and thus we did not have the complication of more than one water (or methyl-β-D-glucopyranoside) molecule interacting with each amine oxide molecule. Although as the titration progresses there are more water or methyl-β-D-

glucopyranoside molecules than amine oxide molecules, this excess is probably solvated by the polar molecules of DMSO.

Several attempts were made to gain information about the interaction of NMMO with both methyl-β-D-glucopyranoside and water using NOE difference spectra. Unfortunately, no reliable information could be attained, partly because of overlapping peaks. Use of the α-anomer of methyl-D-glucopyranoside helped to alleviate some of these overlaps, but nevertheless no significant intermolecular NOE's could be observed.

In the next section ^{13}C shifts of cellobiose and methyl-β-D-cellobioside on addition of various solvent and non-solvent amine oxides will be investigated. Both of these saccharides can be considered as the next highest oligomer, *i.e.* the dimer, of cellulose.

4.3 An evaluation of the interactions between amine oxides and cellobiose or methyl-β-D-cellobioside as soluble model compounds for cellulose

4.3.1 Experimental

4.3.1.1 Cellobiose ^{13}C chemical shift experiments

Cellobiose was purchased from Sigma Chemicals and used without further purification. Samples were prepared with 100 mg of cellobiose, 3 g of NMMO (containing various amounts of water)* and thus the following mole ratios of NMMO (mole ratio of water alongside in brackets) were; 0.111 [0.886], 0.144 [0.853], 0.185 [0.811], 0.311 [0.685], 0.566 [0.427] and 0.591$ [0.400].$ Internal dioxan was used as a shift reference at 67.4 ppm. All experiments were performed at 333 K and about 5000 transients were accumulated for each run.

4.3.1.2 Carbon nT_1 measurements of cellobiose in NMMO solution

An inversion recovery pulse sequence was used to obtain nT_1 values on the above samples. Five delay periods, τ, between the 180° and 90° pulse of 0.01, 0.1, 0.25, 0.75 and 3 seconds were set.

4.3.1.3 Methyl-β-D-cellobioside experiments

Methyl-β-D-cellobioside was purchased from Apin Chemicals and used without further purification. All amine oxides used in this investigation were first dried in a vacuum desiccator over phosphorus pentoxide for several days. 25 mg of methyl-β-D-cellobioside was used in each sample together with 5.5 mmol of each amine oxide in 0.5 ml of water, thus giving mole ratios of 0.164 and 0.836 for the amine oxides and

* The concentration of the NMMO supplied by Courtaulds Research was 89.6 % (w/w). For most samples some water was added so that a range of NMMO concentrations were obtained.

$ This concentration is an estimate since this sample needed to contain the minimum amount of water possible but still be liquid at the experimental temperature; thus the 89.6 % NMMO was heated to evaporate excess water.

water respectively. Six different amine oxides were used, three of which are solvents for cellulose; *i.e.* N-methylmorpholine-N-oxide (NMMO), triethylamine-N-oxide (TEAO) and N, N-dimethylcyclohexylamine-N-oxide (DMCHAO), the other three being non-solvents; *i.e.* N-ethylmorpholine-N-oxide (NEMO), trimethylamine-N-oxide (TMAO) and pyridine-N-oxide (PNO). NMMO, TEAO and DMCHAO were donated by Courtaulds Research. PNO and TMAO were purchased from Lancaster and Aldrich Chemicals respectively, and NEMO was synthesised in our laboratory as described in section 3.2.1.

Various shift references were investigated, *i.e.* internal dioxan at 67.4 ppm and external TSP in D_2O at -1.7 ppm (internal TSP was avoided because of possible chemical interference). About 8000 transients were collected with up to 128 k of data points depending on the sweep width required. All experiments were performed at 333 K.

Some experiments were also performed using DMF-d_7 instead of water. Samples were prepared with 5 mg of methyl-β-D-cellobioside, 20.4 mg of NMMO or 22.8 mg of NEMO in 0.5 ml of DMF-d_7. Therefore, the concentration of each amine oxide in DMF-d_7 was 0.35 M. Experiments for both samples were run at 298 K.

Assignment of carbon resonances for both saccharides was achieved with the aid of 2D NMR spectroscopy. Carbon chemical shift positions assigned for cellobiose[158] and methyl-β-D-cellobioside[159] in the present study are identical to those reported in the literature.

4.3.1.4 Sodium hydroxide experiments

Six samples containing 20 mg of methyl-β-D-cellobioside with 0.6 ml of sodium hydroxide solutions with molar concentrations of 0, 0.15, 0.39, 0.77, 1.75 and 3.48 were prepared. All experiments were run at a temperature of 298 K using 32 k of data points.

4.3.2 Results

Figure 4.7 shows the molecular structure of cellobiose and methyl-β-D-cellobioside, and figures 4.8 and 4.9 show assigned spectra of these two saccharides respectively.

Figure 4.10 shows the carbon $\Delta\delta$ shifts obtained for cellobiose in various concentrations of NMMO solution. To simplify the data only β resonances are shown. All shifts are relative to those obtained for cellobiose in water under identical conditions. C6 carbons are absent from this figure because some of these resonances overlapped with NMMO peaks. Table 4.3 lists nT_1 values for the same set of samples with relative nT_1 values, *i.e.* when the relaxation times of β'_1 carbons are set to one second, in brackets.

Figure 4.11 shows the carbon $\Delta\delta$ shifts for methyl-β-D-cellobioside in various amine oxide solutions. Again, these shifts are relative to those of this saccharide in pure water under identical conditions.

Carbon $\Delta\delta$ shifts obtained from methyl-β-D-cellobioside in various concentrations of sodium hydroxide solutions are shown in figure 4.12. Figure 4.13 shows carbon $\Delta\delta$ shifts obtained for methyl-β-D-cellobioside in DMF-d_7 solutions of NMMO and NEMO.

Work carried out by Thanable *et al.*[160] found that the carbon resonance of internal dioxan was dependent on the concentration of 20 common amino acids. They concluded that external TSP in D_2O gave the most reliable shift reference. In the present investigation, the **Me** carbon resonance of methyl-β-D-cellobioside in each amine oxide solution varied only slightly relative to external TSP in D_2O. Since the **Me** carbon resonance is the most likely peak in this saccharide to be unaffected by solvent, these slight variations in shifts are probably caused by minor differences in susceptibility between samples. Therefore, on the basis of this argument, the **Me** resonance of each sample was used as the final shift reference.

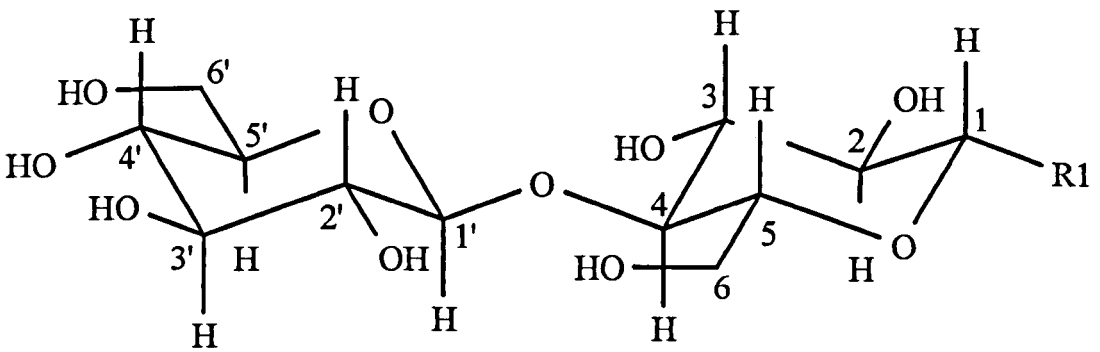

Figure 4.7 Structure of β-D-cellobiose (R1=OH) and methyl-β-D-cellobioside (R1=OMe).

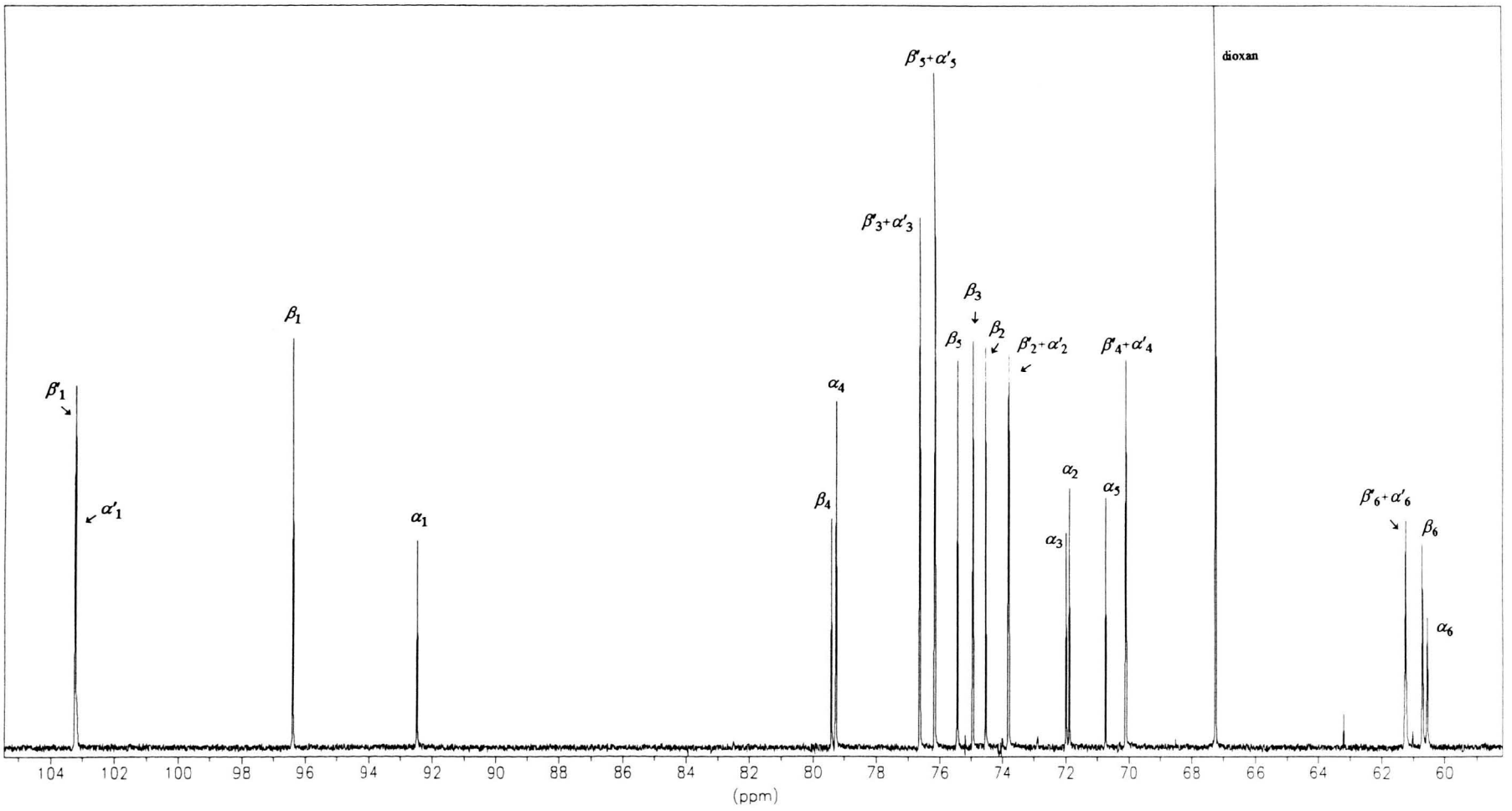

Figure 4.8 ^{13}C spectrum of D-cellobiose in D_2O (0.1 mol dm^{-3}) at 298 K.

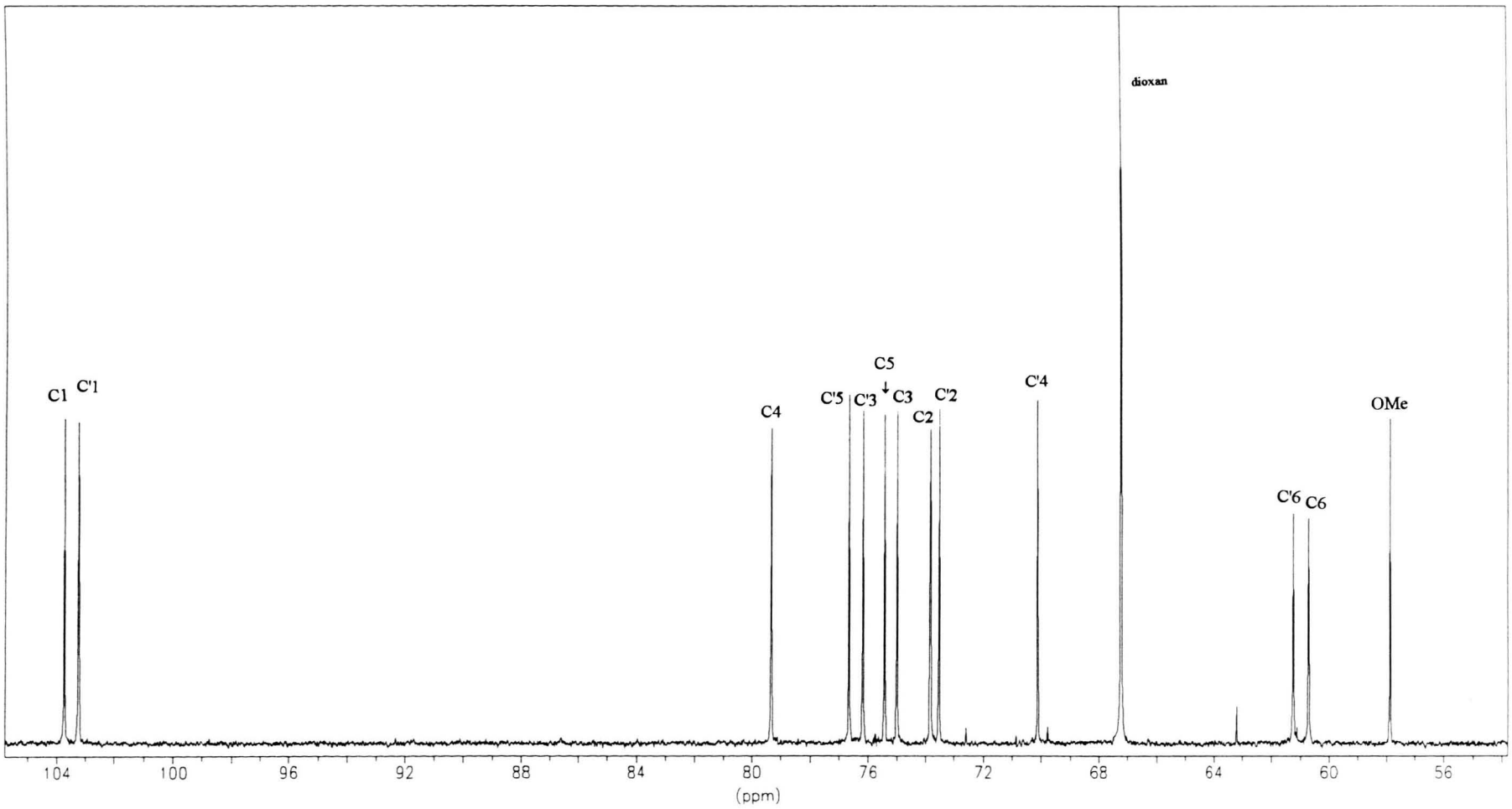

Figure 4.9 ^{13}C spectrum of methyl-β-D-cellobioside in D_2O (0.1 mol dm^{-3}) at 298 K.

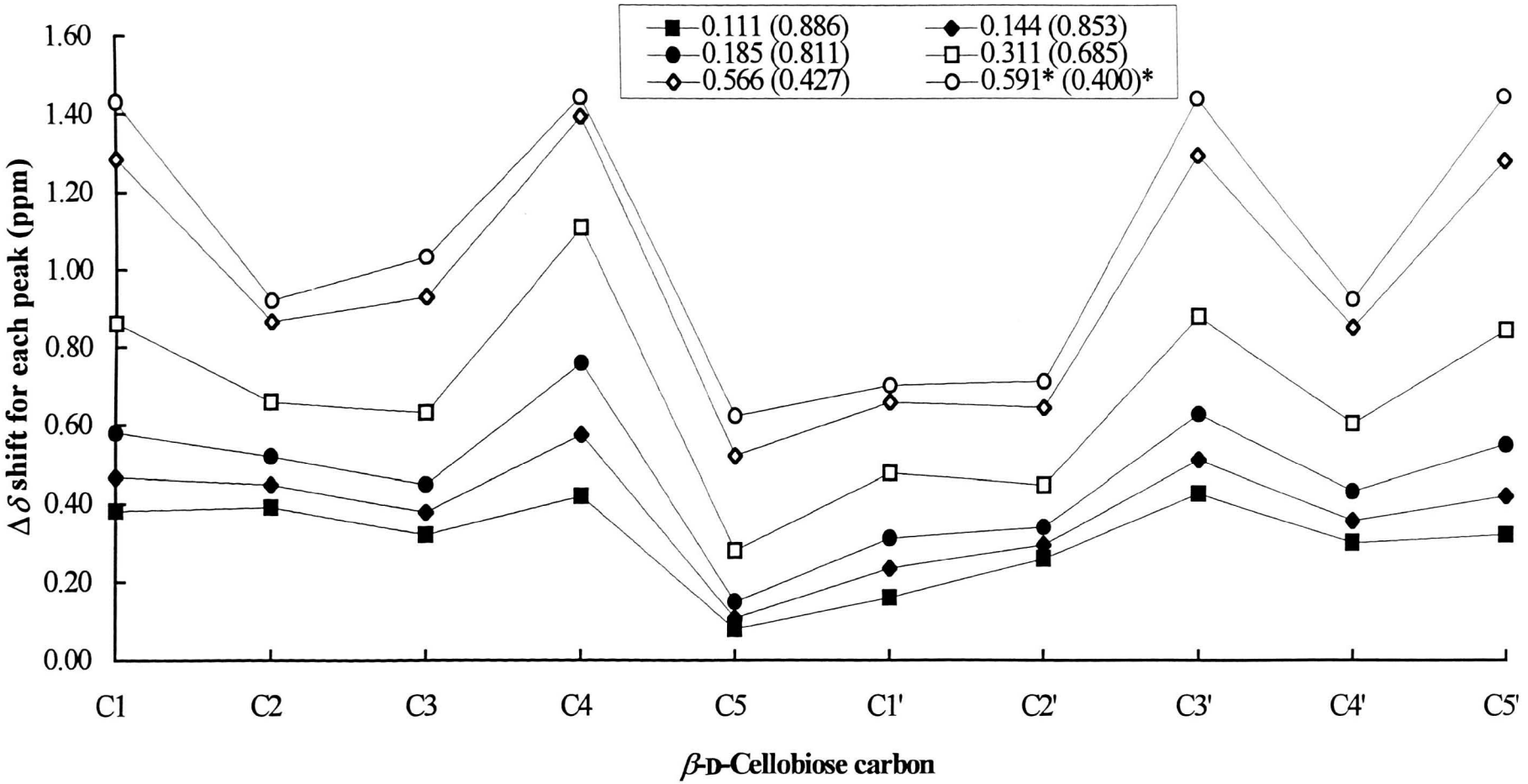

Figure 4.10 $\Delta\delta$ **shifts obtained for each** ^{13}C β-D-**cellobiose resonance obtained with six different aqueous amine oxide solutions at 333 K. Concentration is given as mole fraction of NMMO (mole fraction of water in brackets). * Indicates estimated concentration.**

Table 4.3 nT_1 relaxation times for D-cellobiose in various concentrations of aqueous NMMO solutions at 333 K.

Cellobiose carbon resonance (in chemical shift order)	nT_1 relaxation times obtained with the corresponding mole-fraction of NMMO (mole-fraction of water in brackets) [* indicates an estimated mole-fraction]						
	Water only	**0.111 (0.886)**	**0.144 (0.853)**	**0.185 (0.811)**	**0.311 (0.685)**	**0.566 (0.427)**	**0.591* (0.400)***
β'_1	0.92 (1.00)[a]	0.47 (1.00)	0.35 (1.00)	0.29 (1.00)	0.22 (1.00)	0.28 (1.00)	0.32 (1.00)
α'_1	0.93 (1.01)[a]	0.48 (1.01)	0.34 (0.97)	0.29 (1.00)	0.22 (1.00)	0.28 (1.00)	0.32 (1.00)
β_1	0.96 (1.04)[a]	0.50 (1.06)	0.37 (1.04)	0.30 (1.06)	0.22 (1.00)	0.28 (1.00)	0.30 (0.94)
α_1	0.78 (0.85)[a]	0.40 (0.84)	0.30 (0.86)	0.25 (0.88)	0.20 (0.94)	0.35 (1.25)	0.28 (0.87)
α_4	0.86 (0.93)[a]	0.47 (1.00)	0.33 (0.93)	0.30 (1.04)	0.24 (1.11)	0.27 (0.97)	0.28 (0.89)
β_4	0.88 (0.96)[a]	0.47 (1.00)	0.35 (1.00)	0.30 (1.04)	0.21 (0.98)	0.26 (0.93)	0.31 (0.96)
$\beta'_5+\alpha'_5$	0.91 (0.99)[a]	0.48 (1.01)	0.36 (1.01)	0.30 (1.04)	0.22 (1.00)	0.26 (0.95)	0.33 (1.01)
α'_3	0.91 (0.99)[a]	0.46 (0.97)	0.35 (1.00)	0.30 (1.04)	0.22 (1.00)	0.27 (0.96)	0.33 (1.01)
β'_3	0.93 (1.01)[a]	0.46 (0.97)	0.36 (1.01)	0.30 (1.04)	0.22 (1.00)	0.27 (0.96)	0.33 (1.01)
β_5	0.89 (0.96)[a]	0.48 (1.01)	0.36 (1.01)	0.30 (1.04)	0.23 (1.07)	0.27 (0.96)	0.32 (1.00)
β_3	0.92 (0.99)[a]	0.47 (1.00)	0.36 (1.01)	0.31 (1.07)	0.22 (1.00)	0.27 (0.96)	0.32 (1.00)
β_2	0.97 (1.05)[a]	0.50 (1.05)	0.36 (1.01)	0.31 (1.07)	0.23 (1.07)	0.29 (1.03)	0.32 (1.00)
α'_2	0.86 (0.93)[a]	0.46 (0.97)	0.35 (1.00)	0.29 (1.00)	0.22 (1.00)	0.28 (1.00)	0.33 (1.01)
β'_2	0.92 (0.99)[a]	0.47 (1.00)	0.35 (1.00)	0.30 (1.04)	0.22 (1.00)	0.28 (1.00)	0.33 (1.01)
α_3	0.89 (0.97)[a]	0.51 (1.08)	0.34 (0.97)	0.32 (1.12)	0.25 (1.15)	0.30 (1.08)	0.39 (1.22)
α_2	1.00 (1.08)[a]	0.48 (1.01)	0.37 (1.04)	0.32 (1.12)	0.23 (1.04)	0.33 (1.19)	0.36 (1.11)
α_5	0.93 (1.01)[a]	0.50 (1.06)	0.34 (0.95)	0.32 (1.12)	0.23 (1.04)	0.32 (1.15)	0.35 (1.08)
β'_4	0.86 (0.93)[a]	0.46 (0.97)	0.34 (0.97)	0.30 (1.04)	0.23 (1.04)	0.28 (1.00)	0.34 (1.06)
α'_4	0.98 (1.07)[a]	0.46 (0.97)	0.35 (1.00)	0.30 (1.04)	0.23 (1.04)	0.28 (1.00)	0.34 (1.06)
α'_6	0.97 (1.05)[a]	0.54 (1.13)	0.54 (1.51)	0.55 (1.94)	[b]	0.51 (1.85)	[b]
β'_6	0.98 (1.06)[a]	0.55 (1.16)	0.61 (1.72)	0.46 (1.61)	[b]	0.51 (1.85)	[b]
β_6	0.98 (1.06)[a]	0.49 (1.05)	0.42 (1.19)	0.39 (1.36)	0.32 (1.49)	[b]	[b]
α_6	0.93 (1.01)[a]	0.50 (1.05)	0.46 (1.28)	0.35 (1.23)	0.32 (1.49)	[b]	[b]

[a] bracketed figures are nT_1 values relative to those obtained for β'_1

[b] Overlapping with NMMO resonances

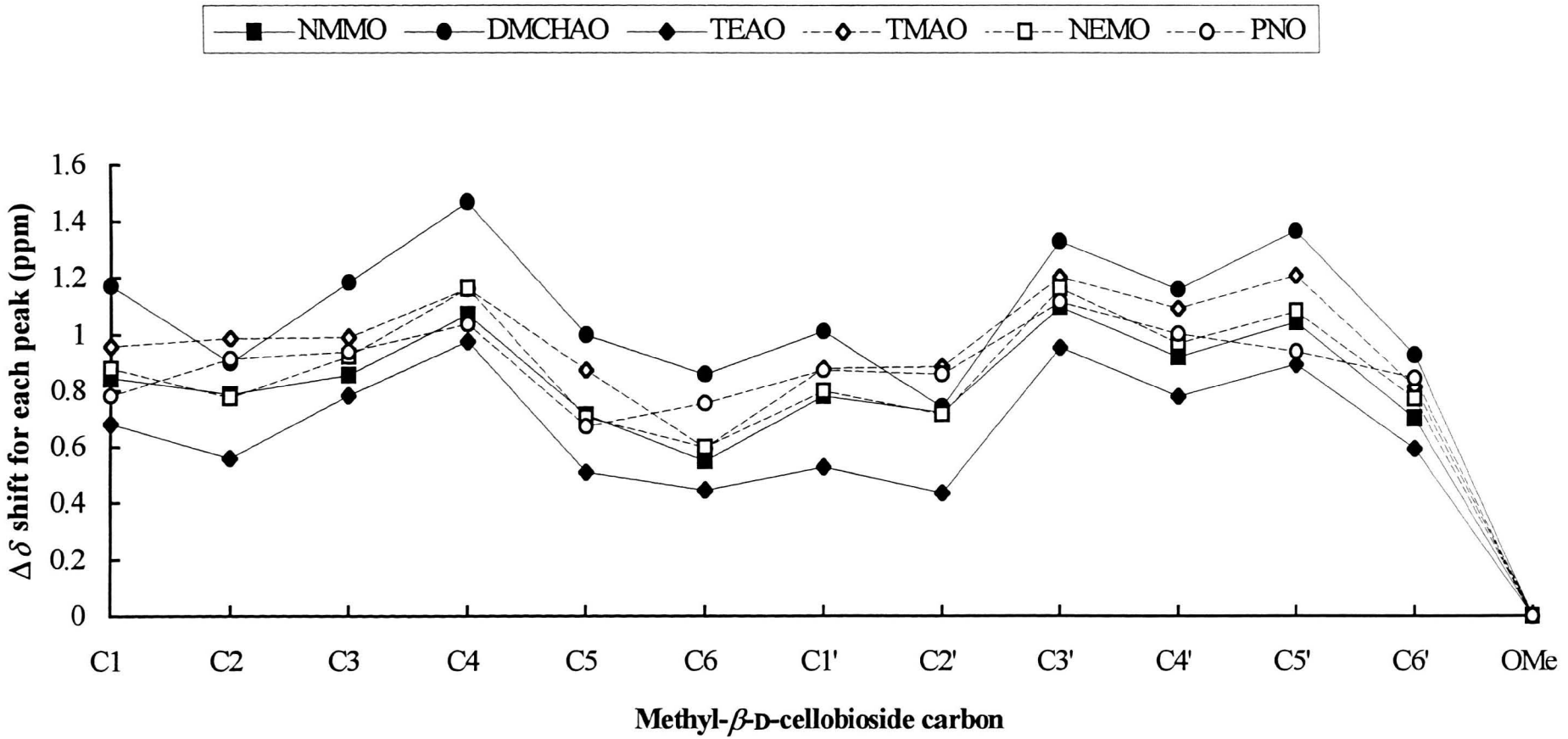

Figure 4.11 $\Delta\delta$ **shifts obtained for each** ^{13}C **methyl-**β**-D-cellobioside resonance obtained with six different aqueous amine oxide solutions at 333 K. Mole ratios for the amine oxides and water were 0.164 and 0.836 respectively.**

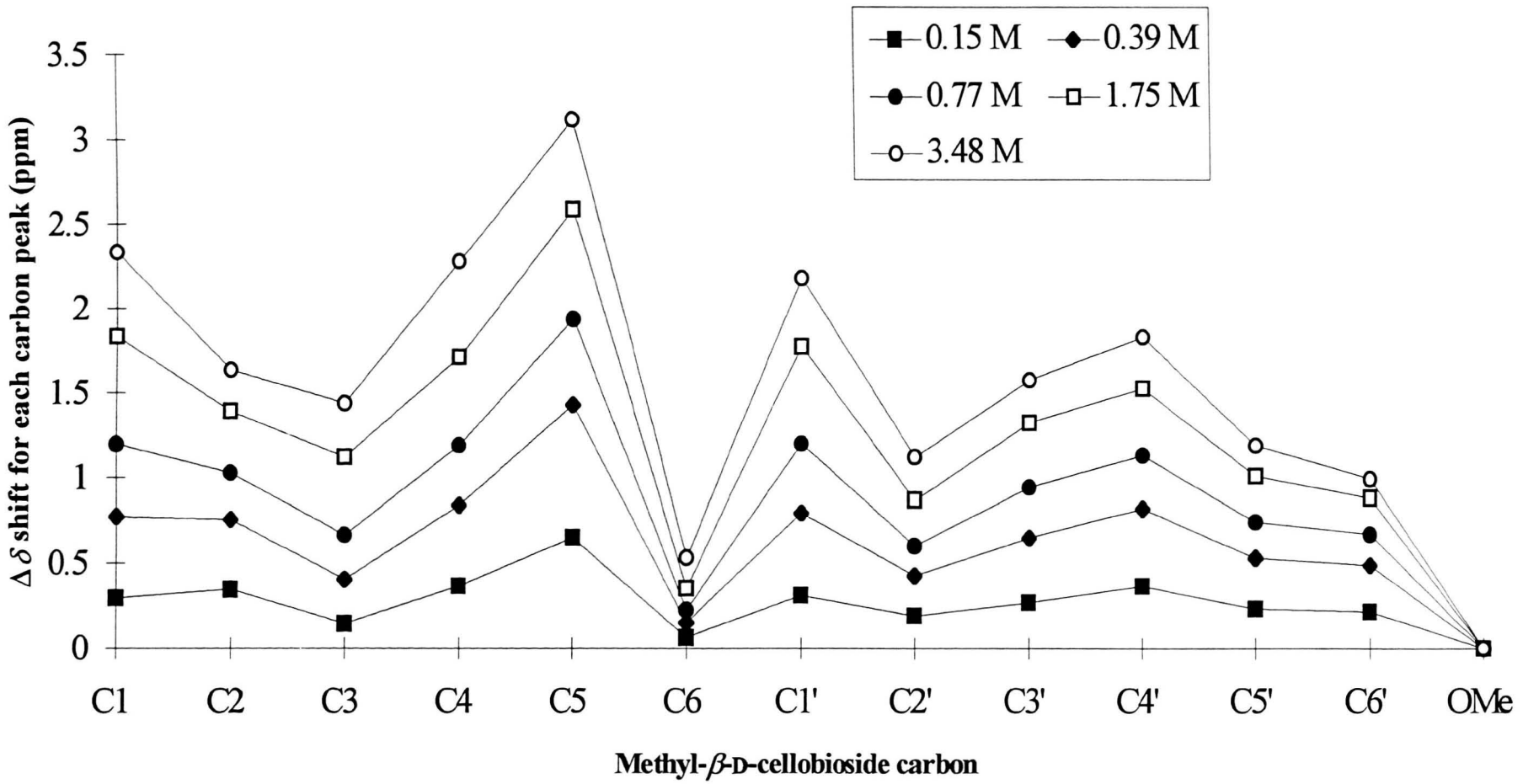

Figure 4.12 $\Delta\delta$ **shifts obtained for each** ^{13}C **methyl-**β**-D-cellobioside resonance obtained with five different aqueous sodium hydroxide solutions at 295 K.**

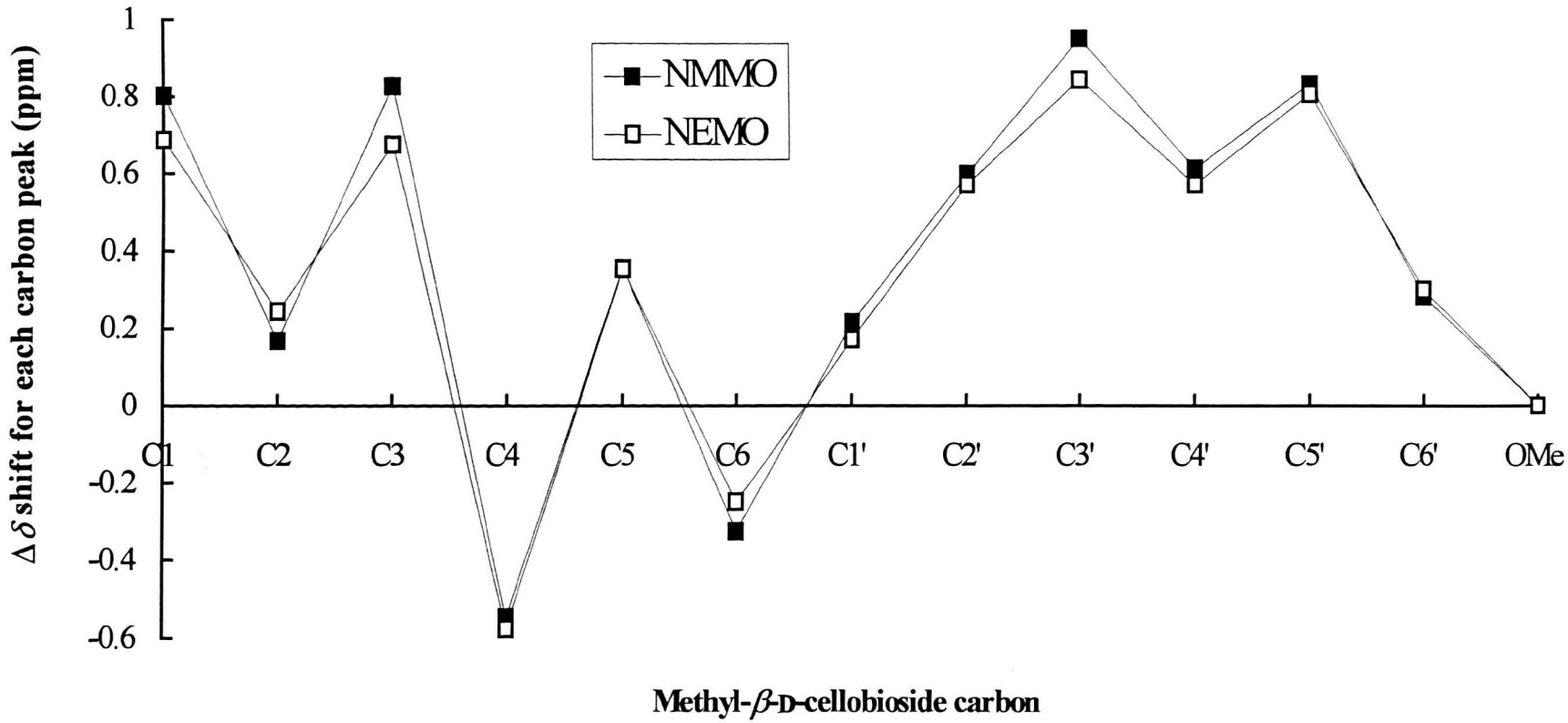

Figure 4.13 $\Delta\delta$ **shifts obtained for each** ^{13}C **methyl-**β**-D-cellobioside resonance obtained with DMF solutions of NMMO and NEMO at 298 K. Concentration for each amine oxide was 0.35 M.**

4.3.3 Discussion

4.3.3.1 ^{13}C chemical shifts of cellobiose in NMMO

Figure 4.10 shows that the carbon resonances of cellobiose in NMMO-water solutions shift downfield with increasing NMMO concentration. Although the amount of NMMO in each sample is in considerable excess relative to the cellobiose concentration, an increase in $\Delta\delta$ values is observed as the NMMO concentration increases still further. This may illustrate the competition between water and NMMO molecules for binding to the saccharide. Section 1.7.3 reports a suggestion by Harmon *et al.*[122] that water is more firmly bound to NMMO at higher H_2O concentrations. Thus, as the number of NMMO molecules increases relative to the number of water molecules, the amine oxide is able to compete more effectively and displace water molecules bound to cellobiose. Another possible reason may be that as the concentration of NMMO increases, the amine oxide is forced to bind with cellobiose because of mass action.

Unfortunately, no shift theory could be extracted from these results, and although some carbon resonances were observed to shift more than others, no pattern could be established. It had been hoped that the relative shifts might reveal the sites of interaction between cellobiose and NMMO.

4.3.3.2 Measurement of nT_1 values of cellobiose in NMMO

The nT_1 value of each cellobiose carbon (table 4.3) first decreases, reaches a minimum, then increases as the NMMO concentration is increased. This pattern of relaxation times may simply arise from the observed increases in viscosity of the sample (*i.e.* the greater the NMMO concentration the higher the viscosity of the sample) and not from the direct interaction of NMMO with cellobiose. The correlation time, τ_r, is linearly dependent on the sample microviscosity in the region of the molecule. Also, the spin-

lattice relaxation times, nT_1, depend on τ_r.* The minimum relaxation time for all but one of the ring carbons measured in this study occurs at about 0.22 s which is identical to the theoretical minimum, assuming isotropic tumbling. This suggests that cellobiose molecules are almost rigid, *i.e.* any significant flexibility in the ring structure would have induced slower relaxation and thus a higher nT_1 minimum value.

The nT_1 values recorded for the ring carbons of cellobiose are similar except for α_1, at all concentrations. The only exception arises in the data recorded with an NMMO mole ratio of 0.566, where α_1 does not relax more rapidly. The slightly shorter nT_1 values recorded for the α_1 carbons at the other concentrations suggest that the tumbling of cellobiose may be slightly anisotropic, with faster rotation about the long axis of the molecules. The reasoning behind this assumption is explained as follows. The proton attached to C1 is in the equatorial position for the α-anomer and axial in the β-anomer. Therefore, if the molecules were rotating faster about the long axis compared to other motions then the C1-H bond in the equatorial position would rotate more slowly than all the other C-H bonds in the molecule. This would lead to faster relaxation for α_1 carbons, unless the nT_1 minimum had been passed. Since cellobiose molecules are essentially rod-shaped it is not surprising that some anisotropic motion occurs. However, for mole ratios ≥ 0.566, the overall motion in the absence of internal motion is sufficiently slow to have passed beyond the nT_1 minimum. In this case the added contribution of the faster rotational motion combines with the main motion in such a way as to bring the overall motion back towards that giving an nT_1 minimum.

Since the anisotropic rotation is observed with and without the presence of NMMO, this indicates that cellobiose molecules continue to be linear after NMMO is added, so that very little bending about the glycosidic bond occurs from the interaction of the amine

* The minimum occurs approximately where $\tau_r = 1/\omega_H$ (ω_H is the resonance frequency of proton). Relaxation of carbon nuclei requires magnetic field fluctuations produced by the rotation of nearby protons around the carbon in question. Therefore the value obtained for nT_1 is a function of the correlation time, τ_r (*i.e.* the average time this C-H vector takes to progress through one radian).

oxide. Had bending occurred then the α_1 carbon would have experience a different tumbling motion and thus the drop in the nT_1 value observed in pure water would have vanished in the presence of NMMO.

A further trend is also apparent from table 4.3. The nT_1 values become longer for the C6 resonances relative to the other resonances (bracketed values in table 4.3) as the NMMO concentration increases. This may indicate an interaction between NMMO and cellobiose molecules about the vicinity of this carbon. H-bonds involving C6 may have been broken by this interaction allowing the C5-C6 bond greater rotational freedom relative to the rest of the molecule. This would result in altered nT_1 times. The importance of C6 for cellulose dissolution in amine oxides has repeatedly been stated in the literature (section 1.7.2), and the results from this study may have given further evidence in support of this hypothesis. Another explanation is that the greater viscosity impedes the tumbling of the molecule but affects the rotational freedom of the C5-C6 bond less. Again, this would lead to two different effective tumbling processes and thus altered nT_1 values. Of course, the relative increase in the nT_1 times for the C6 carbons could be a combination of the two above explanations.

To test our hypothesis that the longer nT_1 values for the C6 carbons indicate greater freedom of rotation about the C5-C6 bond, because of the interaction of NMMO with cellobiose, the following analysis can be considered:

Transition probabilities of combined motion as derived by Woessner[161] and Doddrell *et al.*[162] are given by the following equations:

$$W_0 = \frac{2Ad'\tau_r}{1+(\omega_S-\omega_I)^2\tau_r^2} + \frac{2d'(B+C)\tau_c}{1+(\omega_I-\omega_S)^2\tau_c^2}$$

$$W_1 = \frac{3Ad'\tau_r}{1+(\omega_I\tau_r)^2} + \frac{3d'(B+C)\tau_c}{1+(\omega_I\tau_c)^2}$$

$$W_2 = \frac{12Aa'\tau_r}{1+(\omega_I+\omega_S)^2\tau_r^2} + \frac{12a'(B+C)\tau_c}{1+(\omega_I+\omega_S)^2\tau_c^2}$$

where:

$\omega_I = 2\pi.(100.62\times10^6)$ = carbon resonance frequency in radians s^{-1}

$\omega_S = 2\pi.(400.13\times10^6)$ = proton resonance frequency in radians s^{-1}

$$a = \mu_0^2\gamma_I^2\gamma_S^2\hbar^2\tau_r S(S+1)/240\pi^2r^6$$

and:

μ_0 = permeability of vacuum

γ_I = magnetogyric ratio of ^{13}C and γ_S = magnetogyric ratio of ^1H

h = Planck's constant and $\hbar = h/2\pi$

τ_r = correlation time for main isotropic motion of the molecules

S = spin quantum number (in this case S = ½)

r = heteronuclear distance (normally taken as 0.109 nm)

Therefore:

$$a = \frac{\tau_r}{0.0000000010742} \qquad \text{and} \qquad a' = \frac{a}{\tau_r}$$

and

$$\tau_c = \frac{1}{\tau_r^{-1} + \tau_g^{-1}} = \text{total correlation time for reorientation of the internal mobile group}$$

where:

τ_g = correlation time for internal motion of the molecules

$$A = \tfrac{1}{4}(3\cos^2 \Delta - 1)^2$$
$$B = 3\sin^2 \Delta \cos^2 \Delta$$
$$C = \tfrac{3}{4}\sin^4 \Delta$$

Δ = angle in radians between the C-H vector and the angle of internal reorientation

The overall spin-lattice relaxation time is given by:

$$nT_1 = \frac{1}{2W_1 + W_2 + W_0}$$

If there is no internal motion, *i.e.* $\Delta = 0$, then A is equal to 1.0 and B and C both become zero. In the present study information about the motional freedom of the C5-C6 bond needs to be determined. As discussed in section 1.4 there are 3 possible conformations for this bond. An A value of 1.0 would indicate no rotation about the C5-C6 bond (*i.e.* one fixed conformation) and a value of 0.11 would indicate free rotation (*i.e.* equal occupancy of all three conformations).

The average nT_1 time for the ring carbons of cellobiose in pure water is 0.92 s. The slight anisotropic motion about the long axis of the molecule was ignored for this

analysis. Using the above equations, when Δ is set to zero (*i.e.* no internal motion), a value for τ_r of 1.51×10^{-10} s was calculated. For cellobiose in NMMO the minimum occurs at 0.22 s and this leads to a value for τ_r of 1.12×10^{-9} s. Now that we have calculated the correlation time for the main motion of cellobiose molecules in water and in NMMO solution we can determine values for A and thus assess the rotational freedom of the C5-C6 bond.

nT_1 values of 0.97 and 0.45 s were obtained for the α'_6 carbon of cellobiose in water and in NMMO respectively. The latter figure was an approximation, using the data in table 4.3, of where the minimum occurs. The α'_6 carbon was chosen because the effect on nT_1 is most strongly observed at this site. Also, the data obtained at the minimum were used for our calculations because more variation between these values and those obtained in pure water occurred at this region. For the purpose of these calculations we estimated a value for τ_g (*i.e.* the internal motion of the C5-C6 bond) of 1.00×10^{-10} s. We had to estimate this value because we do not have any other data to help us calculate this parameter. Nevertheless, our estimate seems reasonable for this type of internal motion,[163] and the results below do not depend strongly on its exact value.

If we take τ_r as 1.51×10^{-10} s for cellobiose in pure water, τ_g as 1.00×10^{-10} s and nT_1 for α'_6 as 0.97 s then a value for A of 0.90 is obtained. This indicates that in pure water the C5-C6 bond occupies mainly one conformation. If we now take the value of 1.12×10^{-9} s for τ_r calculated for cellobiose in NMMO solution (*i.e.* assuming the minimum occurs at 0.22 s for the ring carbons), nT_1 as 0.45 s for α'_6 and again fixing τ_g as 1.00×10^{-10} s then A becomes 0.40. Since the value of A has significantly decreased, this indicates an increase of rotational freedom about the C5-C6 bond in the presence of NMMO. Thus our data suggests that there is indeed an interaction of NMMO with the C5-C6 region of cellobiose strong enough to break H-bonds that fix the conformation of

this bond. Thus, this study gives further support that the C5-C6 region of the molecule is very important for the dissolution of cellulose in amine oxides.

4.3.3.3 Methyl-β-D-cellobioside experiments

Figure 4.11 shows that a similar ^{13}C shift pattern is obtained for methyl-β-D-cellobioside in each of the six amine oxide solutions. Only pyridine-N-oxide (PNO) gives a slightly different shift pattern compared to the other five amine oxides. In common with the cellobiose experiments, no shift pattern could be deduced. It had been hoped that the non-solvents would cause smaller shifts, and that the relative shifts might reveal the site of interaction. Malulová *et al.* suggested that carbon co-ordination induced shifts arise because of the polarisation of oxygen atoms.[164] Using a range of complexes, they observed that the ^{13}C resonances shift downfield, which is consistent with the results of the present study.

Figure 4.12 shows shifts obtained for methyl-β-D-cellobioside in sodium hydroxide solutions of various concentrations. The $\Delta\delta$ carbon chemical shifts of the non-reducing ring decrease in the following order; C3' > C5' > C4' > C1' > C2' > C6'. This order is similar to that obtained for methyl-β-D-cellobioside in a concentrated NMMO solution, *i.e.* C3' = C5' > C4' > C1' > C2' > C6'. The non-reducing end of methyl-β-D-cellobioside was chosen for the above comparison because it is more like the central glucose units found in cellulose.

In order to determine if the carbon chemical shifts of methyl-β-D-cellobioside in amine oxides observed in this study are from full deprotonation, the following experiment was carried out. ^{13}C chemical shifts were measured for both ethanol and sodium ethoxide in toluene, using internal dioxan as a reference at 67.4 ppm. The differences in shifts between these two compounds were -0.37 ppm for the methylene carbon and 1.03 ppm for the methyl carbon. Since the shifts obtained for methyl-β-D-cellobioside in the most

concentrated sodium hydroxide solution are greater than these, they are probably caused by the interaction of base with the saccharide and not from full deprotonation. This interaction of base may induce carbon shifts because of polarisation of the methyl-β-D-cellobioside hydroxyls groups as suggested previously.

As stated above the order of decreasing $\Delta\delta$ values obtained for methyl-β-D-cellobioside in NMMO and sodium hydroxide solutions follow a similar shift pattern. Therefore, this suggests that the ^{13}C shifts observed are probably caused mainly by the ability of both these solvents to act as a base towards methyl-β-D-cellobioside and do not depend on the energy of interaction between the solvent and solute. All six amine oxides used in this study gave a similar shift pattern and thus all act as a base towards the saccharide, regardless of whether they are a solvent or non-solvent for cellulose. Since some resonances shift more than others, this suggests that the acidic characters of the hydroxyl groups of methyl-β-D-cellobioside (and cellobiose) molecules are unequal. Nehls *et al.*[165] suggested that the C2 hydroxyl of cellobiose is the most acidic and Berger *et al.*[166] reported the C6 hydroxyl to be the most acidic. However, our results in the present study do not support either of these authors.

Finally, shifts were recorded for methyl-β-D-cellobioside using a DMF solution of NMMO and NEMO. In the literature DMF is stated not to interfere with the interaction between amine oxides and cellulose, allowing the complication of the presence of water to be eliminated.[115] The $\Delta\delta$ values (figure 4.13) are slightly larger for NMMO than for NEMO. This may indicate a stronger interaction between methyl-β-D-cellobioside and NMMO relative to NEMO. However, the shifts are very similar in both cases, so again, these experiments do not give any firm rationalisation on why NMMO can dissolve cellulose while NEMO cannot, even though these two amine oxides are very similar.

4.4 Summary and conclusion

This study has determined that the binding between methyl-β-D-glucopyranoside and NMMO (a solvent for cellulose) in DMSO-d_6 is about twice as strong as the binding between the non-solvent NEMO and the same saccharide (section 4.2). In contrast, the binding between NEMO and water is stronger than that measured between NMMO and water. The reason for the stronger interaction of NMMO (relative to the interaction of NEMO) with the saccharide, and the weaker interaction with water, is not fully understood. Perhaps, because NEMO interacts strongly with water, so that the N→O bond of this amine oxide become less available for binding to saccharides. This would lead to a weaker binding between NEMO and methyl-β-D-glucopyranoside. Other explanations are that NEMO binds more strongly than NMMO with DMSO and so is less willing to bind to the saccharide, or that NEMO molecules bind more strongly to other NEMO molecules, compared to NMMO molecules binding to other NMMO molecules. Again, either of these explanations would lead to a drop in the binding of NEMO with methyl-β-D-glucopyranoside. Of course, the actual reason could be a combination of the above possible explanations.

The ^{13}C shift pattern obtained for methyl-β-D-cellobioside in amine oxides is very similar to that observed for this saccharide in sodium hydroxide solution. In section 4.3.3.3, it was suggested that the reason for this was because amine oxides and sodium hydroxide both act as bases toward methyl-β-D-cellobioside. The ability of amine oxides to act as bases toward cellulose has been presumed for some time, but this work adds further weight to the assumption. As mentioned in section 1.7.1, the "cryptoionic" theory combines the acid-base concept with hydrogen bonding to rationalise the dissolution of cellulose in amine oxides. However, this theory does not explain why some amine oxides can dissolve cellulose while others cannot. All amine oxides have the ability to act as a base towards cellulose and all have a strong dipole moment, arising mainly from

the N→O bond. Thus the "cryptoionic" theory fails to fully explain dissolution of cellulose in these types of solvents.

Our study on methyl-β-D-cellobioside showed that similar ^{13}C chemical shifts occur in amine oxides regardless of whether they are solvents or non-solvents for cellulose. This suggests one or both of the following:

1. The ^{13}C shifts do not reflect the energy of binding between the amine oxides and methyl-β-D-cellobioside, but merely the existence of such binding. Since the solvent is very much in excess, each amine oxide is probably forced to bind with the saccharide, *via* mass action.

2. The interaction of all amine oxides with cellulose is the same and only the interaction with water or between other amine oxide molecules changes. Our experiments on the measurement of shifts of methyl-β-D-cellobioside with the presence of NMMO and NEMO using DMF as the solvent instead of water helps to support this. The ^{13}C shifts in the sugar upon binding were also very similar for either of the amine oxides, so the interaction should be similar in both cases.

nT_1 measurements on cellobiose in various concentrations of NMMO further suggest that the interaction of this amine oxide occurs notably in the region of the C5-C6 bond. Thus, the present study adds further weight to the assumption that this region of the molecule is important for the dissolution of cellulose in amine oxides (see section 1.7.2), and involves the loosening of hydrogen bonds.

So far in the present investigation experiments using solution-state NMR discussed above have been moderately successful in understanding the dissolution process of cellulose with amine oxides using soluble model compounds for this polymer. The next

and final chapter continues this study with further experiments using the technique of solid-state NMR spectroscopy on actual cellulose samples. This investigation was aimed at monitoring the changes that occur to cellulose during the dissolution of this polymer in an NMMO solution. Changes that occurred to ramie fibres (if any) after treatment with non-solvents have also been monitored by the solid-state NMR technique with the anticipation that this will explain why some of these amine oxides cannot dissolve cellulose, but can swell it. Our expectation was that the solid-state NMR experiments would complement the results obtained from the solution-state experiments reported in this chapter and thus provide us with a better understanding of the interactions between cellulose and amine oxides.

CHAPTER FIVE

Solid-State NMR Study of the Interaction of Amine Oxide Solutions With Cellulose

5.1 Introduction

Solid-state NMR experiments were carried out using the spectrometer at Courtaulds research. The purpose of these experiments was to monitor the changes that occur during the production of cellulosic spinning solutions with the hope that this would give insights on the dissolution process of cellulose in NMMO.

Solid-state experiments were also run on ramie fibres treated with several amine oxides that are non-solvents for cellulose. The expectation is that this study will help elucidate the differences between the interaction of solvents and non-solvents with cellulose and assist in the formulation of a dissolution theory.

5.2 Experimental

An initial sample (the premix) was prepared by mixing 36 g of Avicel microcrystalline cellulose (MCC) with 124 g of N-methylmorpholine-N-oxide (NMMO) / water solution (79.6 % w/w) on a glass dish. Thus the components of the initial sample, with overall composition in brackets, were as follows: 36 g cellulose (22.5 % w/w), 98.7 g NMMO (62.7 % w/w) and 25.3 g water (15.8 % w/w). The NMMO solution was maintained at a temperature of 40 °C prior to use, to enable it to be easily mixed with the cellulose (for the NMMO solution becomes solid at room temperature). Two drops of N-propylgallate solution (10 % w/w in propan-2-ol) were added to this mixture as an NMMO stabiliser. The premix was stirred until all the cellulose was soaked with the NMMO solution.

Aliquots of the premix were taken after heating at 120 °C in an oven for 0, 60, 120 and 220 minutes (*i.e.* samples 1, 2, 3 and 4 respectively). The mixture was stirred at intervals of 10 to 15 minutes to ensure homogeneity of each sample. Sample 4 is thought to represent a solution of fully dissolved cellulose.

A Bruker ACP 300 MHz instrument (operating at 75 MHz for ^{13}C spectroscopy) fitted with a solid-state probe and high power pulse units was used to obtain ^{13}C NMR spectra of the four samples, plus pure Avicel microcrystalline cellulose. CPMAS spectra were obtained using a contact time of 2 milliseconds, and a repetition delay of 3 seconds was used for both CPMAS and HPDEC/MAS experiments. 1 k of FID data points were used for each acquisition together with a sweep width of 80 ppm. An exponential window function was applied with a line broadening of 25 Hz to enhance the signal-to-noise ratio. Spin rates of between 2.3 and 3.75 kHz were used depending on the stability of the rotor during acquisition. Spectra using both CPMAS and HPDEC/MAS techniques were acquired at 298 K and at 363 K.

The magic angle was optimised using the bromide resonance of KBr until maximum signal was obtained. Adamantane was utilised to find the Hartmann-Hahn condition and also to calibrate the spectrometer, using the peak at 38.4 ppm.

A CPMAS spectrum was also run at 298 K on an amorphous* sample of cellulose, donated by Courtaulds Research, using a contact time of 2 ms.

As a comparison, a ^{13}C solution-state spectrum of a 7 % (w/w) NMMO solution was also run at 100 °C on a Bruker ACP 400 spectrometer.

* Amorphous refers to a disordered phase of cellulose (see section 1.4.7). This disordered phase may occur naturally or be created by the action of solvent on crystalline cellulose.

Ramie fibres treated with non-solvents (*i.e.* 90 % w/w NEMO / water, 68 % w/w TMAO / water and 100 % PNO) at 100 °C for about an hour were also run using CPMAS at 298 K with a 2 ms contact pulse. More details about these experiments are given in section 5.8.

5.3 Results

Figure 5.1 shows a comparison of ^{13}C spectra obtained from amorphous and crystalline cellulose, both in the solid-state (CPMAS), and a solution-state NMR spectrum of fully dissolved cellulose in NMMO at 373 K. Table 5.1 lists the ^{13}C shifts of these three spectra. The crystalline spectrum was obtained by subtracting a spectrum acquired from cellulose pulp with that of amorphous cellulose.

Table 5.2 shows ^{13}C chemical shift positions of cellulose and NMMO obtained using the four samples prepared, plus pure Avicel MCC, obtained from CPMAS and HPDEC/MAS experiments. Intensity data using arbitrary units are shown in table 5.3. These values also depend on the amount of sample packed into the rotor, and since this inevitably will vary with each run, they are shown as a rough guide only. Figure 5.2 shows a comparison of ^{13}C spectra obtained from MCC using CPMAS at 298 K and HPDEC/MAS at 363 K. CPMAS ^{13}C spectra obtained at 298 K of samples 1 to 4 are shown in figures 5.3 and HPDEC/MAS spectra obtained at 363 K for the same set of samples are shown in figure 5.4.

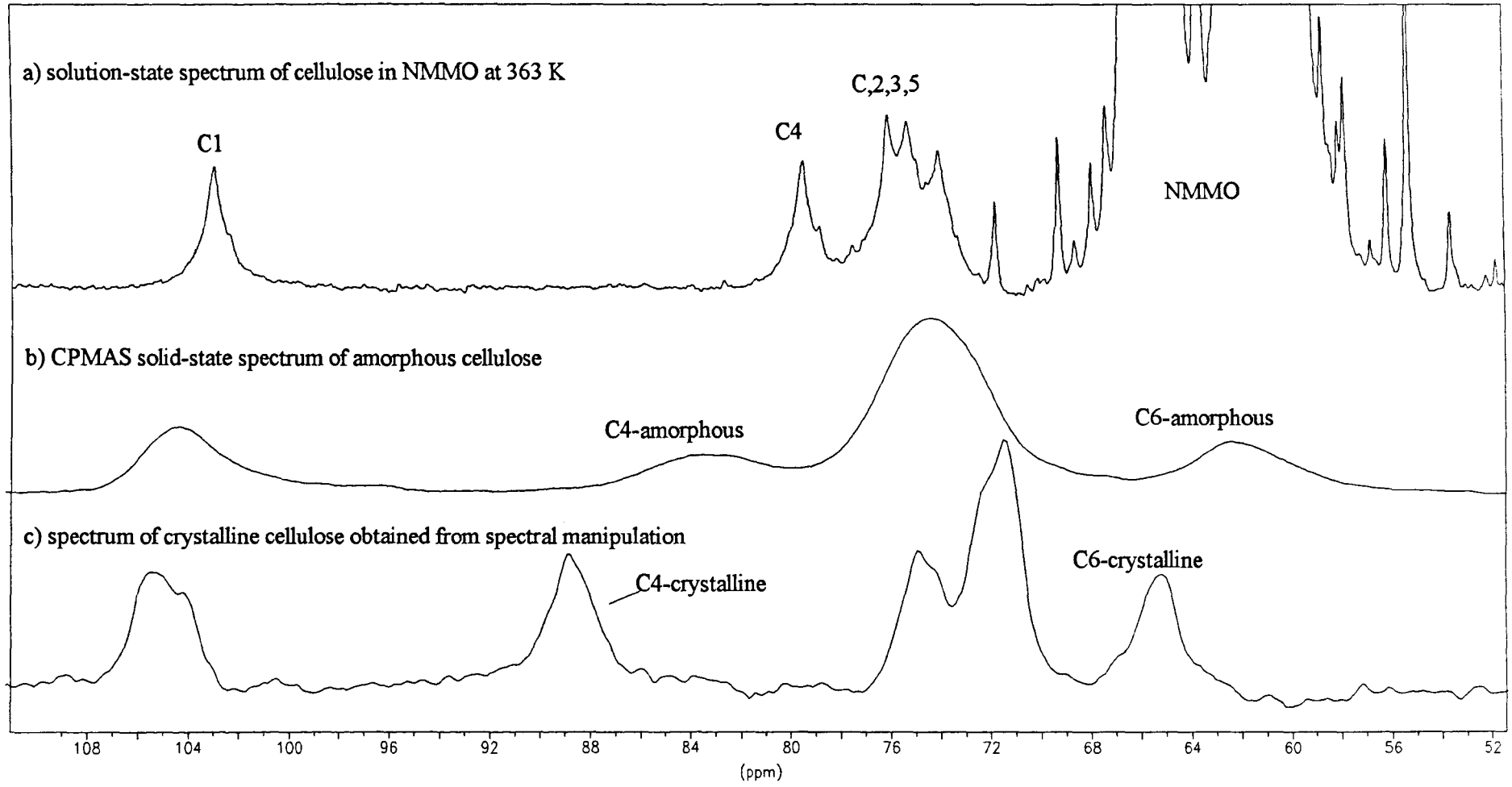

Figure 5.1 Comparison of amorphous and crystalline cellulose using CPMAS at 298 K with a solution-state spectrum of cellulose in NMMO recorded at 373 K. Smaller unlabelled peaks (top spectrum) are impurities from the NMMO sample.

Table 5.1 Carbon chemical shifts of amorphous and crystalline cellulose in the solid phase compared with solution-state shifts of cellulose in an NMMO solution. The solid-state spectra were recorded at 298 K and the solution-state spectrum was recorded at 373 K.

Spectrum	C1 peak	C4 peak	C2,3,5 peak	C6 peak
crystalline cellulose[a]	105 (ppm)	88.6	74.66, 71.3	65.2
amorphous cellulose	104.4 (ppm)	83.3	74.5	62.4
NMMO cellulose solution	103 (ppm)	79.5	76.1, 75.4, 74.1	[b]

[a] obtained from spectral manipulation (see text)
[b] overlapped by NMMO peaks

Table 5.2 ^{13}C shifts obtained for MCC and those recorded for samples 1 to 4.

Material	Technique	Temperature	Chemical shifts of cellulose carbons (ppm)			
			C1 peak (ppm)	C4 peak	C2,3,5 group of peaks	C6 peak
MCC	CPMAS	298 K	105.0c	89.0[c], 84.1[a]	74.8, 72.2	65.2[c], 62.9[a]
sample 1			105.0	88.7, 83.8	74.8, 71.8	hd
sample 2			105.3, 104.3[s]	88.41[c], (85.8, 83.8)[a]	75.1, 72.5	hd
sample 3			106.3, 105.0	85.5, 82.93	75.1, 72.5	hd
sample 4			104.7	81.1	75.47	hd
MCC	CPMAS	363 K	105.0[c]	88.8[c], 83.7[a]	74.9, 72.8	65.2[c], 62.9[a]
sample 1			nr			
sample 2			105.3, 104.3[s]	88.4[c], 83.8	75.1, 72.8	hd
sample 3			105.8, 104.2	83.7, 80.1	75.3	hd
sample 4			nr			
MCC	HPDEC	298 K	104.7[a]	nd	74.5, 72.8	62.5[a]
sample 1			nr			
sample 2			nd	nd	74.5	hd
sample 3			nd	nd	74.6	hd
sample 4			nr			
MCC	HPDEC	363 K	104.7[a]	84.5[a]	74.6, 73.0	62.5[a]
sample 1			105.0, 103.34	84.8, 80.5	76.1, 74.5	hd
sample 2			103.3	80.1	76.13, 75.1[s]	hd
sample 3			103.4	79.56	75.4	hd
sample 4			103.2	80.1	75.8	hd

nd = not detected
nr = not run
hd = hidden by NMMO peaks

[a] amorphous
[c] crystalline
[s] shoulder

Table 5.3 ^{13}C intensity data obtain for MCC and those recorded for samples 1 to 4.

Material	Technique	Temperature	Intensity of cellulose resonances (arbitrary units)			
			C1 peak (ppm)	**C4 peak**	**C2,3,5 group of peaks**	**C6 peak**
MCC	CPMAS	298 K	18.6[c]	12.2[c], 5.9[a]	30.8, 33.6	14.0[c], 7.5[a]
sample 1			22.0	13.9, 6.3	29.1, 36.9	hd
sample 2			12.4, 10.7[s]	5.4[c], (5.3, 4.3)[a]	19.4, 23.5	hd
sample 3			8.0, 7.5	4.5, 4.0	16.4, 13.2	hd
sample 4			6.6	3.4	16.6	hd
MCC	CPMAS	363 K	9.7[c]	5.3c, 2.9[a]	15.5, 15.9	6.0[c], 4.3[a]
sample 1			nr			
sample 2			7.9, 7.0[s]	2.6[c], 3.3	16.1, 12.4	hd
sample 3			3.8, 3.3	2.0, 2.5	11.6	hd
sample 4			nr			
MCC	HPDEC	298 K	1[a]	nd	2..0, 2.2	2.6[a]
sample 1			nr			
sample 2			nd	nd	4.8	hd
sample 3			nd	nd	7.3	hd
sample 4			nr			
MCC	HPDEC	363 K	1.6[a]	0.7[a]	3.5, 3.0	2.5[a]
sample 1			1.7, 2.5	0.2, 0.9	5.4, 4.7	hd
sample 2			5.7	5.9	13.6, 12.2[s]	hd
sample 3			6.1	8.1	14.4	hd
sample 4			4.6	6.4	12.7	hd

nd = not detected
nr = not run
hd = hidden by NMMO peaks

[a] amorphous
[c] crystalline
[s] shoulder

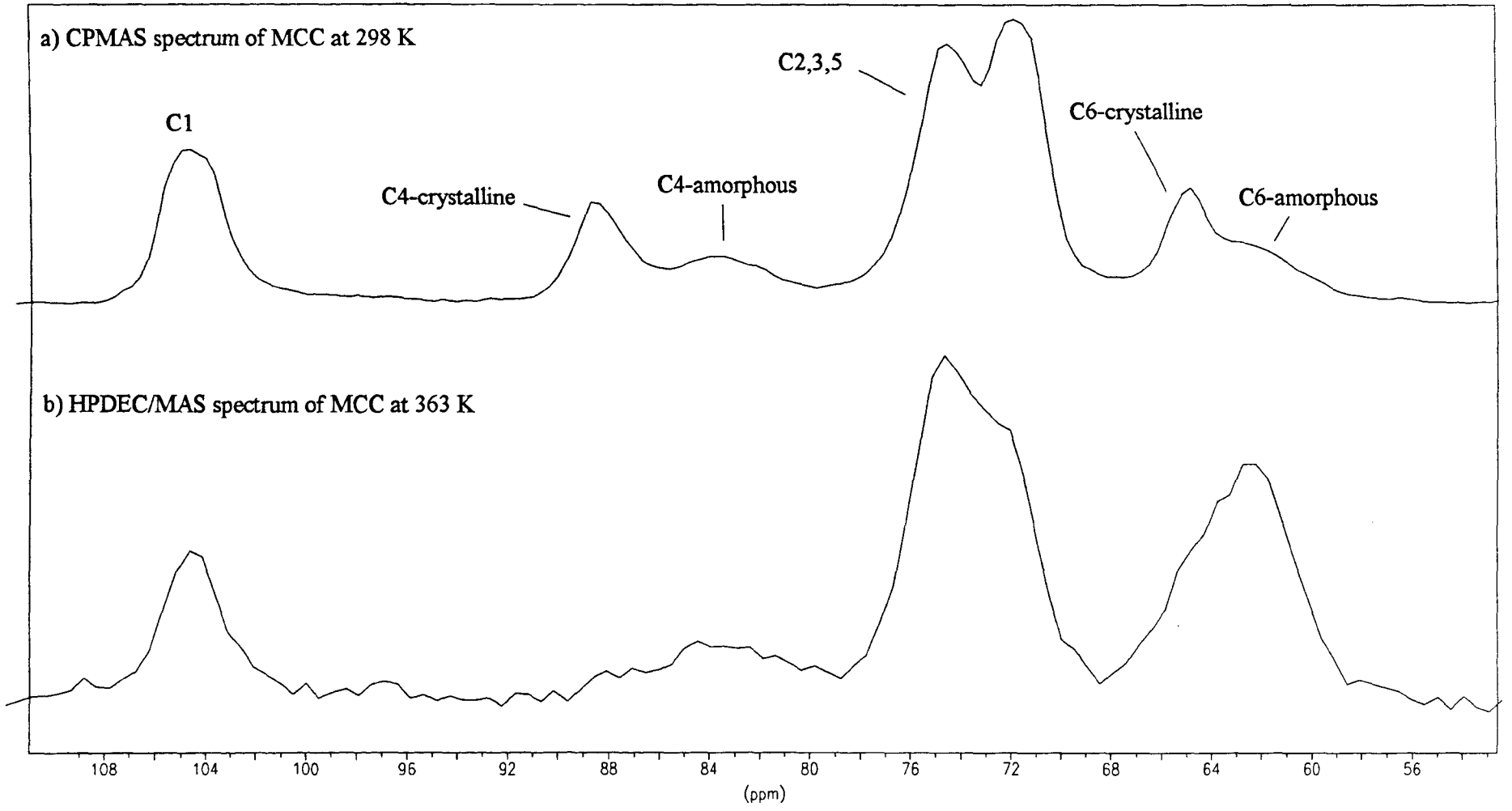

Figure 5.2 A comparison of spectra obtained from MCC using; a) CPMAS at 298 K and b) HPDEC at 363 K.

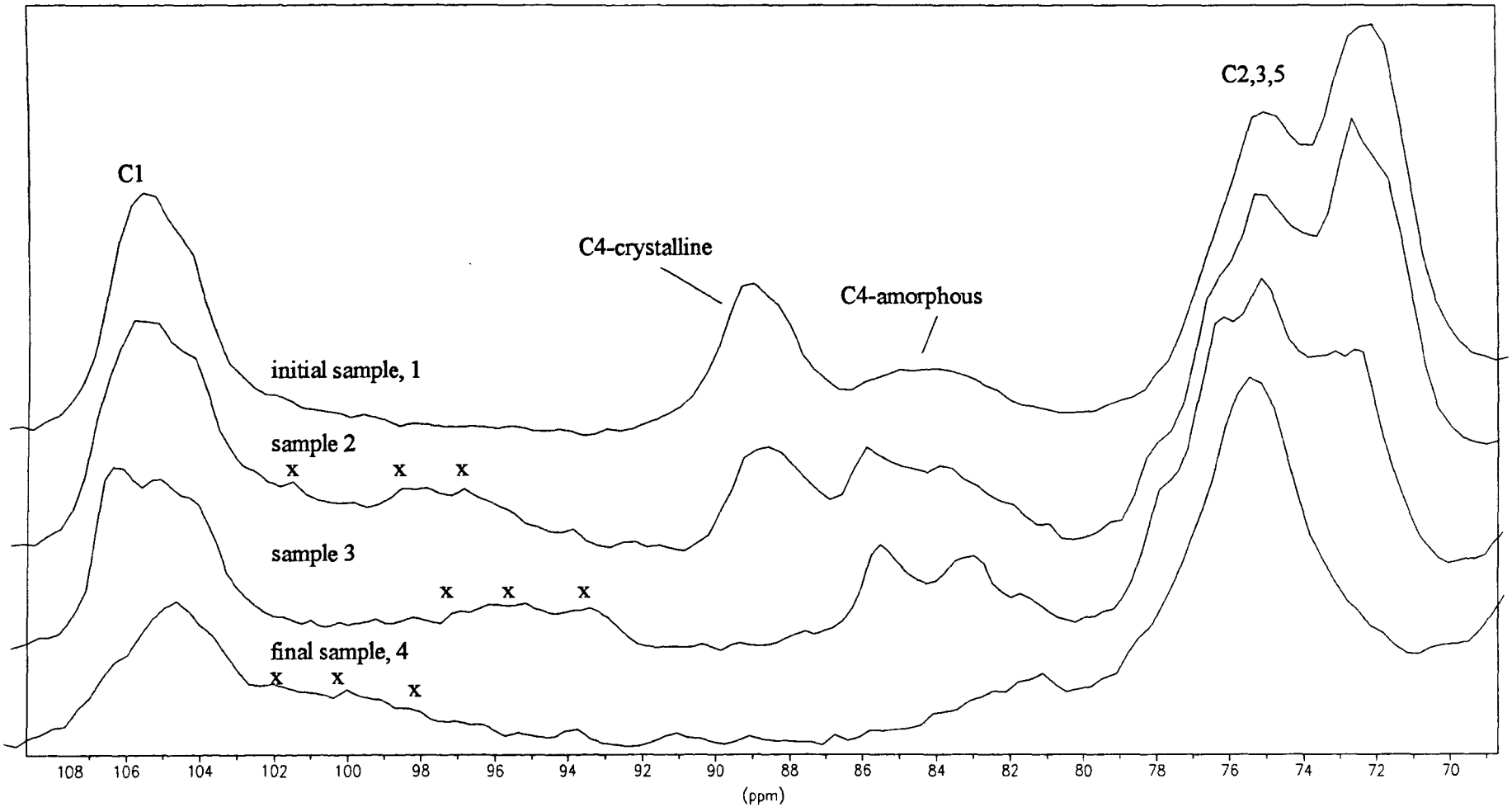

Figure 5.3 Sequence of CPMAS spectra recorded at 298 K obtained from samples 1 to 4. Spinning side-bands are marked by X.

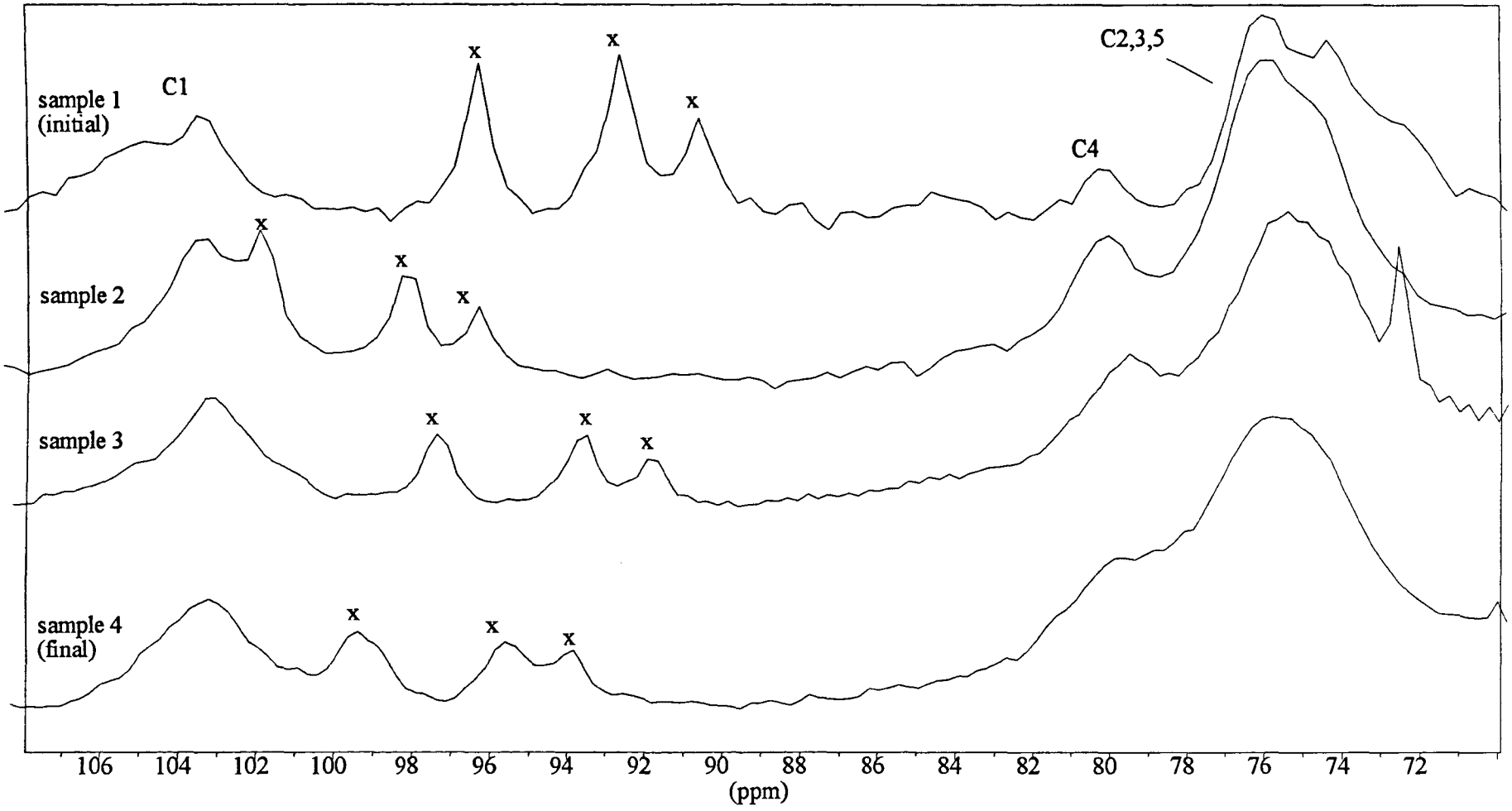

Figure 5.4 Sequence of HPDEC spectra recorded at 363 K obtained from samples 1 to 4. Spinning side-bands are marked by X.

5.4 Discussion

5.4.1 Pure Avicel samples

In the CPMAS spectra of MCC, the peaks have approximately twice the intensity at 298 K than at 363 K (not shown). This is probably because CPMAS experiments favour rigid structures, and at the lower temperature the molecules would be expected to move less. In HPDEC/MAS only amorphous regions (*i.e.* ~84 ppm for C4 and ~63 ppm for C6) show. This indicates that they have somewhat enhanced mobility relative to the crystalline region. In contrast, CPMAS shows crystalline regions (*i.e.* ~89 ppm for C4 and ~65 ppm for C6) plus some amorphous regions as above.

5.4.2 Samples 1-4

At 298 K the cellulose solutions made in this study are highly viscous; the higher the cellulose concentration the more viscous the sample becomes. When the samples were heated to 363 K, they softened to form a syrupy solution. The temperature where each highly viscous sample becomes a syrupy solution is referred to in this chapter as the softening point. The softening point in this case is equivalent to the glass transition point of polymer materials.

Unfortunately, the C6 resonance of cellulose overlaps with NMMO peaks and thus no information about this carbon was obtained in this study. However, it may be possible to repeat the procedure adopted in this investigation using a different amine oxide that does dissolve cellulose but does not overlap with the cellulose NMR peaks. However, because of time constraints with the solid-state spectrometer, we were unable to do this.

5.4.2.1 CPMAS at 298 K

At this temperature all samples were highly viscous or glassy. The CPMAS spectrum (sample 1) is initially similar to that of MCC under the same conditions except for a shoulder on C1 at about 104.5 ppm. This shoulder grows at the expense of the main peak at 105 ppm as the premix is heated. Possibly, this shoulder is an amorphous phase formed by the penetrating action of solvent on crystalline cellulose, its position being very similar to the C1 shift of solid amorphous cellulose (see table 5.1). However, the shifts could simply be from the influence of solvent on solid crystalline cellulose, and thus, the solvent-penetrated phase could have coincidentally the same chemical shifts as solid amorphous cellulose. Section 5.5 will discuss why a reduction in shift of C1 implies a rotation about the glycosidic bond as solid cellulose enters fully into solution.

The crystalline region of C4 reduces steadily in intensity as the preheating time increases, while the amorphous region of C4 splits into two and reduces in intensity more slowly, moving upfield, as with the amorphous region of C1. It appears that the crystalline component is dissolving faster than the amorphous phase. However, this is very unlikely, for the amorphous phase probably dissolves before the crystalline component enters fully into solution. The above observation that the crystalline region, evident in the peak at about 89 ppm, appears to dissolve before the solid amorphous phase may be explained as follows. Solvent penetrates the crystalline structure of cellulose, possibly creating an amorphous phase near the solvent regions, before complete dissolution of the polymer occurs. This explanation supports the theory proposed by Kabrelian (section 1.7.1) that NMMO has the ability to act as a wedge and penetrates into the ordered regions of the fibre structure before the polymer chains becomes completely separated.[111]

Since the peak at 84 ppm splits into two, there is possibly more than one phase of amorphous cellulose. Unfortunately this work so far does not give any firm evidence to

suggest that the structure of solvent-penetrated cellulose is similar to the structure of amorphous cellulose, and there is considerable doubt about its nature.

The C1 resonance shifts slightly downfield at about 106 ppm relative to the pure MCC at about 105 ppm during the intermediate stages of the sequence. This peak then shifts upfield to about 104.6 ppm as the cellulose enters fully into solution. These observations may arise from the formation of other polymorphs of cellulose, during the intermediate stages of dissolution. There is a possibility that cellulose I_{α}, being less stable* than the I_{β} polymorph, dissolves first. However, this was impossible to confirm in the present study.

The right-hand component of the C2,3,5 group of resonances (~72 ppm) reduces in intensity much faster than the left-hand region C2,3,5 component at about 75 ppm. The left-hand component loses less than half its intensity during the sequence and moves slightly downfield. This component may represent solvent-penetrated cellulose and the slight shift downfield is possibly the resonance from fully dissolved cellulose.

The NMMO peaks broaden (not shown) as the dissolution process proceeds. Some broadening is likely to arise in part from an increase in viscosity of the samples (*i.e.* as more cellulose dissolves the viscosity of the sample becomes greater) but may also involve the interaction of NMMO with cellulose. At room temperature the solvent molecules must have less mobility because of the high viscosity of each sample, and may also experience a range of chemical environments (*e.g.* some bound with cellulose and some not, *etc.*) creating a spread of resonances. As the temperature is raised above the softening point of each sample, the solvent molecules will have more mobility and experience an average chemical environment, thus, the peaks become narrower.

* See section 1.4.4.1

The final shifts obtained (*i.e.* sample 4) under these conditions are similar to those obtained for amorphous cellulose with CPMAS solid-state NMR. This indicates that the range of conformations of cellulose in an NMMO cellulosic spinning sample at ambient temperature may be similar to those of the solid amorphous component of this polymer.

Experiments using CPMAS at 298 K of similar sequences of samples to those used in this section were repeated using cellulose pulp and ramie fibres, in place of MCC. These spectra are similar to those described above.

The sequence of CPMAS spectra in this work is very similar to that obtained by Yokota *et al.* using cotton linters in sodium hydroxide solution of various concentrations.[167] They stated that the crystalline and amorphous phases seem to be attacked simultaneously by sodium hydroxide. However, the more likely explanation is that as the sodium hydroxide concentration increases the solvent penetrates the crystalline region and this leads to a broad peak with similar chemical shifts to solid amorphous cellulose (*i.e.* at about 84 ppm for C4). As with NMMO described above, complete dissolution occurs after solvent-penetration of the crystalline phase has taken place. The solid amorphous phase is presumably dissolved directly before the crystalline region has been completely attacked by the solvent.

5.4.2.2 CPMAS at 363 K

The CPMAS spectra obtained at 363 K (samples 2 and 3 only) are similar to that at 298 K except for the NMMO peaks being less broad at the higher temperature because of a fall in viscosity. Also, the cellulose peaks, as expected, have less intensity since CPMAS disfavours mobile species. Although there is little CPMAS enhancement, the solvent peaks appear because of the high concentration of NMMO in each sample.

5.4.2.3 HPDEC/MAS at 298 K

HPDEC/MAS spectra at 298 K show very little other than NMMO peaks becoming broader as preheating increases, for the same reasons as discussed above. Cellulose peaks are not detectable because at 298 K the polymer molecules move too slowly.

5.4.2.4 HPDEC/MAS at 363 K

There is no overall broadening of the NMMO peaks as the preheating time increases. Molecules of dissolved cellulose at this temperature move much more than those in the highly viscous solution and so are more readily detected under these conditions. The spectra show that the peaks from dissolved cellulose (~103 ppm for C1, ~80 ppm for C4 and ~76 ppm for C2,3,5) grow as the preheating time increases. These shifts are identical to those obtained in true solution-state NMR spectroscopy of cellulose dissolved in NMMO (see table 5.1). The transition of the CPMAS shifts of C1 (~104.7 ppm) and C4 (~81 ppm) at 298 K to the ones obtained for HPDEC/MAS stated above occurs at the softening point of the highly viscous solution. This temperature is very dependent on the composition of the highly viscous solution (see section 1.7.4), and is inevitably different depending on the particular sample studied.

Since there are differences between sample 1 and pure MCC, this indicates that the solvent interacts with the polymer during acquisition. Since the acquisition took several hours at 363 K it is not surprising that some cellulose passes into solution.

The C1 and C4 shifts obtained for solvent-penetrated and amorphous cellulose in the CPMAS spectra appear about halfway between the shifts observed for crystalline and dissolved cellulose. This indicates that solvent-penetrated cellulose could be an intermediate state of this polymer and is probably similar in nature to amorphous cellulose. Evidence to support this will be discussed in section 5.8.

5.5 NMR shift theory of the dissolution of cellulose

Kochetkov *et al.*[168] have suggested that the glycosidic and aglycone (*i.e.* C1 and C4 in this case) ^{13}C chemical shifts in disaccharides correlate with the distance between the two protons on these carbon atoms, *i.e.* protons 1 and 4 in figure 5.5. Bock *et al.* also attempted to correlate this distance with the anomeric and aglycone ^{13}C glycosylation shifts (figure 5.6) and found that the smaller the distance between these two protons, the greater are the shifts.[169] This helps to account for the marked difference in shift recorded between the C4 peak at 89 ppm from the crystalline component of native cellulose, and the C4 peak at 79 ppm from dissolved cellulose. In the solid phase of cellulose I,* the crystalline component has all its C5-C6 bonds positioned in the *tg* conformation (figure 5.7 shows the three possible conformations about the C5-C6 bond of a glucose unit). This pattern of H-bonding prevents the glycosidic linkage from taking up other conformations, and therefore ensures a rigid chain structure and partly explains the unusually high shifts of the C1 and C4 peaks of solid cellulose relative to those recorded for monosaccharide molecules in solution. Since the H-bonds involving C6 break as solvent penetrates the crystalline phase during dissolution of cellulose, the glycosidic bond is now free to occupy other conformations. Rotations about the glycosidic bond from the angles set in cellulose will always increase the distance between the two protons on the glycosidic and aglycone carbons, and according to figure 5.6, this will lead to a

* The structure of cellulose I is described in section 1.4.2.

reduction of δ_C. Therefore we conclude that the -10 ppm shift difference between the C4 peak from crystalline cellulose and dissolved cellulose is mainly because of rotations about the glycosidic bond. The -2 ppm shift difference for the anomeric carbon between crystalline and dissolved cellulose (*i.e.* from 105 to 103 ppm) is also likely to arise from those glycosidic bond angles, permitted only in the solution-state. The origin of these shifts is not yet fully understood, but are almost certainly related to the γ-*gauche* effect (see section 1.1), but other steric effects may be involved.

Hobley *et al.* found that larger ^{13}C shifts were observed when a C-O bond in pyranose monosaccharides is *syn-axial* to the C-H bond, relative to a C-O bond being *syn-axial* to another C-O bond.[20] Because cellulose I has C5-C6 bonds in the *gt* conformation the C6-O and C4-O bonds are positioned *syn-axial* to one another. But as cellulose dissolves, the C5-C6 bond will occupy other conformations. Thus, rotations about the C5-C6 bond will also contribute to shift changes that occur at C4 as cellulose passes into solution.

In the solid-phase NMR spectrum of amorphous cellulose the C5-C6 bonds will also occupy various conformations because of the irregular packing of the chains. This leads to a distribution of shifts, not averaged by motions. Thus a broad C4 peak is observed from the amorphous component of the cellulose, with the intermediate shift of *ca.* 84 ppm.

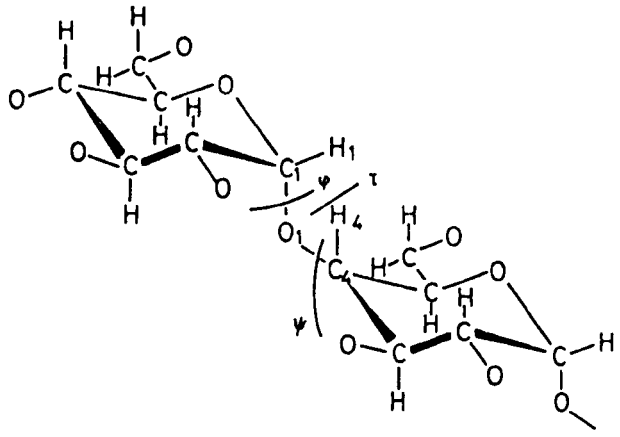

Figure 5.5 Definition of the torsional angles φ and Ψ which determines the conformation of the glycosidic linkage.

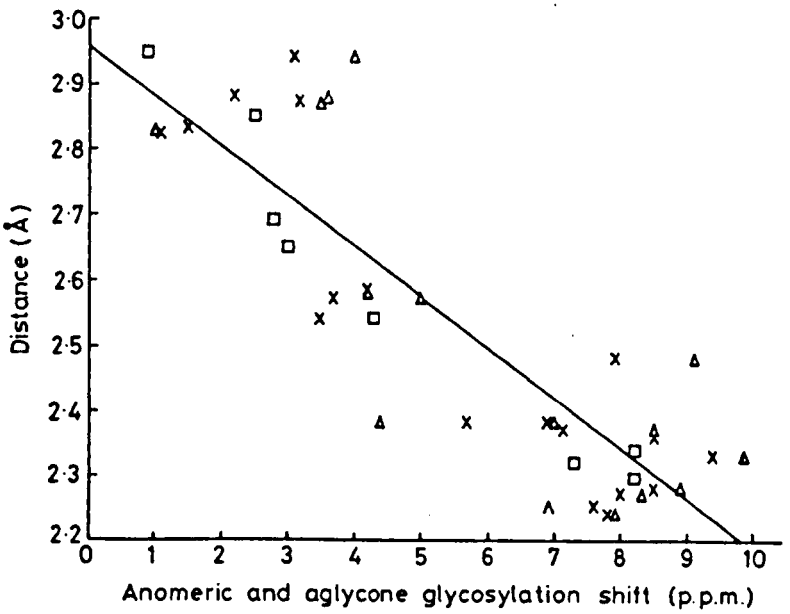

Figure 5.6 Correlation of glycosidation shifts for anomeric and glycone carbons with the distance between the protons attached to the anomeric and aglycone carbon atoms, respectively. x, Data from glycosidic carbon atoms of α-D-glucose; Δ, those from corresponding aglycone carbon atoms; □, those from glycoside carbon atoms of α-D-galactose.

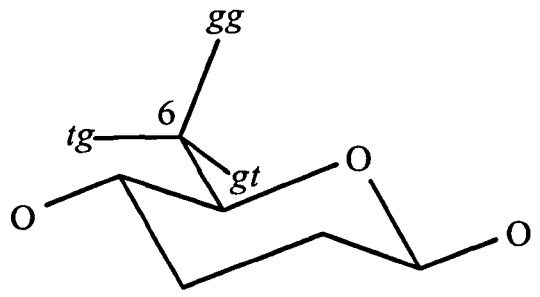

Figure 5.7 A glucose unit with 3 possible staggered positions for C6.

5.6 Comparison of NMR solid-state spectra with the microscopy study of cellulose

The optical microscopy photographs in chapter 3 (figure 3.2) clearly show the solvent-penetrated region of the outer layers of a ramie fibre. Swelling continues until these outer fibre layers become unobservable. They will then appear in the HPDEC/MAS spectra at 363 K as effectively dissolved cellulose, if we assume that the swelling process also induces significant chain motions.

The inner layers around the lumen are still largely untouched by solvent when swelling begins, since we observe breaks in this centre channel. This would not be observed unless the lumen was surrounded by solid material. The CPMAS sequence of spectra shows this solid material as undissolved crystalline cellulose and as the preheating time increases these peaks diminish in intensity. With time, the rest of the fibre swells (giving the solvent-penetrated region observed in CPMAS spectra) before complete dissolution occurs. After this stage, all crystalline components in the CPMAS spectra have gone.

5.7 Summary

Below is a summary of the dissolution sequence of cellulose in NMMO and the detection of each component using CPMAS at 298 K and HPDEC/MAS at 363 K. The assumption is that amorphous cellulose can be dissolved directly by the action of NMMO, whereas the crystalline components must first be penetrated by the solvent, breaking H-bonds between chains of this polymer, and thus forming a solvent-penetrated phase. Evidence in this work suggests that this solvent-penetrated phase of crystalline cellulose may be similar to amorphous cellulose, both having very similar shifts in the CPMAS spectra. However, the similar shifts observed for amorphous and solvent-penetrated crystalline cellulose could be coincidental. The shift recorded for penetrated cellulose may be from the influence of solvent and thus this phase may possibly have a different nature to amorphous cellulose. However, evidence in the next section will suggest that solvent-penetrated cellulose and amorphous cellulose are indeed similar.

Phase	CPMAS spectra	HPDEC/MAS spectra
Crystalline Cellulose	strongly visible	not visible
↓		
Solvent-Penetrated Cellulose	visible	weakly visible
↓		
Dissolved Cellulose	not visible	strongly visible
↑		
Amorphous Cellulose	visible	strongly visible

Figure 5.8 Sequence of cellulose dissolution and the detection of the various phases with CPMAS at 298 K and HPDEC/MAS at 363 K.

5.8 An investigation of the interaction of non-solvents on ramie

Optical microscopy experiments (section 3.3.1.4) have shown that although some amine oxides cannot dissolve cellulose, a subset of these do have the ability to swell ramie fibres without dissolving them. Chapter 3 showed that ramie fibres swelled when treated by NEMO and TMAO but were unaffected by PNO. Therefore, the purpose of these experiments was to acquire solid-state spectra of ramie fibres treated with these three non-solvents and detect if any morphological change had occurred. CPMAS and HPDEC/MAS experiments were run at 298 K and 343 K respectively. The results might help to elucidate the difference between the interaction of cellulose with solvents and non-solvents, and ultimately lead to a theory of dissolution.

The concentrations of the three amine oxide non-solvents (w/w with water) used for our solid-state NMR experiments are identical to those used during the microscopy study reported in chapter 3:

1. N-ethylmorpholine-N-oxide (NEMO) (90 %)
2. Trimethylamine-N-oxide (TMAO) (68 %)
3. Pyridine-N-oxide (PNO) (100 %)

All samples were prepared by heating ramie fibres in each of the above named amine oxides for about an hour at 373 K. Each spectrum of ramie obtained in this study was acquired without washing out the excess amine oxide from each sample (unless otherwise stated).

Some wide-angle X-ray diffraction experiments were also run on ramie fibres using a Phillips XRD instrument. The purpose of these experiments was to monitor the change (if any) of the morphology of the cellulose when treated with amine oxides that are non-

solvents for the polymer. However, limited information was gained because of overlapping solvent peaks.

5.8.1 Ramie treated with N-ethylmorpholine-N-oxide (NEMO)

The middle spectrum in figure 5.9, obtained under CPMAS conditions at 298 K, is of ramie treated with NEMO. This spectrum is identical to one published by Isogai *et al.* of cellulose III_I derived from ramie fibres.[170] Clearly, there has been an interaction between NEMO and cellulose, strong enough to slide sheets of the polymer relative to each other (thus altering the polymorphism) but too weak to break the strong H-bonds between adjacent chains. Cellulose I and III_I do not have any hydrogen bonds between sheets (see figure 1.4) and so the inter-sheet region can be more easily penetrated by a solvent than the region where adjacent chains are tightly bound together by H-bonds. Our optical microscopy photographs (figure 3.5) show ramie fibres swelling on application of NEMO. This observed swelling is probably because solvent has penetrated between cellulose layers. This consequent structural change is seen in the CPMAS spectrum as a conversion from cellulose I to cellulose III_I.

The CPMAS spectrum of ramie treated with NEMO shows only sharp peaks from crystalline cellulose. No peaks are observed from amorphous cellulose. However, a HPDEC/MAS spectrum recorded at 343 K of the same sample (top spectrum in figure 5.9) reveals the C1 and C4 peaks from the amorphous phase. Therefore, an amorphous phase associated with the cellulose III_I is still present but is not detected by our CPMAS experiments. It may therefore be more mobile than the corresponding amorphous phase in untreated ramie.

Figure 5.10 shows a CPMAS spectrum of ramie treated with NEMO (the same sample as discussed above) and then washed with water to remove the amine oxide, in comparison to a spectrum of untreated ramie (*i.e.* cellulose I). Clearly, the cellulose III_I formed by treatment with NEMO has reverted back to cellulose I. Wide-angle X-ray diffraction experiments confirmed that cellulose III_I has indeed reverted back to cellulose I. However, the intensity of the amorphous peaks of C4 and C6 from ramie treated with NEMO and then washed has significantly increased at the expense of the crystalline peaks. This shows that the NEMO has had the effect of decrystallising the cellulose, probably because this amine oxide was able to penetrate between the sheets of cellulose chains during the conversion from cellulose I to cellulose III_I.

A suggestion was made in section 5.4.2.1 that NMMO-penetrated cellulose has a similar C4 shift to amorphous cellulose. There were considerable doubts about what this observation meant. Had the crystalline phase become amorphous because of the structural loosening induced by the penetration of solvent, or did the shifts arise from the direct effects of bound NMMO, with these coincidentally giving the same chemical shift as amorphous cellulose? However, in the present case there is a relative increase in the amorphous peaks when ramie is treated with NEMO, followed by complete washing out with water. It therefore now seems likely that the solvent-penetrated phase of cellulose is indeed similar to amorphous cellulose and that the direct shift influence of the amine oxide, where present, is negligible.

5.8.2 Ramie treated with trimethylamine-N-oxide (TMAO)

Although TMAO was unable to convert cellulose I to the III_I polymorph (figure 5.11), there is evidence that some decrystallisation has occurred (*i.e.* the intensity of the C4 peak of the amorphous phase has increased at the expense of the crystalline peak). Clearly, there has been some interaction between cellulose and TMAO, but not strong enough to convert this polymer into another polymorph or to dissolve it. The microscopy study described in chapter 3 showed that TMAO can swell ramie fibres without any dissolution occurring. Since the CPMAS spectrum in figure 5.11 shows an increase in intensity of the amorphous peaks at the expense of the crystalline peaks after treatment with TMAO, the swelling observed under the microscope may occur because of a partial crystalline → amorphous transition in this cellulose sample, as well as through the intercalation of solvent.

5.8.3 Ramie treated with pyridine-N-oxide (PNO)

Figure 5.12 shows a spectrum of ramie treated with the non-solvent pyridine-N-oxide (PNO). Changes are again observed, but this time the C4 and C6 peaks from the amorphous regions are less easily detected. An explanation for this observation might be that some amorphous cellulose has dissolved in PNO even though this amine oxide is reported as a non-solvent. However, this is very unlikely and the observation mentioned above is probably because the experimental conditions in this case favoured detection of crystalline cellulose relative to the amorphous phase. The signal-to-noise ratio in this spectrum is low which makes the detection of the amorphous regions even more difficult. The microscopy study in chapter 3 showed no visible interaction of PNO with ramie fibres. Perhaps the interaction is too weak, or non-existent, and thus the cellulose in this case has been unaffected. An equivalent explanation is that the interaction between PNO

molecules is too strong for this amine oxide to dissolve cellulose. Since PNO was unable to swell ramie fibres, intercalation of solvent probably does not occur.

5.8.4 Summary of the interaction of non-solvent amine oxides on ramie fibres

In this study the interaction of three different non-solvent amine oxides with ramie fibres were investigated with solid-state NMR spectroscopy. The CPMAS spectra obtained showed that interactions between cellulose and two of the non-solvents (*i.e.* NEMO and TMAO) do indeed occur. Only NEMO was able to convert cellulose I to cellulose III_I. Both the solid-state experiments reported in this chapter and the optical microscopy experiments reported in chapter three showed that PNO had no effect on ramie. The results of these experiments also suggest that NEMO and TMAO begin to penetrate between sheets of cellulose that are held together only by relatively weak Van der Waals forces. However, the strength of this interaction is not sufficient enough to disrupt the strong H-bonds that hold adjacent chains of cellulose together, and thus dissolution does not occur.

Solid-state NMR experiments in this study have shown that some amine oxides that are non-solvents for cellulose can interact with this polymer. Therefore, it is not perhaps surprising that the solution-state experiments discussed in chapter 4 showed a similar carbon chemical shift pattern for methyl-β-D-cellobioside in various amine oxide solutions regardless of whether they are solvents or non-solvents for cellulose. The solution-state experiments also showed a slightly different shift pattern for methyl-β-D-cellobioside in a PNO solution. Hence, the interaction between PNO and cellulose may be slightly different from the others discussed in this study.

Finally, there was no effect on the solid-state NMR spectrum, and no swelling was observed with a microscope, when ramie fibres were heated in pure water. Therefore, any change that did occur to ramie fibres treated with the non-solvents must have occurred because of the interaction of these amine oxides on this polymer and not from the application of heat and water only.

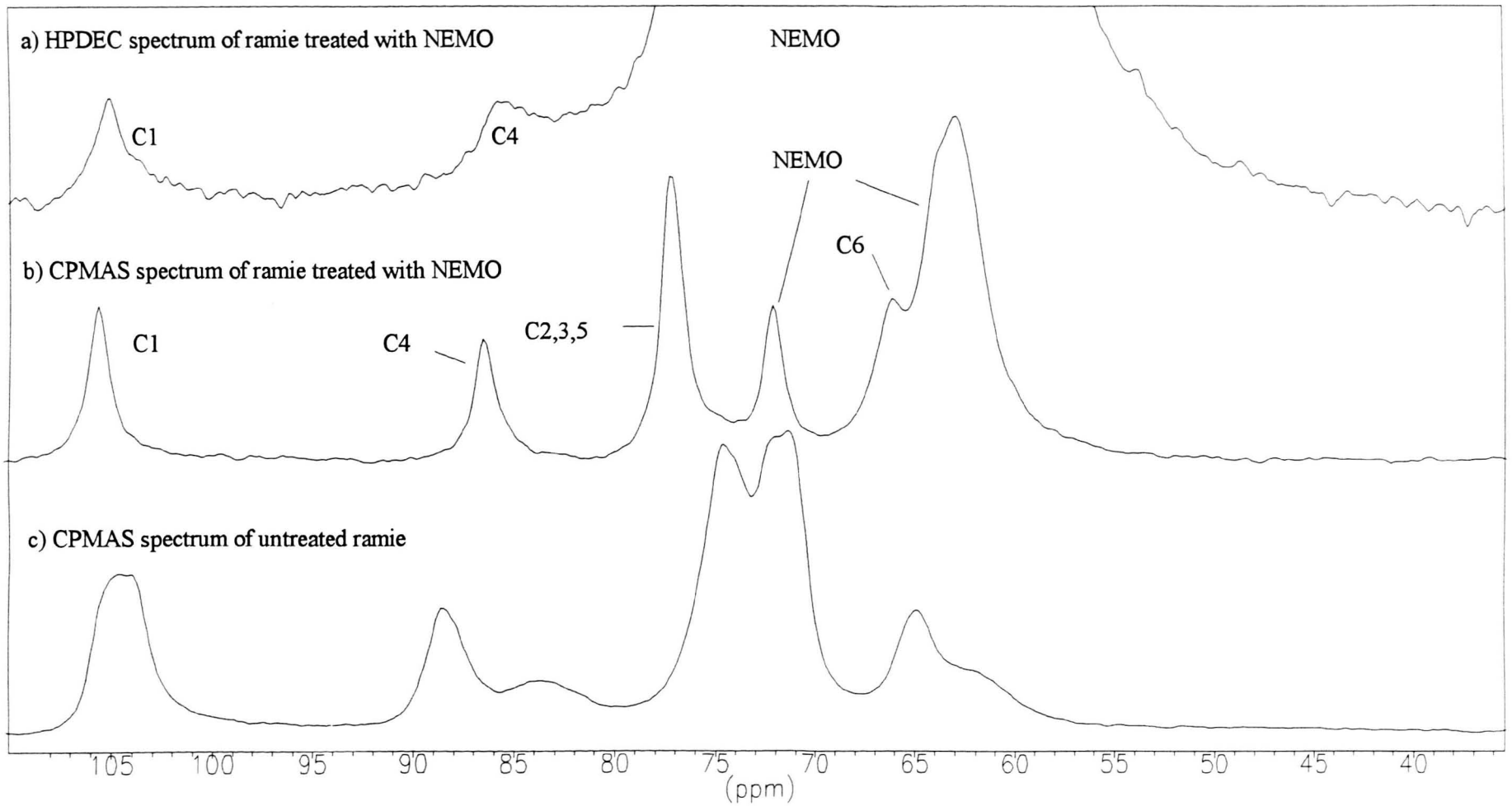

Figure 5.9 a) HPDEC spectrum at 343 K of ramie after treatment with NEMO b) CPMAS spectrum of ramie at 298 K after treatment with NEMO and c) CPMAS of untreated ramie. Concentration of NEMO in water used was 90 % w/w.

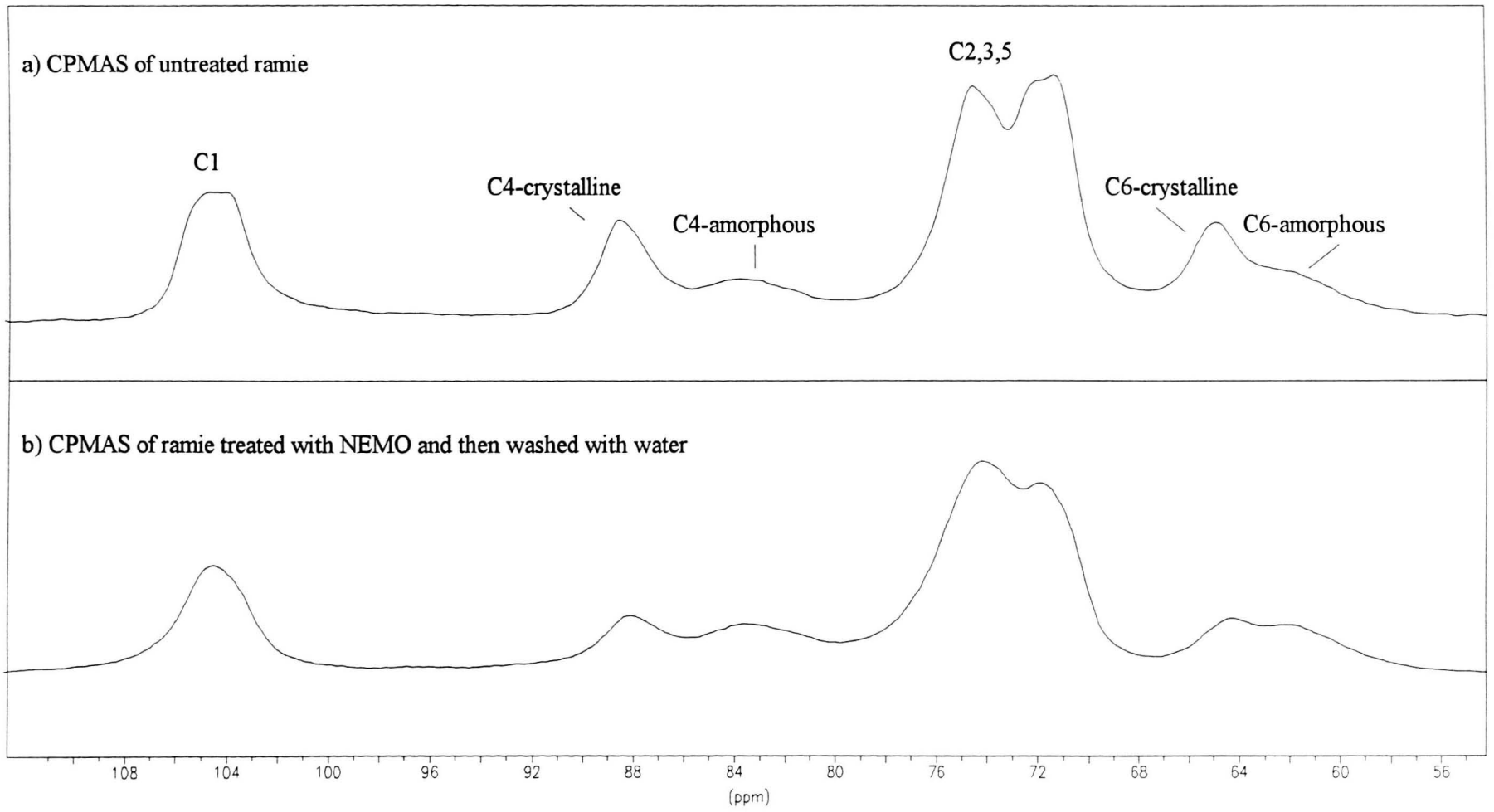

Figure 5.10 CPMAS spectra of ramie fibres at 298 K; a) untreated and b) after treatment with NEMO and then washed with water to remove the amine oxide.

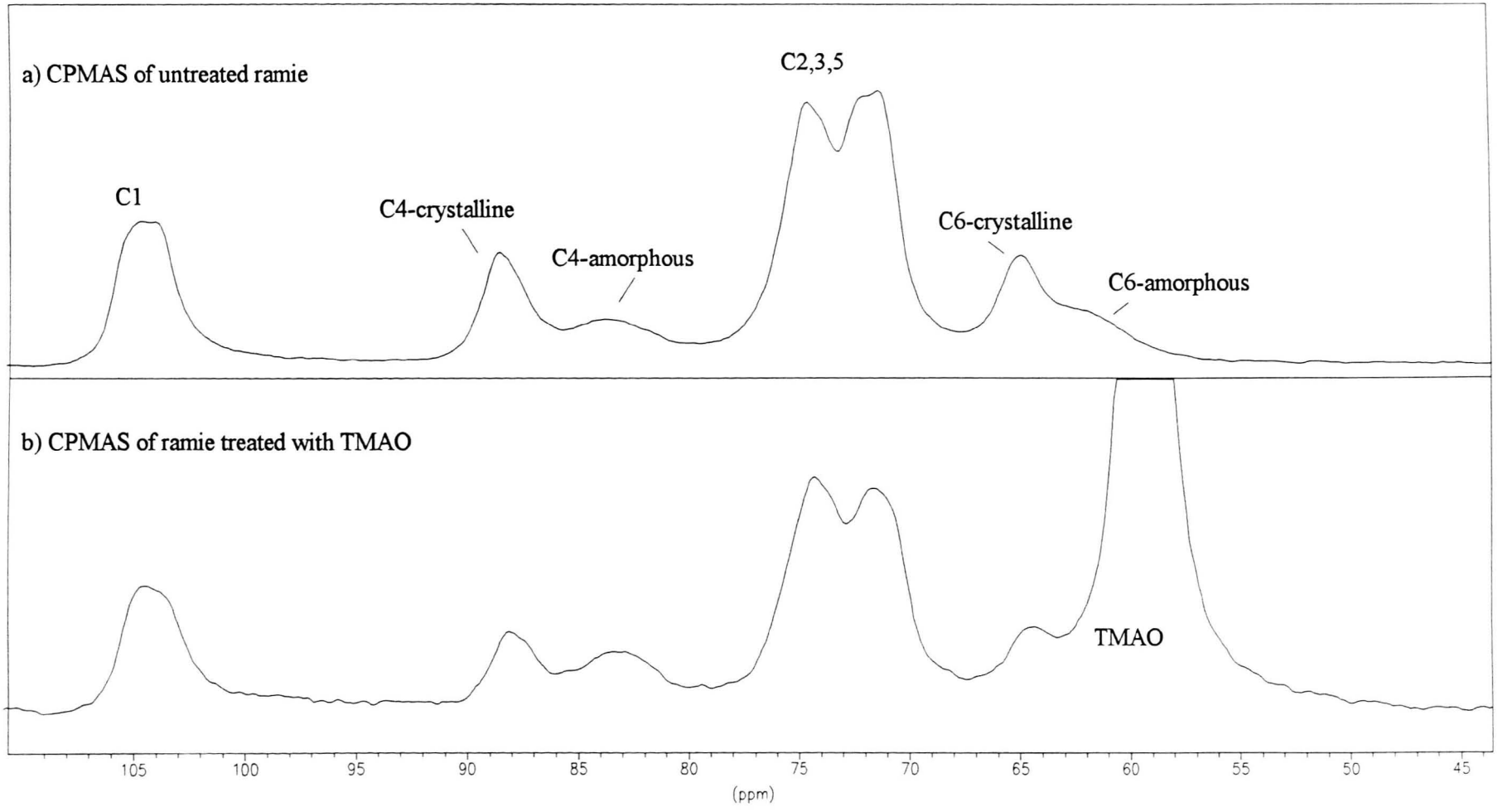

Figure 5.11 CPMAS spectra at 298 K of ramie fibres; a) untreated and b) after treatment with TMAO. The TMAO peak is covering the C6 amorphous peak.

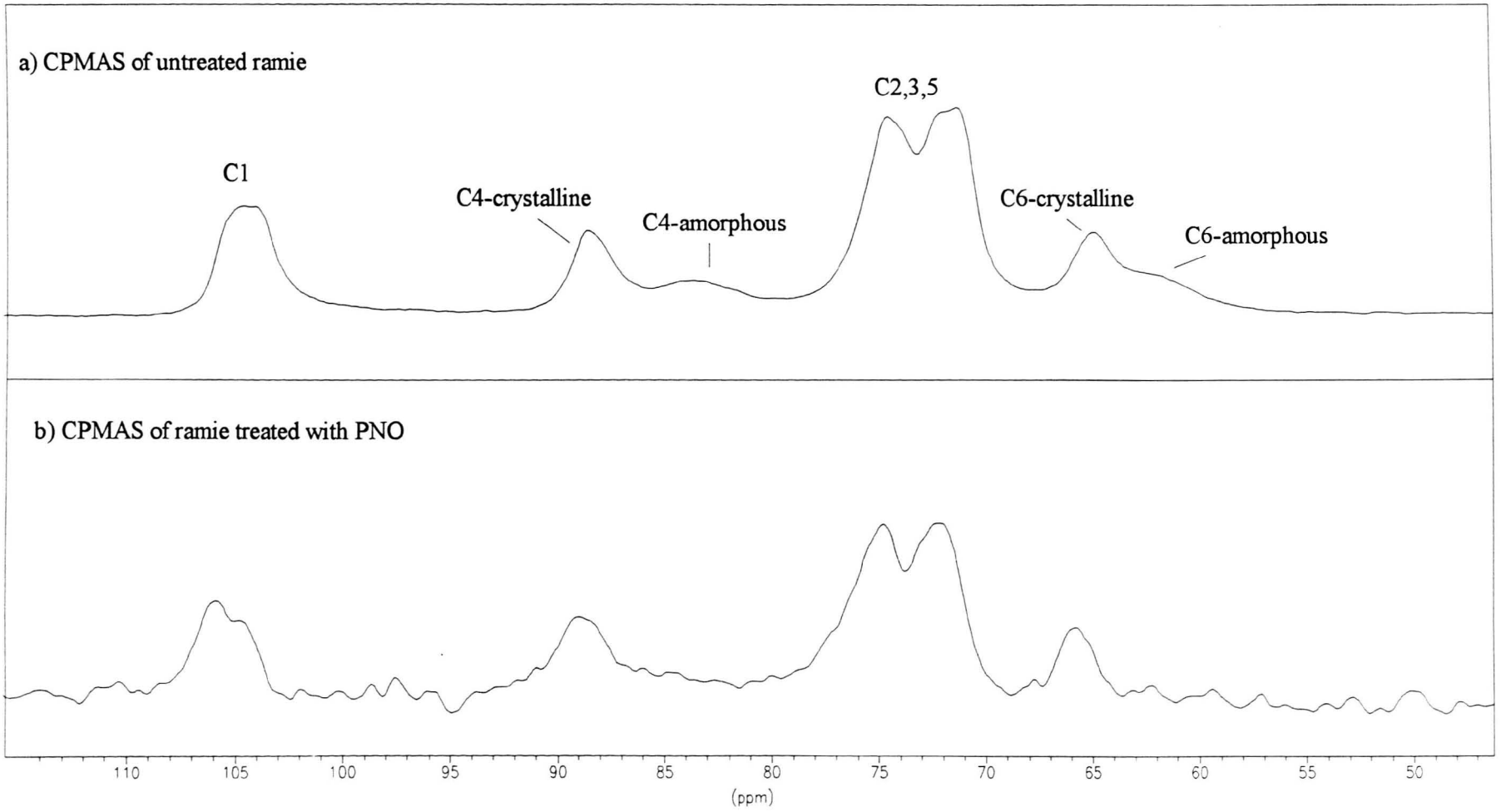

Figure 5.12 CPMAS spectra at 298 K of ramie fibres; a) untreated and b) after treatment with PNO.

REFERENCES

1. D. G. Smith, R. L. Jaffe and D. Y. Yoon, *J. Am. Chem. Soc.*, **117**, 530 (1995).
2. F. Müller-Plathe and W. F. van Gunsteren, *Macromolecules*, **27**, 6040 (1994).
3. G. D. Smith, R. L. Jaffe and D. Y. Yoon, *J. Phys. Chem.*, **98**, 9072 (1994).
4. D. G. Smith, R. L. Jaffe and D. Y. Yoon, *J. Phys. Chem.* **97**, 12752 (1993).
5. R. L. Jaffe, G. D. Smith and D. Y. Yoon, *J. Phys. Chem.* **97**, 12745 (1993).
6. M. A. Murcko and R. A. DiPaola, *J. Am. Chem. Soc.*, **114**, 10010 (1992).
7. S. Tsuzuki, T. Uchimaru, K. Tanabe and T. Hirano, *J. Phys. Chem.*, **97**, 1346 (1993).
8. A. Abe and J. E. Mark, *J. Am. Chem. Soc.*, **98**, 6468 (1976).
9. N. E. Franks and K. V. Julianna, United States Patent, No. 4,196,282 (1980).
10. A. E. Tonelli, *NMR Spectroscopy and Polymer Microstructure: The Comformation Connection*, PP 49-50, VCH Publishers, Inc. (1989).
11. R. U. Lemieux and K. Bock, *Jap. J. Antibiotics*, **32**, 163 (1979).
12. A. De Bruyn and M. Antenuis, *Bull. Soc. Chem. Belg.*, **84**, 799 (1975).
13. A. De Bruyn, M. Antenuis and J. van Beeumen, *Bull. Soc. Chem. Belg.*, **86**, 259 (1977).
14. L. M. Jackman and S. Sternhell, *Application of Nuclear Magnetic Resonance Spectroscopy in Organic Chemistry*, 2nd edn., Pergamon, Oxford (1969).
15. L. Braunschweiler and R. R. Ernst, *J. Magn. Reson.*, **53**, 521 (1983).
16. A. Bax and R. Freeman, *J. Magn. Reson.*, **44**, 542 (1981).
17. H. J. Jennings and I. C. P. Smith, *Methods in Carbohydrate Chemistry*, Vol. 8, Academic Press Inc., New York and London, p97 (1980).
18. J. A. Schwarcz and A. S. Perlin, *Canad. J. Chem.*, **48**, 2596 (1970).
19. K. Bock and C. Pedersen, *Carbohyd. Res.*, **71**, 319 (1979).
20. P. Hobley, O. W. Howard and R. N. Ibbett, *Magn. Reson. Chem.*, **34**, 755 (1996).
21. A. Pines, M. G. Gibby and J. S. Waugh, *J. Chem. Phys.*, **59**, 569 (1973).
22. J. Schaefer and E. O. Stejskal, *J. Am. Chem. Soc.*, **98**, 1031 (1976).
23. S. R. Hartmann and E. L. Hahn, *Phys. Rev.*, **128**, 2042 (1962).
24. J. T. Edward, *Chem. Ind (London)*, 1102 (1955).
25. E. Juaristi and G. Cuevas, *Tetrahedron*, **48**, 5019 (1992).
26. I. Tvaroška and T. Bleha, *Adv. Carbohydr. Chem. Biochem.*, **47**, 45 (1989).
27. N. S. Zefirou, *Tetrahedron*, **33**, 3193 (1977).
28. I. Tvaroška and T. Bleha, *Tetrahedron Letts.*, **4**, 249 (1975).
29. L. Phillips and V. Wray, *J. C. S. Chem. Comm.*, 90 (1973).
30. G. Baddeley, *Tetrahedron Letts.*, **18**, 1645 (1973).
31. E. A. C. Lucken, *J. Chem. Soc.*, 2954 (1959).

32. S. David, O. Eisenstein, W. J. Hehre, L. Salem and R. Hoffmann, *J. Am. Chem. Soc.*, **95**, 3806 (1973).
33. E. L. Eliel, C. A. Giza, *J. Org. Chem.*, **33**, 3754 (1968).
34. S. Wolfe, *Acc. Chem. Res.*, **5**, 102 (1972).
35. T. K. Brunck F. Weinhold, *J. Am. Chem. Soc.*, **101**, 1700 (1979).
36. N. S. Zefirov, V. S. Blagoveshchensky, I. V. Kazimirchik and N. S. Surova, *Tetrahedron*, **27**, 3111 (1971).
37. R. H. Marchessault and P. R. Sundararajan, *The Polysaccharides*, Vol. 2, Ed. G. O. Aspinall, Academic, New York (1983).
38. A. Payen, *Extrait des memoires de l'Acédemie Royale des Science: Tomes III des Savents Éntrangers*, Imprimerie Royale, Paris (1842).
39. W. N. Haworth, *Helv. Chim. Acta 11, 534; idem, Ber Dtsch. Chem. Ges. (A)*, **65**, 43 (1928).
40. H. Staudinger, *Die hochmolekularen organishen Verbindungen-Kautschuk und Cellulose 2nd Edn.*, Springer Verlag, Berlin (1960).
41. K. H. Mayer and H.F. Mark, *Z. Physik Chem.*, **2B**, 115 (1929).
42. K. H. Mayer and L. Misch, *Ber.* **70B**, 266 (1937).
43. K. H. Mayer and L. Misch, Helv. *Chim. Acta*, **20**, 232 (1937).
44. K. H.Gardner and J. Blackwell, *Biopolymer*, **13**, 1975 (1974).
45. A. Sarko and R. Muggli, *Macromolecules*, **7**, 486 (1974).
46. A. Sarko, *Appl. Polymer Sci. Symp.*, **28**, 729 (1976).
47. C. Woodcock and A. Sarko, *Macromolecules*, **13**, 1183 (1980).
48. P. Zulgenmaier and A. Sarko, *Biopolymer*, **12**, 435 (1973).
49. R. H. Marchessault and C.Y. Liang, *J. Polymer Sci.*, **43**, 71 (1960).
50. J. Blackwell and R. H. Marchessault, *Cellulose and Cellulose Derivatives*, Ed. N. M. Bikales and L. Segal, Part IV, John Wiley & Son, Ney York (1971).
51. J. Blackwell, J. Kolpak and K. H. Gardner, *Cellulose Chemistry and Technology*, Ed. J. C. Arthur, ACS-symp. Series No.48, American Chem. SDoc., Washington (1977).
52. A. J. Stipanovic and A. Sarko, *Macromolecules*, **9**, 851 (1976).
53. F. J. Kolpak and J. Blackwell, *Macromolecules*, **8**, 563 (1975).
54. F. J. Kolpak and J. Blackwell, *Polymer*, **9**, 273 (1976).
55. F. Kolpak, M. Weih and J. Blackwell, *Polymer*, **19**, 123 (1978).
56. S. Arnott and A. J. Wonacott, *Polymer*, **7**, 157 (1966).
57. T. Okano and A. Sarko, *J. Appl. Sci.*, **29**, 4175 (1984).
58. T. Okano and A. Sarko, *J. Appl. Sci.*, **30**, 325 (1985).
59. A. Sarko, J. Southwick and J. Hayashi, *Macromolecules*, **9**, 857 (1976).

60. J. Hayashi, A. Sufoka, J. Ohkita and S. Watanabe, *J. Polym. Sci., Polymer Letters* Ed., **13**, 23 (1975).
61. J. Sugiyama, J. Persson and H. Chanzy, *Macromolecules,* **24**, 2461 (1991).
62. R. H. Atalla and D. L. VanderHart, *Science*, **223**, 283 (1984).
63. R. H. Atalla and D. L. VanderHart, *Macromolecules,* **17**, 1465 (1984).
64. F. Horii, H. Yamamoto, R. Kitamaru, M. Tanahashi and T. Higuchi, *Macromolecules,* **20**, 2946 (1987).
65. H. Yamamoto, F. Horii, H. Odani, *Macromolecules,* **22**, 4130 (1989).
66. E. M. Debzi, H. Chanzy, J. Sugiyama, P. Tekely, G. E xcoffier, *Macromolecules,* **24**, 6816 (1991).
67. J. Sugiyama, J. Persson and H. Chanzy, *Macromolecules,* **24**, 2461 (1991).
68. J. Sugiyama, R. Vuong and H. Chanzy, *Macromolecules,* **24**, 4168 (1991).
69. M. Wade, J. Sugiyama and T. Okano, *J. Appl. Polym. Sci.,* **49**, 1491 (1993).
70. D. L. VanderHart, W. L. Earl and A. N. Garroway, *J. Magn. Reson.*, **44**, 361 (1981).
71. W. L. Earl and D. L. VanderHart, *Macromolecules,* **14**, 570 (1981).
72. J. O. Warwicker, R. Jeffries, R. L. Colbron and R. N. Robinsson, Shirley Institute Pamphlet No. 93, Manchester, England (1966).
73. S. P. Rowland, *Applied Fibre Science*, Ed. F. Happey, Academic Press, London (1970).
74. J. Blackwell and F. J. Kolpak, *Macromolecules,* **8**, 322 (1975).
75. C. H. Haigler, R. M. Brown Jr. and M. Benjamin, *Science*, **210**, 903 (1980).
76. J. Blackwell and F. J. Kolpak, *Appl. Polym. Symp.*, **28**, 751 (1976).
77. G. E. Marcel, L. W. L. Kolodziejski, M. S. Bertran and B. E. Dale, *Macromolecules,* **15**, 686 (1982).
78. C. Nägeli, *Die Stärkekörner*, Schulhub, Zürich (1858).
79. J. Hengstenberg and H. F. Mark, *Z. Krist.,* **69**, 271 (1928).
80. W. Seifritz, *Am. Naturalist,* **63**, 423 (1929).
81. K. H. Mayer and A. J. A. van der Wyk, *Z. Elektrochem.*, **47**, 353 (1941).
82. H. F. Mark, *J. Phys. Chem.*, **44**, 764 (1940).
83. A. Frey-Wyssling, *Protoplasma*, **25**, 261 (1936).
84. S. M. Mukherjee, S. Sikorski and H. J. Woods, *Nature*, **167**, 821 (1952).
85. K. Hess, H. Mahl and E. Gütter, *Kolloid. Z.*, **155**, 1 (1957).
86. K. Hess, E. Gütter and H. Mahl, *Kolloid. Z.*, **158**, 115 (1958).
87. O. Kratky and G. Porod, *Physik der Hochpolymeren*, Vol. 3, Ed. H. A. Stuart, Sect. A, Springer Verlag, Berlin (1955).
88. A. Frey-Wyssling, *Submikropische Morphologie des Protoplasmas und seiner Derivate*, Gebr. Borntträger, Berlin (1949).

89. J. W. S. Hearle, *Fiber Structure*, Ed. J. W. S. Hearle and R. H. Peters, Butterworth, London (1963).
90. H. Krässig, *Textilveredelung*, **4**, 26 (1969).
91. T. Kerr and I. W. Bailey, *J. Arnold Arboretum*, **15**, 327 (1934).
92. P. A. Roelofsen, *Text. Res. J.*, 21 (1951).
93. P. Flory, *J. Chem. Phys.*, **10**, 51 (1942).
94. M. Huggins, *J. Phys. Chem.*, **46**, 151 (1942).
95. A. F. Turbak, R. B. Hammer, R. E. Davies and H. L. Hergert, *Chemtech.*, 51 (1980).
96. K. Kamide, K. Yasuda, T. Matsui, K. Okajima and T. Yamashiki, *Cellulose Chem. Technol.*, **24**, 23 (1990).
97. H. Chanzy, S. Nawrot, A. Peguy, *J. Polym. Sci., Poly. Phys. Ed.*, **20**, 1909 (1982).
98. P. Scherer and C. Philip, *J. Am. Chem. Soc.*, **53**, 4009 (1931).
99. H. Schleicher and B. Phillip, *C. A.*, **74**, 127361b (1971).
100. A. F. Turbak, R. B. Hammer, R. E. Davies and H. L. Hergert, *Chemtech.*, 51 (1980).
101. V. Petrov, *C. A.*, **63**, 10161g (1965).
102. A. Turbak, *Tappi J.*, January (1984).
103. H. Mertel, Ch. Michels, S. Kaufmann and P. Malitzke, *Papier*, **46**, 101 (1992).
104. D. Cole and A. Jones, *Lenzinger Ber.*, **40**, 1114 (1990).
105. J. Brisson, M. Guimond and B. Riedl, *Polym. J.*, **28**, 1299 (1992).
106. M. Garcia-Ramirez, J. Cavaille, A. Dufresne and D. Dupeyre, *J. Appl. Polym. Sci.*, **59**, 1995 (1996).
107. M. Garcia-Ramirez, J. Cavaille, A. Dufresne and D. Dupeyre, *J. Polym. Sci., Polym Phys Ed.*, **32**, 1437 (1994).
108. D. Loubinoux and S. Chaunis, *Textile Res.*, **57**, 61 (1987).
109. R. Armstrong, J. Varge and C. Mccorsley, U.S. Patent 4,196,282 (1980).
110. D. Mancier, Thèse Docteur-Ingènièur, Universite de Grenoble, France (1979).
111. V. Kabrelian, Dissertation, T. U. Dresden (1988).
112. H. Schleicher, B. Philipp and V. Kabrelian, *Papier*, **42**, 653 (1988).
113. W. Berger, M. Keck and B. Philipp, *Cellulose Chem. Technol.*, **22**, 387 (1988).
114. A. V. Yakimanskii, A. M. Bochek, V. A. Zubkov and G. A. Petropavlovskii, *Khimicheskie Volokna*, **64**, 622 (1991).
115. A. M. Bochek, G. A. Petropavlovsky and O. V. Kallistov, *Cellulose Chem. Technol.*, **27**, 137 (1993).
116. T. I. Borisova, N. V. Afanaseva, L. L. Burshtein, O. E. Borodina and L. K. Golova, *Poly. Sci.*, **35**, 1099 (1993).

BRITISH LIBRARY

IMAGING SERVICES NORTH

Boston Spa, Wetherby
West Yorkshire, LS23 7BQ
www.bl.uk

PAGE MISSING IN ORIGINAL

145. V. F. Bystrov, *Progress in NMR Spectroscopy*, Vol. 10, Ed. J. W. Emsley, J. Feeney and L. H. Sutcliffe, Pergamon Press, pp41-81 (1976).
146. P. J. Flory, *Macromolecules*, **7**, 381 (1974).
147. J. E. Mark and P. J. Flory, *J. Am. Chem. Soc.*, **87**, 1415 (1965).
148. J. E. Mark and P. J. Flory, *J. Am. Chem. Soc.*, **88**, 3702 (1966).
149. J. E. Anderson and A. I. J. Ijeh, *J. Chem. Soc., Perkin Trans. II*, 1965 (1994).
150. M. H. Abraham, P. L. Grellier, J. L. M. Doherty and R. W. Taft, *Can. J. Chem.*, **66**, 2673 (1988).
151. E. Juaristi and G. Cuevas, *Tetrahedron*, **48**, 5019 (1992).
152. M. Björling, G. Karlström and P. Linse, *J. Phys. Chem.*, **95**, 6706 (1991).
153. J. Cymerman-Craig and K. K. Purushothman, *J. Org. Chem.*, **5**, 1721 (1970).
154. G. G. Osbourn, *Text. Res.*, **5**, 360 (1935).
155. H. Chanzy, P. Noe, M. Paillet and P. Smith, *J. Appl. Polym. Science*, **37**, 239 (1983).
156. P. H. Hermans and A. Weidinger, *J. Polym. Sci.*, **4**, 135 (1949).
157. A. Pizzi and N. Eaton, *J. Macromol. Sci.-Chem.*, **A21**, 1443 (1984).
158. R. L. Dudley, C. A. Fyfe, P. J. Stephenson, Y. Deslandes, G. K. Hamer and R. H. Marchessault, *J. Am. Chem. Soc.*, **105**, 2469 (1983).
159. G. K. Hamer, F. Balza, N. Cyr and A. S. Perlin, *Can. J. Chem.*, **56**, 3109 (1978).
160. V. Thanabal, D. O. Omecinsky, M. D. Reily and W. I. Cody, *J. Biomolecular NMR*, **4**, 47 (1994).
161. D. E. Woessner, *J. Chem. Phys.*, **36**, 1 (1962).
162. D. Doddrell, V. Glushko and A. Allerhand, *J. Chem. Phys.*, **56**, 3683 (1972).
163. O. W. Howarth and L. Yun Lian, *J. Chem. Soc., Perkin Trans. II*, 263 (1982).
164. M. Malulová, J.-F. Verchère, S. Chapelle, *Carbohydr. Res.*, **287**, 37 (1996).
165. I. Nehls, W. Wagenknecht and B. Philipp, *Cellulose Chem. Technol.*, **29**, 243 (1995).
166. W. berger, M. Keck and B. Philip, *Cellulose Chem. Technol.*, **22**, 387 (1988).
167. H. Yokota, T. Sei, F. Horii and R. Kitamaru, *J. Appl. Polym. Sci.*, **41**, 783 (1990).
168. N. K. Kocketkov, O. S. Chizkov and A. S. Shashkov, *Carbohydr. Res.*, **133**, 173 (1984).
169. K. Bock, A. Brignole and B. W. Sigurskjold, *J. Chem. Soc., Perkin Trans. II*, 1711 (1986).
170. A. Isogai, M. Usuda, T. Kato, T. Urya and R. H. Atalla, *Macromolecules*, **22**, 3168 (1989).